

NASA CR-189230
RI/RD 92-114

(NASA-CR-189230) ORBIT TRANSFER
VEHICLE ENGINE TECHNOLOGY PROGRAM.
TASK B-6 HIGH SPEED TURBOPUMP
BEARINGS Final Report, Jun. 1987 -
Sep. 1989 (Rockwell International
Corp.) 97 p

N92-31892

Unclas

G3/37 0116940

FINAL REPORT

Orbit Transfer Vehicle Engine Technology Program Task B-6 High Speed Turbopump Bearings

by

Rocketdyne Engineering

Rocketdyne Division

Rockwell International

prepared for

NATIONAL AERONAUTICS AND SPACE ADMINISTRATION

January 1992

NASA-Lewis Research Center
Cleveland, Ohio 44135

Contract NAS3-23773

G. P. Richter, Project Manager

**NASA CR-189230
RI/RD 92-114**

FINAL REPORT

Orbit Transfer Vehicle Engine Technology Program Task B-6 High Speed Turbopump Bearings

by

Rocketdyne Engineering

Rocketdyne Division

Rockwell International

prepared for

NATIONAL AERONAUTICS AND SPACE ADMINISTRATION

January 1992

**NASA-Lewis Research Center
Cleveland, Ohio 44135**

Contract NAS3-23773

G. P. Richter, Project Manager



Report Documentation Page

1. Report No. CR-189230	2. Government Accession No.	3. Recipient's Catalog No.	
4. Title and Subtitle Orbit Transfer Vehicle Engine Technology Program Task B-6 High Speed Turbopump Bearings		5. Report Date January 1992	
		6. Performing Organization Code	
7. Author(s) Rocketdyne Engineering		8. Performing Organization Report No. RI/RD92-114	
		10. Work Unit No.	
9. Performing Organization Name and Address ROCKWELL INTERNATIONAL Rocketdyne Division 6633 Canoga Avenue Canoga Park, California 91304		11. Contract or Grant No. NAS 3-23773	
		13. Type of Report and Period Covered Final Report; June 87 to Sept. 89	
12. Sponsoring Agency Name and Address National Aeronautic Space Administration-Lewis Research Center Space Vehicle Propulsion Branch 21000 Brookpark Road Cleveland, Ohio 44135		14. Sponsoring Agency Code	
15. Supplementary Notes Project Manager, G. P. Richter, NASA Lewis Research Center, Cleveland, Ohio			
16. Abstract <p>Bearing types were evaluated for use on the OTV high pressure fuel pump. The high speed, high load, and long bearing life requirements dictated selection of hydrostatic bearings as the logical candidate for this engine. Design and fabrication of a bearing tester to evaluate these cryogenic hydrostatic bearings was then conducted. Detailed analysis, evaluation of bearing materials, and design of the hydrostatic bearings were completed resulting in fabrication of Carbon P5N and Kentanium hydrostatic bearings. Rotordynamic analyses determined the exact bearing geometry chosen. Instrumentation was evaluated and data acquisition methods were determined for monitoring shaft motion up to speeds in excess of 200,000 RPM in a cryogenic atmosphere. Fabrication of all hardware was completed, but assembly and testing was conducted outside of this contract.</p>			
17. Key Words (Suggested by Author(s)) Rocket Engine, Hydrostatic, Bearings, Cryogenic, Turbopump, Rotordynamic		18. Distribution Statement Unclassified - Unlimited	
19. Security Classif. (of this report) Unclassified	20. Security Classif. (of this page) Unclassified	21. No. of Pages 94	22. Price

TABLE OF CONTENTS

LIST OF FIGURES	i i
LIST OF TABLES	i v
SUMMARY	1
INTRODUCTION	2
BEARING CONCEPT EVALUATION.....	2
HYDROSTATIC JOURNAL BEARING ANALYSIS	8
BACKGROUND.....	8
ANALYSIS	8
TESTER DETAIL DESIGN AND ANALYSIS	20
TESTER DESIGN	20
ROTORDYNAMIC ANALYSIS	22
STRUCTURAL ANALYSIS.....	25
HYDROSTATIC BEARING MATERIALS EVALUATION	28
TESTER FABRICATION AND ASSEMBLY.....	31
INSTRUMENTATION	37
CONCLUSION	39
REFERENCES.....	40
APPENDIX A - OTV TESTER COASTDOWN STUDY.....	41
APPENDIX B - OTV AXIAL THRUST BEARING DESIGN.....	44
APPENDIX C - RADIAL LOAD DEVICE.....	46
APPENDIX D - THERMAL ANALYSIS.....	47
APPENDIX E - ROTORDYNAMIC ANALYSIS	50
APPENDIX F - STRUCTURAL ANALYSIS.....	62
APPENDIX G - TEST PLAN	66
APPENDIX H - COPPER PLATING METHOD.....	90

LIST OF FIGURES

Figure 1 - Hybrid Bearing Types.....	4
Figure 2 - Garrett Multi-Leaf Foil Bearing	5
Figure 3 - MTI Bumper -Supported Foil Bearing	5
Figure 4 - AMPEX/Teledyne Tension Foil Bearing.....	6
Figure 5 - Multi-Layer Single Leaf Foil Bearing.....	6
Figure 6 - Pressure Ratio Effects.....	10
Figure 7 - Rotor Speed versus Direct Stiffness Prediction.....	10
Figure 8 - Rotor Speed versus Direct Damping Prediction.....	10
Figure 9 - Rotor Speed versus Cross-Coupled Stiffness Prediction	11
Figure 10 - Rotor Speed versus Leakage Prediction.....	11
Figure 11 - Rotor Speed versus Torque Prediction.....	11
Figure 12 - Hydrogen Vapor Pressure Curve.....	12
Figure 13 - Shaft Diameter versus Direct Damping Prediction	13
Figure 14 - Shaft Diameter versus Direct Damping	14
Figure 15 - Shaft Diameter versus Cross-Coupled Stiffness Prediction.....	14
Figure 16 - Shaft Diameter versus Leakage Prediction	14
Figure 17 - Shaft Diameter versus Torque.....	15
Figure 18 - Bearing Length versus Direct Stiffness Prediction.....	16
Figure 19 - Bearing Length versus Direct Damping Prediction	17
Figure 20 - Bearing Length versus Cross-Coupled Stiffness Prediction.....	17
Figure 21 - Bearing Length versus Leakage Prediction	17
Figure 22 - Bearing Length versus Torque Prediction.....	18
Figure 22A- Final Bearing Design	19
Figure 23 - OTVE Hydrostatic Bearing Tester	20
Figure 24 - Tester Components.....	32
Figure 25 - Tester Nozzle and Baseplate.....	33
Figure 26 - Tester Shaft.....	34
Figure 27 - Tester Baseplate	35
Figure 28 - Radial Bearing Inner View.....	36
Figure A-1 - Turbine Torque vs Coastdown Time (1 to 5 in-lbs).....	42
Figure A-2 - Turbine Torque vs Coastdown Time (0.1 to 1 in-lbs)	42
Figure A-3 - Turbine Torque vs Leakage Mass (1 to 5 in-lbs).....	43
Figure A-4 - Turbine Torque vs Leakage Mass (0.1 to 1 in-lbs)	43
Figure A-5 - Speed vs Coastdown Time.....	43
Figure A-6 - Speed vs Leakage Mass.....	43
Figure E-1 - Rotor Spin Speed vs Damped Natural Frequency.....	50
Figure E-2 - Rotor Spin Speed vs Log Decrement	51

Figure E-3 - First Critical Rotor Group Mode Shape.....	5 2
Figure E-4 - Second Critical Rotor Group Mode Shape.....	5 3
Figure E-5 - Rotor Spin Speed vs Damped Natural Frequency.....	5 4
Figure E-6 - Rotor Spin Speed vs Log Decrement.....	5 5
Figure E-7 - First Critical Rotor Group Mode Shape.....	5 6
Figure E-8 - Second Critical Rotor Group Mode Shape.....	5 7
Figure E-9 - Rotor Spin Speed vs Damped Natural Frequency.....	5 8
Figure E-10 - Rotor Spin Speed vs Log Decrement.....	5 9
Figure E-11 - First Critical Rotor Group Mode Shape.....	6 0
Figure E-12 - Second Critical Rotor Group Mode Shape	6 1
Figure F-1 - Carbon P-5N Hydrostatic Bearing.....	6 2
Figure F-2 - Kentanium Hydrostatic Bearing	6 3
Figure F-3 - Bolt Torque Specifications.....	6 4
Figure F-4 - Tester Materials.....	6 5
Figure G-1 - Program and Test Schedule.....	7 0
Figure G-2 - Tester Hardware.....	7 1
Figure G-3 - Facility Plumbing Schematic.....	7 2
Figure G-4 - Speed/Pressure vs Time	7 4

LIST OF TABLES

Table 1 - OTVE Turbopump Bearing Comparison Summary	3
Table 2 - Results of OTV Hydrostatic Bearing Analysis	1 5
Table 3 - Bearing Length Study.....	1 8
Table 4 - KXX, KXY, and CXX for Various Bearings at 200,000 RPM.....	2 3
Table 5 - Hydrostatic Bearing Material Candidates	2 9
Table F-1 - Material Summary	6 2
Table F-2 - Stress Summary.....	6 3
Table G-1 - Tester Port Identification.....	8 0
Table G-2 - Instrumentation, Dynamic Tests.....	8 1
Table G-3 - Instrumentation, Hardware Limitations.....	8 3
Table G-4 - Accelerometer Instrumentation Parameters	8 4
Table G-5 - Valve Sequencing.....	8 4
Table G-6 - Tester Parameter Identifiers.....	8 5

SUMMARY

Conventional rolling element, hybrid, foil, and hydrostatic bearings were evaluated for use in the Orbit Transfer Vehicle Engine (OTVE) High Pressure Fuel Turbopump. The imposed turbopump speed, load, cryogenic requirements, and engine life and duty cycle of the OTV motivated the selection of the hydrostatic bearings as the prime candidate for this engine.

Detail analysis and design of the hydrostatic bearings and evaluation of bearing materials were completed. The final bearing configuration was carbon P5N with a bore diameter of 1.0 inch and a length of 0.8 inches. Each bearing contained 6 square recesses with orificed isolation pins to provide controlled uniform bearing flow. The tester design included a one inch diameter Titanium shaft supported at each end by the hydrostatic journal bearings and driven by a terry turbine which was designed for shaft speeds up to 200,000 RPM. Two axial hydrostatic thrust bearings were designed to control axial transients and were made from Kel-F polymer with Teflon material properties.

Rotordynamic analyses determined the exact bearing design chosen. Stiffness, damping, and leakage were optimized for the bearing configuration selected. Critical speeds for the final configuration were determined to be under 40,000 RPM, far below the planned test dwell speeds.

Instrumentation was selected and included Bently proximitors probes and fiberoptics. The fiberoptic probe measurement capabilities were determined accurate up to the high rotational speeds planned for testing. A method for copper plating titanium was developed during this effort. The instrumentation was selected to monitor shaft orbit, speed, and axial and radial position under cryogenic operating conditions.

At the completion of this contract, all the tester components were fabricated, but funding limitations precluded actual testing.

INTRODUCTION

The Orbit Transfer Vehicle (OTV) has, as a goal, the same basic characteristics as the Space Shuttle, i.e., reusability, operational flexibility, and payload retrieval with high reliability and low operating cost. The OTV is thus planned to be a manned, reusable cryogenic upper stage engine of high performance and reliability. The requirements for the engine of a vehicle of this type have been derived from NASA-sponsored vehicle and engine studies (ref. RI/RD 92-127). To achieve these requirements and the engine operating needs, the OTV Fuel Turbopump may be required to operate at nearly 230,000 RPM. Conventional rolling element, hybrid, foil, and hydrostatic bearings were evaluated against turbopump imposed speed, load, and cryogenic requirements and engine life and duty cycle requirements.

This evaluation led to the selection of the hydrostatic bearings as the prime candidate design for the OTV Fuel Turbopump. Subsequently a program was conducted to design, fabricate, and assemble a hydrostatic bearing tester. It was planned to test the candidate bearings, in a follow on program, to quantify bearing wear rates and fluid flows required for the selected hydrostatic bearing designs. However, budget constraints limited the scope of work at the time to the fabrication of the tester.

This report includes the evaluation of the bearing concepts, the detailed design of the selected bearing, the evaluation of the bearing materials, the tester fabrication, and assembly.

BEARING CONCEPT EVALUATION

Conventional rolling element, hybrid, foil, and hydrostatic bearings were evaluated as the bearing candidates for the OTVE High Pressure Turbopump. Table 1 summarizes Rocketdyne's estimate of capabilities for each bearing type based on Rocketdyne experience.

Rolling element bearings were evaluated for the OTVE high speed fuel turbopump with a design point shaft speed of approximately 200,000 RPM. Life calculation results of 5 hours, as shown in Table 1, for an appropriate bearing size of 25 mm, fall short of the OTVE requirement of 20 hours. The DN speed limit value of 1.8×10^6 also falls short of a DN goal of 5.0×10^6 for the turbopump. These limitations exclude rolling element bearings from further consideration.

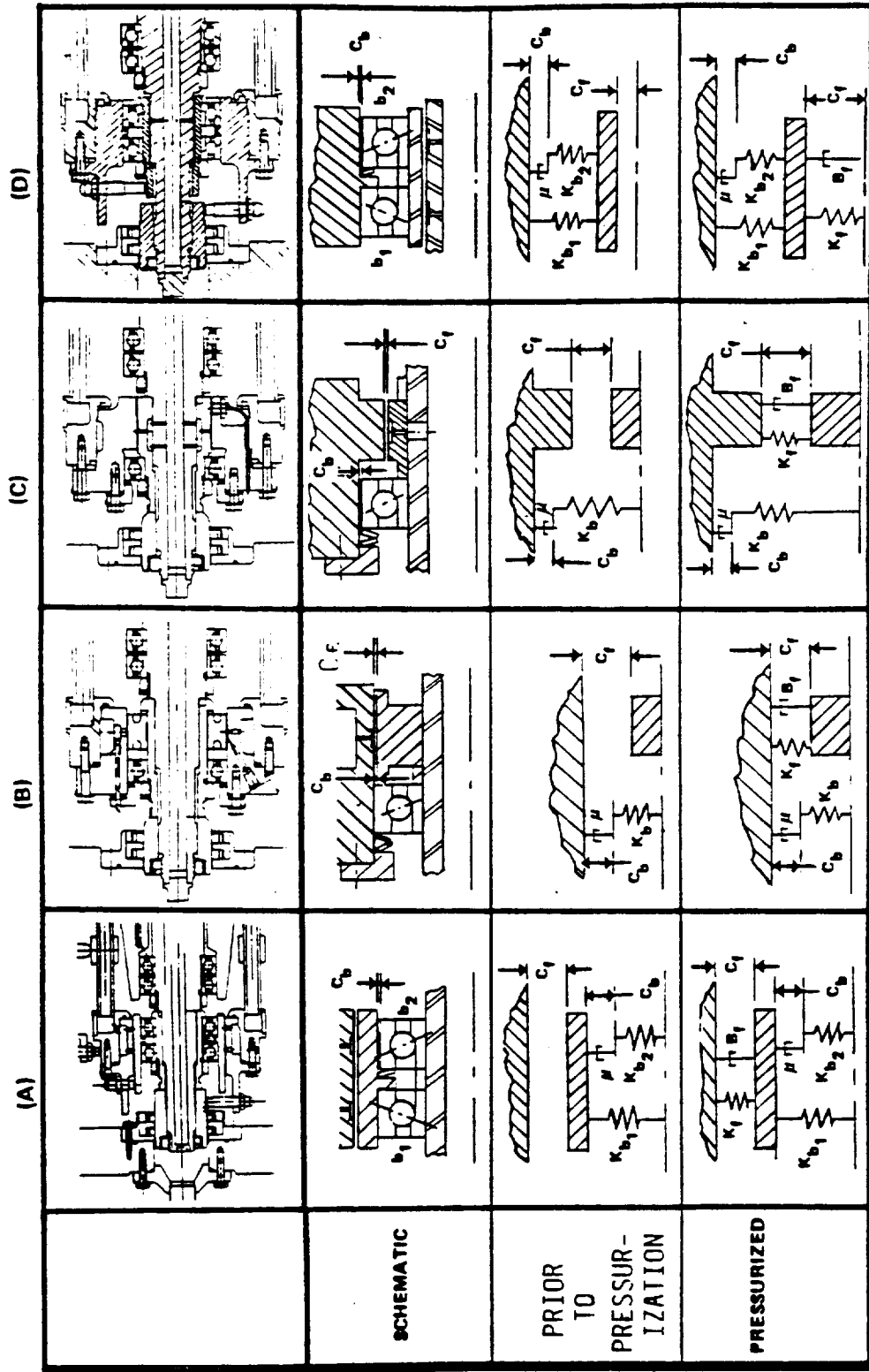
Hybrid bearing configurations as shown in Figure 1, offer improved life (approx. 50 hours); however, these configurations have larger turbopump cross sectional requirements in both the radial and axial directions. This space requirement makes these bearings less suitable for use

Table 1 - OTVE Turbopump Bearing Comparison Summary

BRG TYPE	LOAD CAPACITY RAD (LB)	STIFFNESS (LB/IN)	DAMPING $\left(\frac{\text{LB/SEC}}{\text{IN}}\right)$	LIFE (HR)	SPEED LIMIT (DN) $\times 10^{-6}$	BRK AWAY TORQUE (LB/IN)	LEAKAGE (LBM/S)	LIFT OFF SPEED (RPM)	REQD PRESSURE (LB/IN)
ROLLING ELEMENT (BALL)	150	20000 TO 80000	1.0	5.0	1.8	0.3	COOLANT FLOW ~.05	0	MAINTAIN LIQUID OR HI DENSITY
ROLLING ELEMENT (ROLLER)	300	60000 TO 1.5×10^6	1.0	5.0	1.8	0.15	.05	0	MAINTAIN LIQUID OR HI DENSITY
FOIL	30-40 FOR 1" L X 1" D BRG @ SPEED	2K-10K	≤ 1.0	55000- 95000 IN ECU	UNKNOWN	≤ 2 IN-LB FOR 1" L X 1" D BEARING	FLOW THRU FOR COOLING <ROLLING ELEMENT	~3K	~10' PSI ΔP ACROSS FOR COOLING
HYBRID	150 OR .25 (ΔP)	100000	50	50	3.0	0.3	0.15 (H_2)	~1.5K	~2000 (ΔP)
HYDRO- STATIC	.25 (ΔP)	400 (ΔP)	50	START LIMITED TO ∞	NONE	0.05 X wt	0.2 (H_2)	~1.5K	~2000 (ΔP)

LH₂ Capacities

Figure 1 - Hybrid Bearing Types



in the small diameter OTVE high speed fuel turbopump. The rolling element bearing in the hybrid combination has the capability of reacting transient axial loads but will continue to rotate and generate parasitic losses during steady state operation.

Foil bearings were reviewed for applicability to the OTVE high speed fuel turbopump. The four types of foil bearings reviewed include the multi-leaf type, the bumper supported, the tension type, and the multi-layer single leaf. These foil bearings are shown in Figures 2 thru 5 respectively.

Figure 2 - Garrett Multi-Leaf Foil Bearing

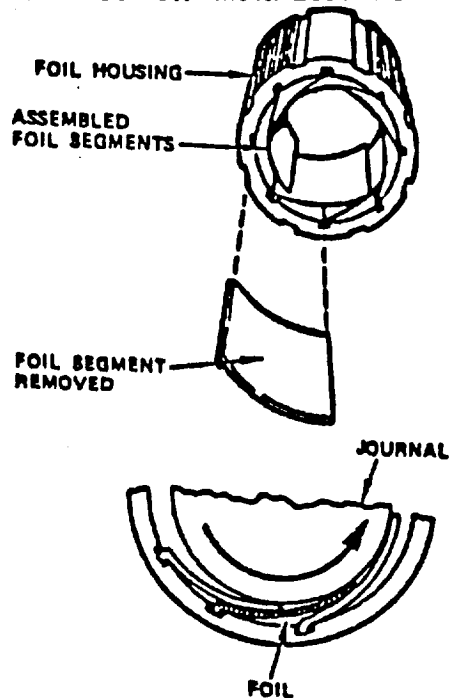


Figure 3 - MTI Bumper -Supported Foil Bearing

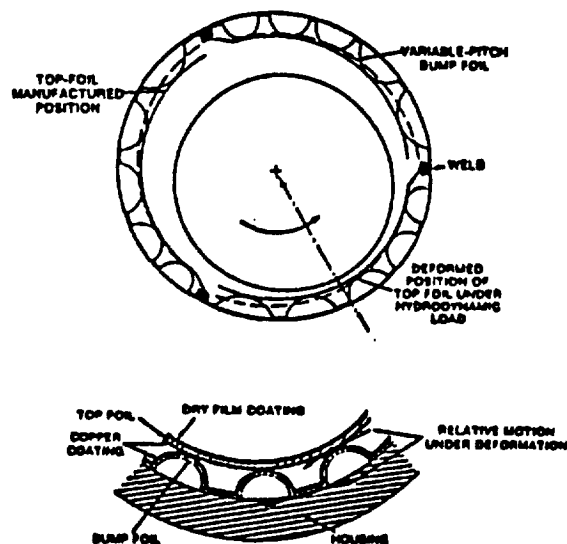


Figure 4 - AMPEX/Teledyne Tension Foil Bearing

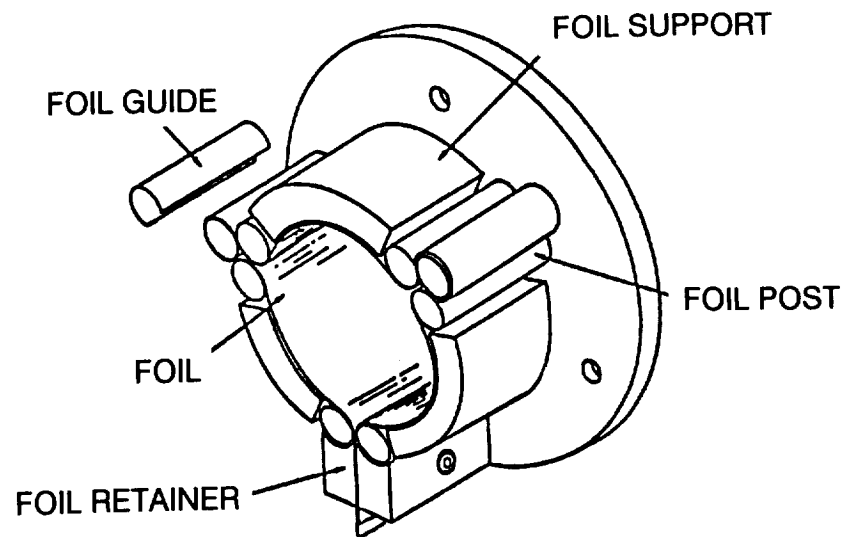
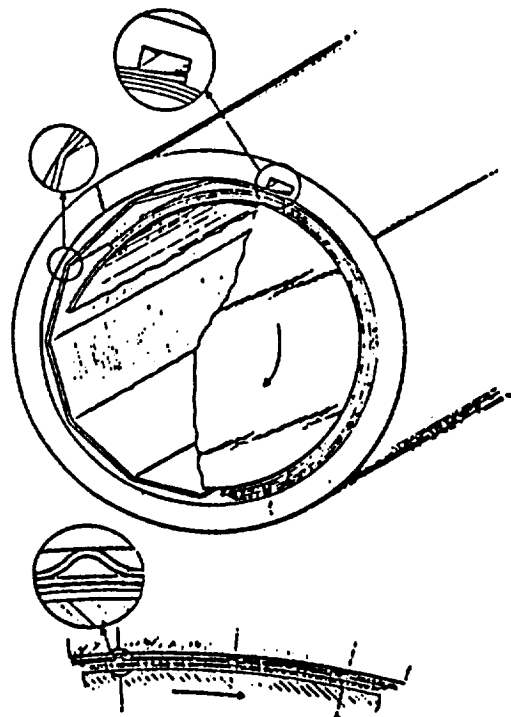


Figure 5 - Multi-Layer Single Leaf Foil Bearing



The multi-leaf bearing has been used in various aircraft for air-conditioning and heating applications and has gained the most experience to date. In these applications the bearing has been employed in compressors which operate at low pressures and consequently low radial loads. However, liquid cryogenic turbomachinery operate at high pressures and high radial loads. Under these conditions there has been no experience with the foil bearings. Rotordynamic characteristics are difficult to acquire and are unavailable. Additionally, the impact of foil bearings on minimal clearance soft seals is undefined.

Significant attributes make the foil bearings attractive however. The foil bearings operate in a bath of fluid and generate little heat after lift-off from the foil and as a result require little cooling and minimal process fluid replenishment. They have demonstrated long life and reliability, and simplified rotordynamics. The characteristic foil bearing aspect ratio (journal diameter divided by bearing length approximately equal to one) results in shafts of large diameter and increased shaft stiffness which may result in simplified rotordynamics.

Foil bearings are worthy of investigation as turbopump bearings; however, uncertainty about their rotordynamic characteristics prompts the recommendation of a follow-on program to evaluate their application into high speed turbopumps for pumping liquid propellants.

Hydrostatic bearings offer predictable stiffness and damping and unlimited DN. Bearing life, while predicted to be infinite, needs to be quantified and process fluid flow requirements need to be defined. The predicted attributes of long life, high reliability and operational experiences resulted in the selection of the hydrostatic bearings for use in the OTVE High Pressure Turbopump.

HYDROSTATIC JOURNAL BEARING ANALYSIS

BACKGROUND

Hydrostatic bearings were invented in 1862 by L. Girard and since that time have been used in applications ranging from telescopes to turbomachinery rotors. The current state-of-the-art of hydrostatic bearing analysis is still based on the classical analysis by Reynolds (1886). There have been many papers detailing minor revisions to the original theory to account for such things as turbulent viscosity, inertial pressure loss, surface roughness, two-phase flow, cavitation, and various numerical methods for solving Reynolds' equations. Improvement in analysis can be accomplished with experimental measurements inside the flow field.

Considering the long history of hydrostatic bearings, most of the experimental data can be considered recent. Ho and Chen (1984) presented detailed pressure measurements in a hydrostatic bearing. Raimondi and Boyd (1957) (oil), Aerojet (1965) (water), Pratt and Whitney (1967) (liquid hydrogen and liquid oxygen), Ghosh (1973) (oil), Ho and Chen (1980) (oil), Chaomleffel (1983) (oil), Yoshimoto et al (1984) (air), Spica et al (1986) (liquid hydrogen) and Yoshimoto (1988) (air) performed static displacement tests to yield stiffness, leakage and torque as a function of eccentricity. Mullan and Richardson (1964) presented experimental stiffness and damping coefficients for lateral motion of a rotor supported in gas bearings. Heller (1974) used a model matching technique to obtain direct and cross-coupled stiffness and damping for a hydrostatic bearing in water. However, the technique used did not produce repeatable or reliable results. Butner and Murphy (Rocketdyne - 1986) measured stiffness and damping coefficients for internal and external hydrostatic bearings in liquid hydrogen and Freon. However, their force coefficients could not be separated since the test apparatus produced synchronous, circular orbits. There are a multitude of other authors who have measured secondary quantities such as onset speed of instability, response to unbalance, and critical speed for a rotor supported in hydrostatic bearings. There are no experimental data in the open literature to support the high speed and small size bearings for the OTVE (7.5K pound thrust) hydrogen turbopump. This data will be acquired in testing the OTVE bearing tester.

ANALYSIS

The externally fed hydrostatic bearing analysis used at Rocketdyne is based on the work of Artiles et al (1982). This work solves Reynolds' equations for turbulent flow utilizing a Newton-Raphson type of solution algorithm and accounts for turbulent flow, inertial losses, and eccentricity of the rotor. This analysis has been correlated with the available stiffness,

leakage, and torque data and has been found to be in general agreement. No reliable data exists for the cross-coupled stiffness and direct damping of hydrostatic journal bearings.

The first step in the design of the hydrostatic bearing was to do a parametric study to define the geometry of the bearing based on rotordynamic considerations and the available envelope in the turbopump. To start the study, a scaled down version of the hydrostatic bearing tested by Butner and Murphy (1986) was chosen. For a 1.0 inch diameter and a 1.2 inch length, the geometry became:

Number of recesses = 6

Recess circumferential width = 0.237 in.

Recess axial width = 0.22 in.

Using this geometry, the effects of rotor speed, supply pressure, and rotor diameter on the stiffness, damping, leakage, and torque of the hydrostatic bearing were examined. For the rotor speed study the following geometry was used:

Radial clearance = 0.00125 in.

Bearing length = 1.2 in.

Rotor diameter = 1.0 in.

The supply pressure for the rotor speed study was assumed to be 1000, 2000, or 4000 psi at 200,000 rpm and proportional to rotor speed squared for off design speeds. The hydrostatic bearing orifice was optimized to yield a pressure ratio of 0.5 which has been shown to yield the optimum stiffness and damping (see Figure 6). The results for the rotor speed study are illustrated in Figures 7 thru 11. Figure 7 shows that the direct stiffness of the bearing increases non-linearly with rotor speed increase. This is to be expected since direct stiffness is proportional to supply pressure, as shown, and supply pressure is proportional to rotor speed squared. Figure 8 shows that direct damping is linearly proportional to rotor speed and increases with increased supply pressure. Figure 9 shows that cross-coupled stiffness increases non-linearly with increased rotor speed and increases with increased supply pressure. Figure 10 illustrates that the bearing leakage is linearly proportional to rotor speed for the 2000 psi case. However, the leakage is slightly nonlinear with rotor speed for both the 1000 and 4000 psi cases. Figure 11 shows the bearing torque as a function of rotor speed. This figure shows that the torque increases non-linearly with increasing speed. The torque for the 2000 and 4000 psi cases were virtually the same. This rotor speed study was a necessary first step to provide information for the critical speed analysis. The interesting information that resulted from this study concerned the temperature of the hydrogen being supplied to the tester. Originally it was assumed that the fluid temperature would be 80

Figure 6 - Pressure Ratio Effects

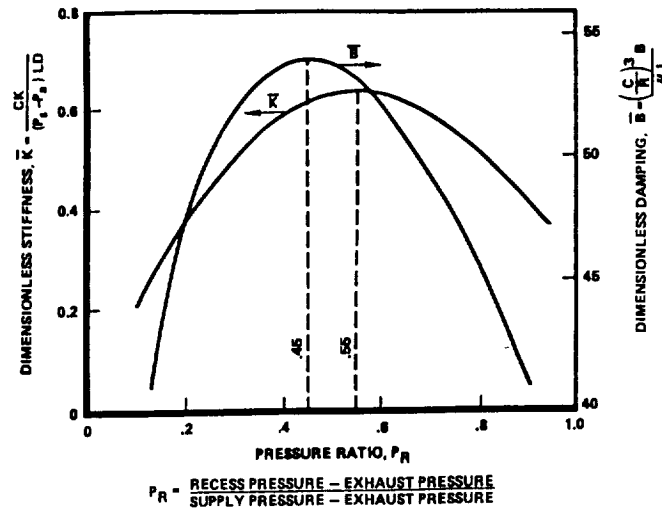


Figure 7 - Rotor Speed versus Direct Stiffness Prediction

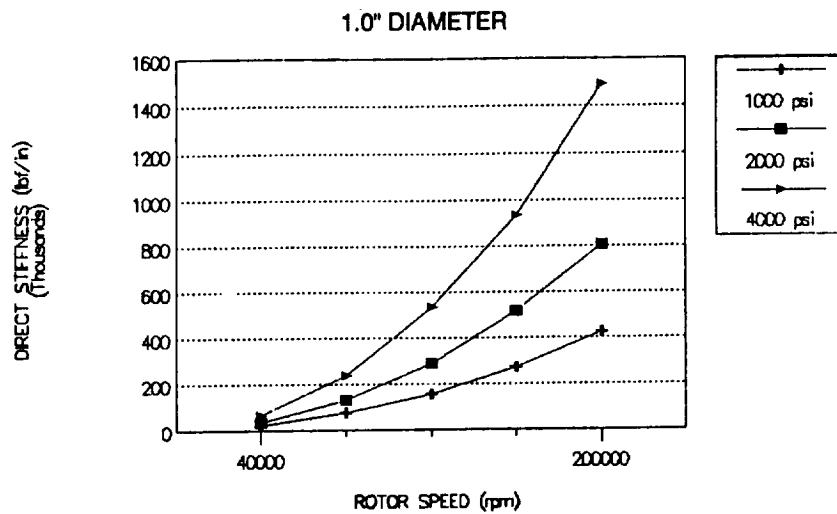


Figure 8 - Rotor Speed versus Direct Damping Prediction

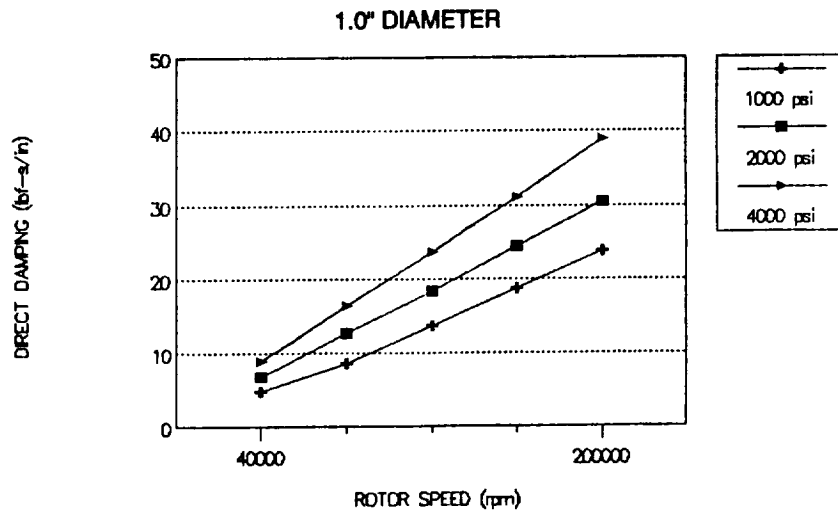


Figure 9 - Rotor Speed versus Cross-Coupled Stiffness Prediction

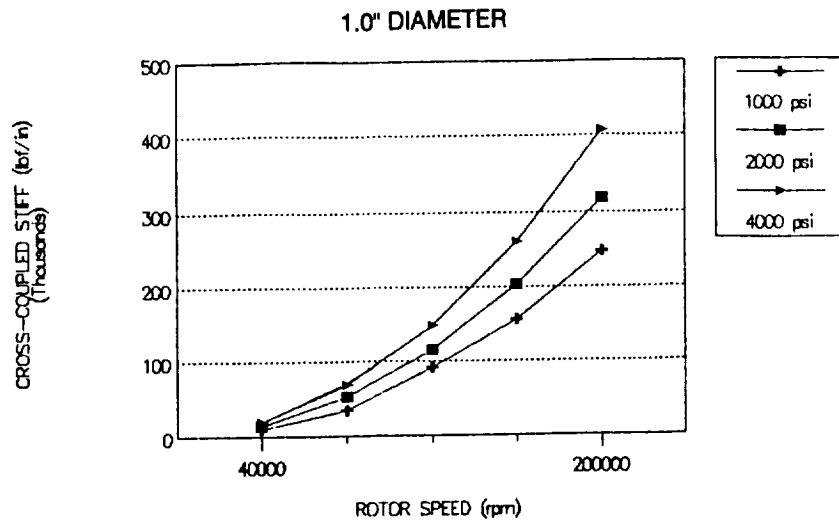


Figure 10 - Rotor Speed versus Leakage Prediction

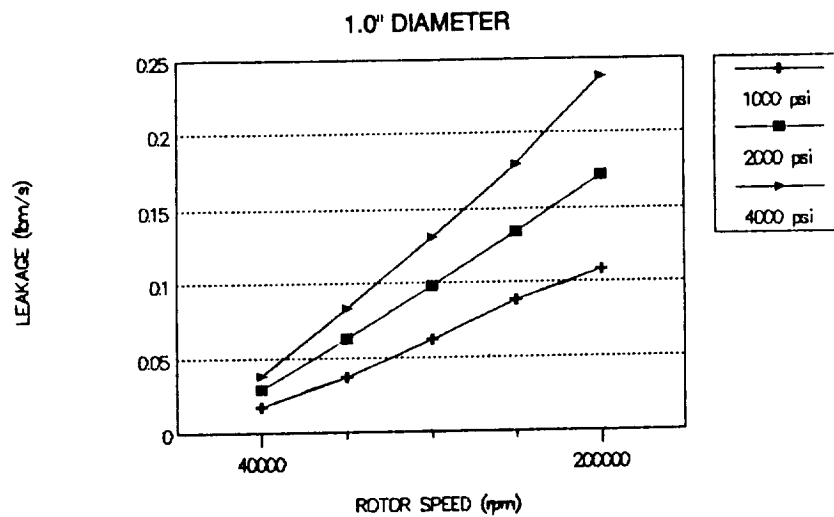
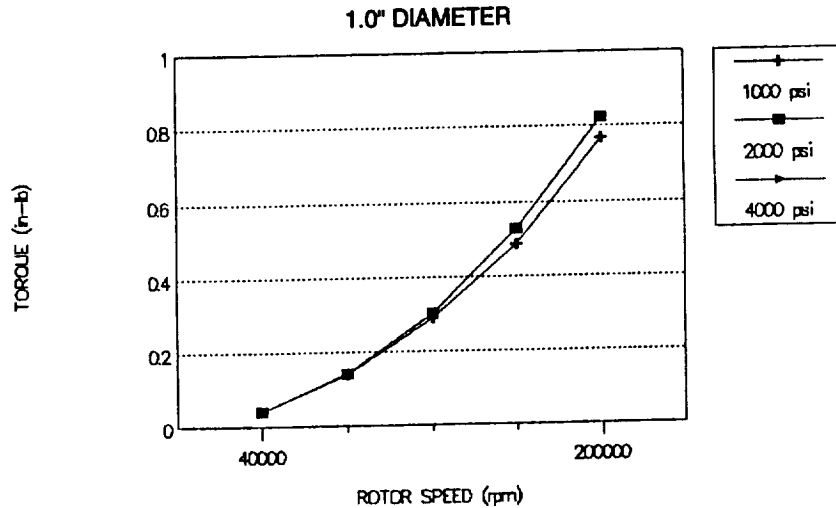


Figure 11 - Rotor Speed versus Torque Prediction

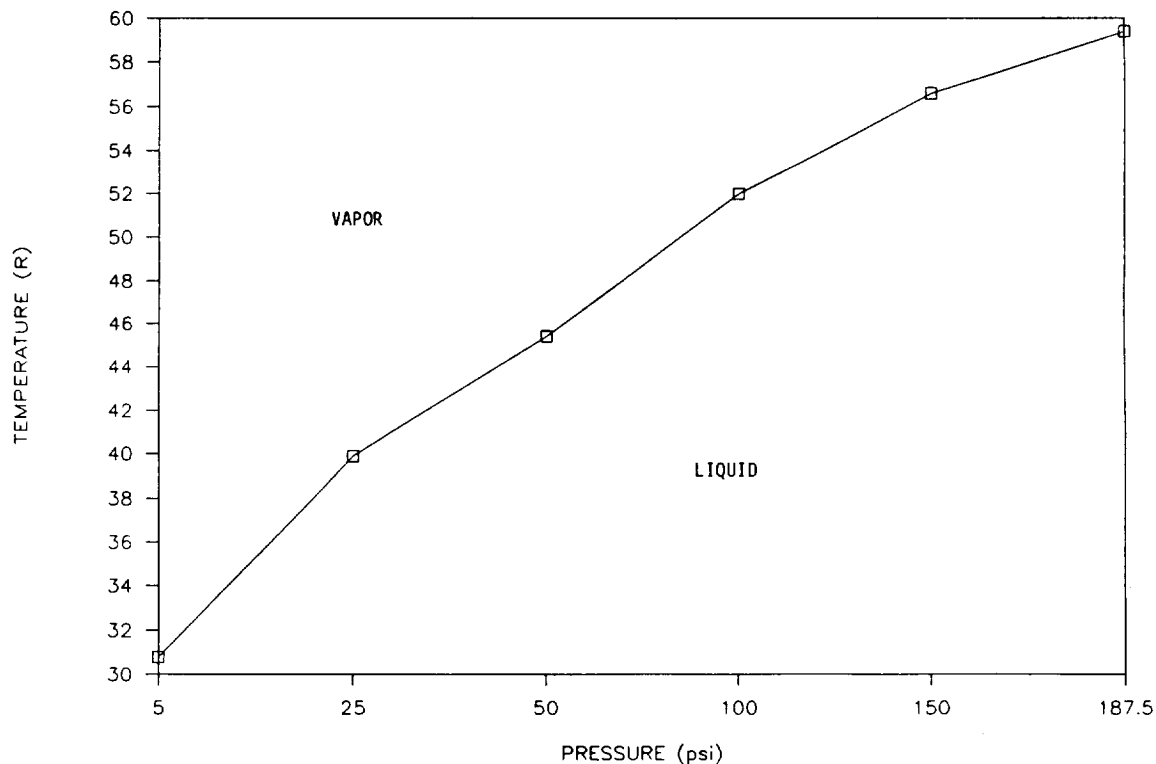


degrees Rankine. The pressure and rotor speed relationship was as follows:

SPEED (RPM)	Supply Pressure (psi)	Recess Pressure (psi)
40,000	80	40
80,000	320	160
120,000	720	360
160,000	1280	640
200,000	2000	1000

For calculation purposes, the sump pressure was assumed to be zero. The properties of the fluid were calculated at each pressure condition using the computer program MIPROPS developed by the National Bureau of Standards. The vapor pressure curve for hydrogen is shown in Figure 12. The figure shows that below the critical pressure of 187.5 psi, the hydrogen will vaporize for temperatures greater than 59 degrees Rankine. This means that the hydrogen in the bearing recess will vaporize at speeds less than 85,000 rpm, for a 2000 psi supply pressure at design speed. Vaporization of the fluid would result in reduced load capacity and subsequent rubbing of the shaft and changes in the rotordynamics. To avoid this condition, it was decided that the supply temperature of the fluid would be maintained at 36 degrees Rankine.

Figure 12 - Hydrogen Vapor Pressure Curve



The second part of this study was to examine the influence of rotor diameter on the stiffness, damping, leakage, and torque. This study was carried out using the following assumptions:

Bearing length = 1.2 in
Rotor speed = 200,000 RPM
Radial clearance = 0.00125 in
Recess dimensions = 0.22 x 0.237 in.
Number of recesses = 6
Supply pressure = 2000 psi

Generally, the bearing length, recess geometry, number of recesses, and radial clearance would be optimized for each rotor diameter. For convenience, these parameters were held constant in this study. Figure 13 shows shaft diameter versus direct stiffness. This figure shows that the stiffness increases as shaft diameter increases. It also shows that the stiffness gradient has a inflection point near the 1.0 inch diameter size. Figure 14 shows direct damping versus shaft diameter. Figure 15 shows cross-coupled stiffness versus shaft diameter. This figure shows the same phenomenon as the damping plot; the cross-coupled stiffness increases monotonically with increasing diameter up to 1.25 inches and then levels off. Figure 16 shows leakage versus shaft diameter. Like the direct stiffness plot, this figure shows an inflection point near the 1.0 inch diameter. Therefore, optimum leakage performance would be obtained for a 1.0 inch diameter shaft. Figure 17 shows the bearing torque as a function of the rotor diameter. The figure shows that the torque increases non-linearly as shaft diameter increases. Also, the torque increases sharply for diameters greater than 1.0 inch. The tabulated results for the aforementioned studies are given in Table 2.

Figure 13 - Shaft Diameter versus Direct Stiffness Prediction

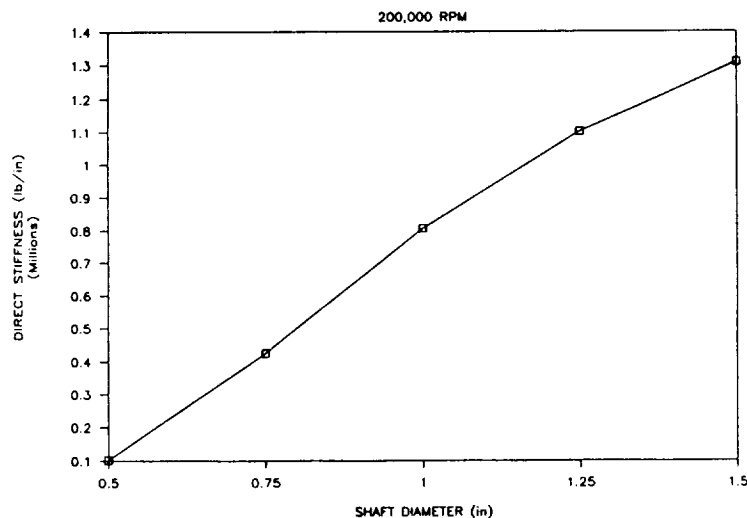


Figure 14 - Shaft Diameter versus Direct Damping

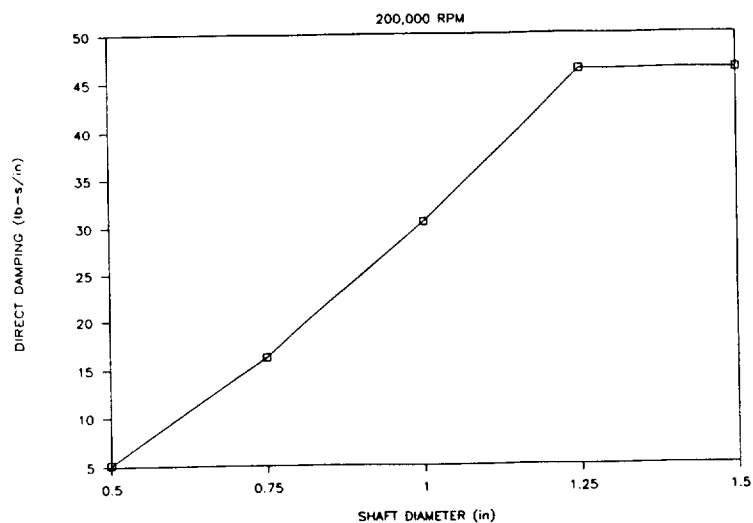


Figure 15 - Shaft Diameter versus Cross-Coupled Stiffness Prediction

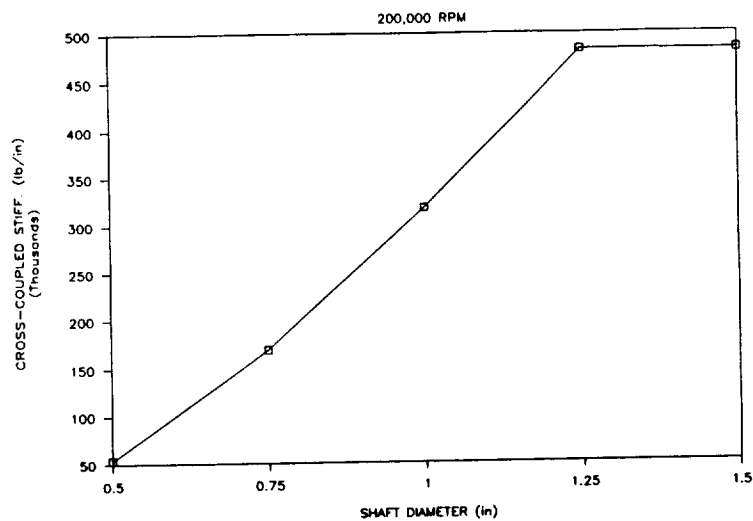


Figure 16 - Shaft Diameter versus Leakage Prediction

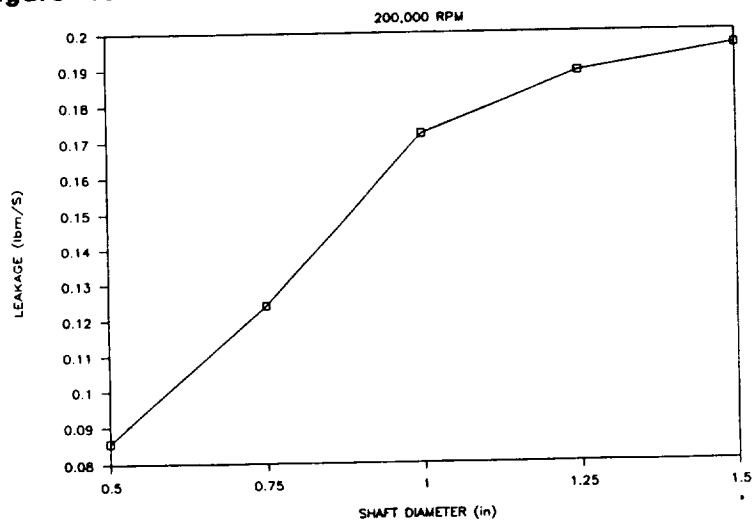


Table 2 - Results of OTV Hydrostatic Bearing Analysis

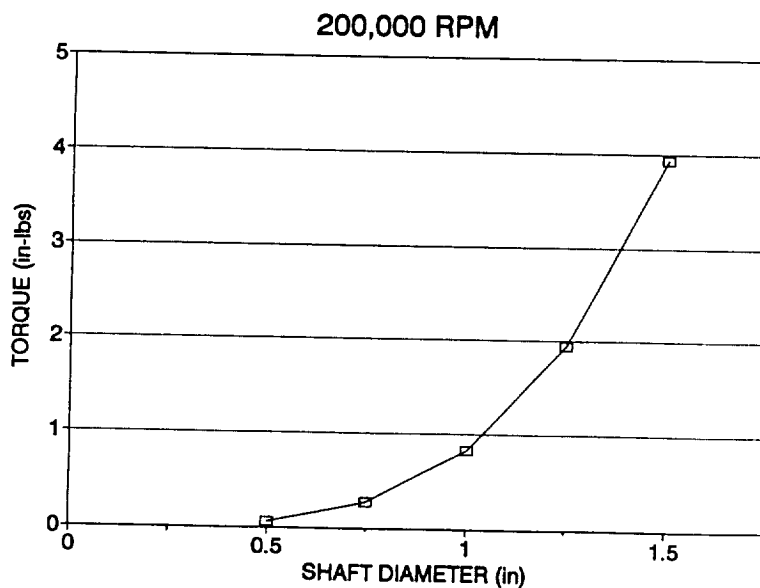
2000 psi supply		200K RPM			
DIAMETER	KXX	CXX	KXY	MDOT	TORQUE
(in)	(lb/in)	(lb-s/in)	(lb/in)	(lbm/s)	(in-lbs)
0.50	102394	5.2	53742	0.086	0.056
0.75	425105	16.2	169362	0.124	0.269
1.00	806732	30.5	318265	0.172	0.823
1.25	1102312	46.3	482579	0.189	1.948
1.50	1308573	46.3	482311	0.196	3.932

1000 PSI	SUPPLY	1.0" DIA.			
RPM	KXX	KXY	CXX	MDOT	TORQUE
40000	19534	9769	4.68	0.017	0.041
80000	73461	34258	8.44	0.037	0.139
120000	154483	91869	14.67	0.062	0.290
160000	273953	155884	18.66	0.088	0.487
200000	424557	248229	23.80	0.108	0.769

2000 PSI	SUPPLY	1.0" DIA			
RPM	KXX	KXY	CXX	MDOT	TORQUE
40000	33497	14151	6.78	0.029	0.041
80000	129269	53060	12.7	0.063	0.143
120000	290508	115444	18.43	0.098	0.302
160000	516124	203366	24.35	0.134	0.527
200000	806732	318265	30.48	0.172	0.822

4000 PSI	SUPPLY	1.0" DIA			
RPM	KXX	KXY	CXX	MDOT	TORQUE
40000	63998	18593	8.9	0.038	0.041
80000	237711	68591	16.4	0.083	0.143
120000	531597	148466	23.7	0.131	0.302
160000	935754	260261	31.15	0.179	0.527
200000	1494694	407091	38.98	0.238	0.822

Figure 17 - Shaft Diameter versus Torque



Based on these investigations, the 1.0 inch diameter was chosen for the test rotor and the 2000 psi bearing supply pressure was selected as most nearly approximating the turbopump bearing supply pressure from the impeller discharge. The next step was to investigate the bearing length. Until now, the bearing length was assumed to be 1.2 inches. The bearing geometry assumptions remained the same.

Figure 18 illustrates the effect of bearing length on direct stiffness as a function of shaft speed. The figure shows that the stiffness increases with increasing length. It appears that if there were an optimum it would occur near 0.6 inches. Figure 19 shows direct damping versus bearing length as a function of shaft speed. This figure shows that damping increases non-linearly as length increases. Figure 20 shows cross-coupled stiffness versus length as a function of shaft speed. Like the damping, the cross-coupled stiffness increases non-linearly with increasing length. Figure 21 shows the leakage versus bearing length as a function of shaft speed. The figure shows that leakage decreases as length increases. The plot is probably distorted because the same recess geometry (0.22 x 0.237) was used for each length. A constant area ratio (total recess area/total bearing area) would most likely produce a more linear plot. Figure 22 shows torque versus length as a function of shaft speed. This figure illustrates that the torque increases linearly as length increases. The data used for these plots is given in Table 3.

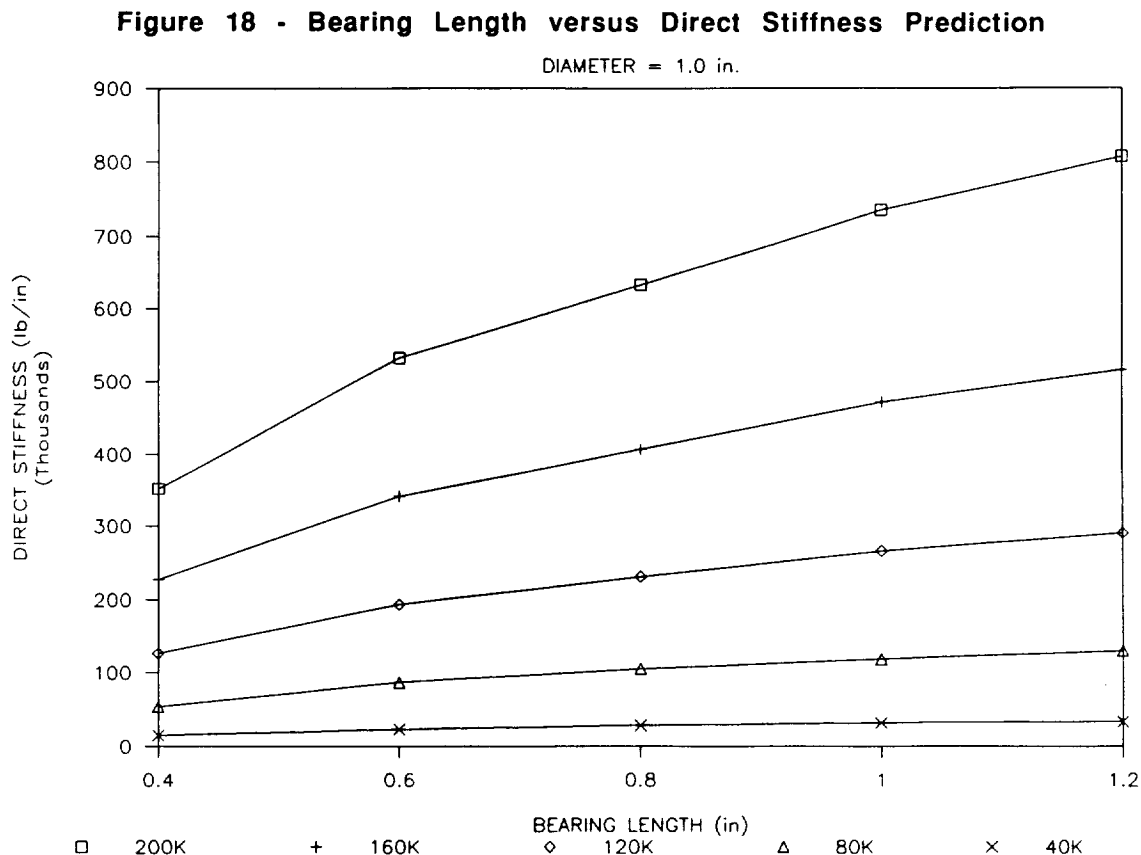


Figure 19 - Bearing Length versus Direct Damping Prediction

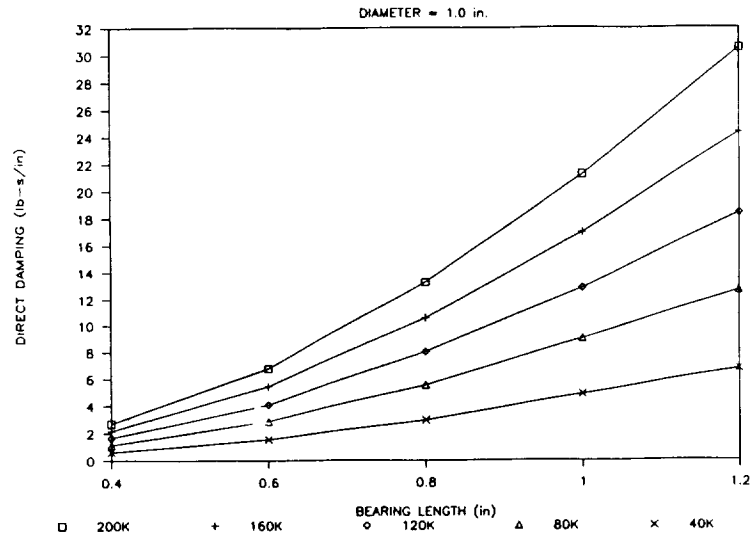


Figure 20 - Bearing Length versus Cross-Coupled Stiffness Prediction

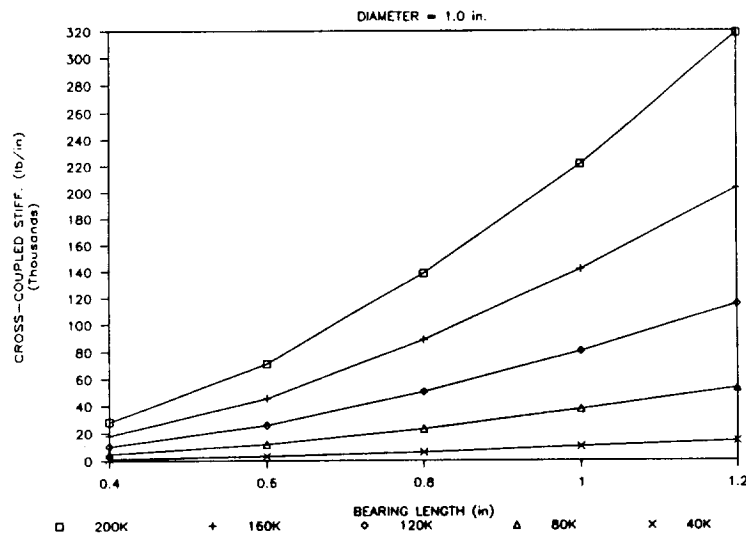


Figure 21 - Bearing Length versus Leakage Prediction

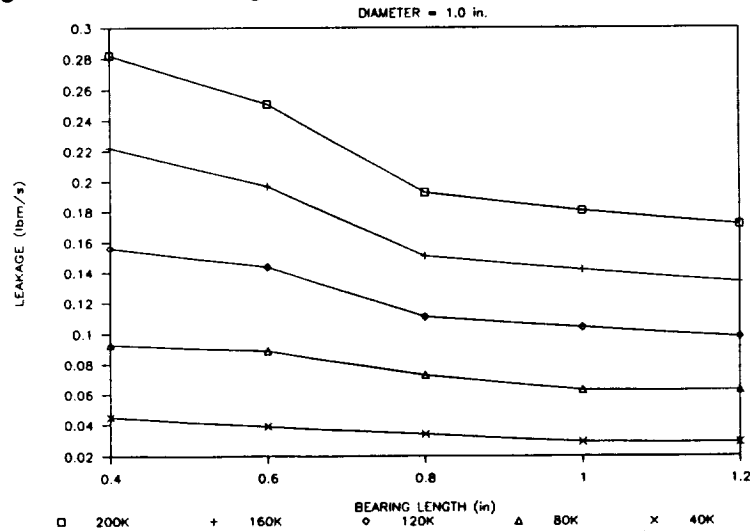


Figure 22 - Bearing Length versus Torque Prediction

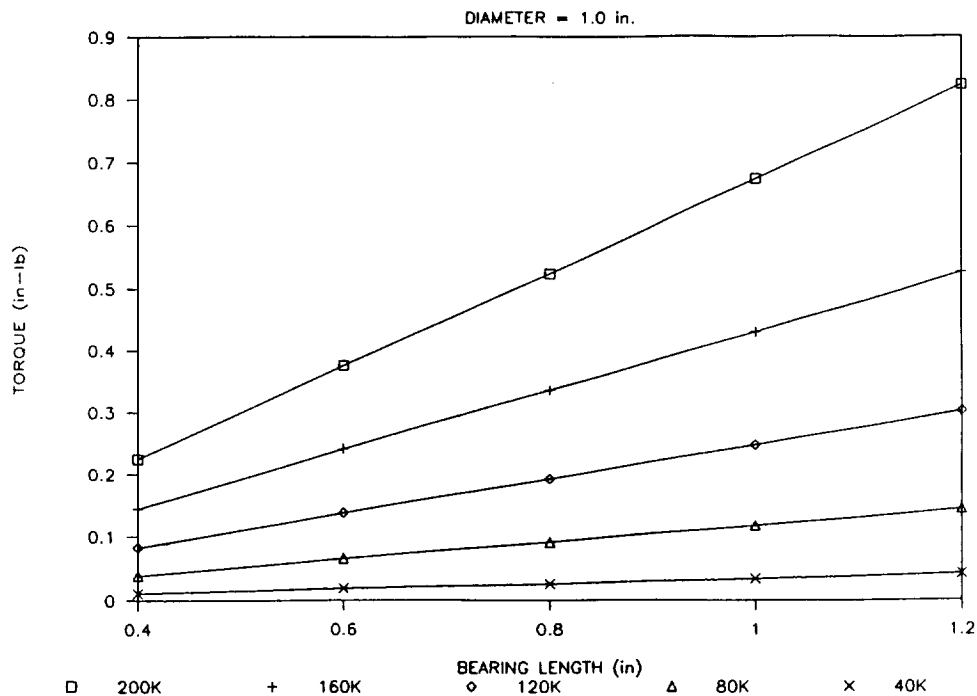


Table 3 - Bearing Length Study

LENGTH (IN)	SUPPLY PRESSURE (psi)	ROTOR SPEED (RPM)	KXX (lb/in)	KXY (lb/in)	CXX (lb-s/in)	MDOT (lbm/s)	TORQUE (in-lbs)
0.4	2000	200000	352350	28227	2.7	0.282	0.225
0.6	2000	200000	533100	71297	6.8	0.251	0.375
0.8	2000	200000	632379	138785	13.3	0.193	0.524
1	2000	200000	735554	221573	21.2	0.181	0.674
1.2	2000	200000	806732	318265	30.5	0.172	0.822
0.4	1280	160000	227611	18155	2.2	0.222	0.144
0.6	1280	160000	342486	45655	5.5	0.197	0.240
0.8	1280	160000	406923	88949	10.6	0.151	0.336
1	1280	160000	471813	141818	17.0	0.142	0.430
1.2	1280	160000	516124	203366	24.4	0.134	0.526
0.4	720	120000	126485	10384	1.7	0.156	0.083
0.6	720	120000	193781	25924	4.1	0.144	0.137
0.8	720	120000	231105	50601	8.1	0.111	0.192
1	720	120000	266584	80527	12.9	0.104	0.247
1.2	720	120000	290508	115444	18.4	0.098	0.302
0.4	320	80000	54081	4792	1.1	0.093	0.039
0.6	320	80000	86973	12110	2.9	0.089	0.065
0.8	320	80000	104946	23249	5.6	0.0729	0.091
1	320	80000	118359	37746	9.0	0.063	0.117
1.2	320	80000	129269	53060	12.7	0.063	0.143
0.4	80	40000	14982	1284	0.6	0.045	0.011
0.6	80	40000	23022	3289	1.6	0.039	0.019
0.8	80	40000	28123	6200	3.0	0.034	0.026
1	80	40000	31780	10187	4.9	0.029	0.034
1.2	80	40000	33497	14151	6.8	0.0288	0.041

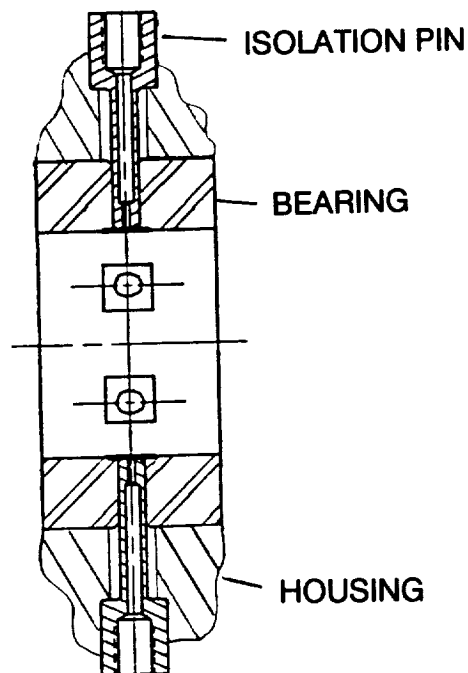
Based on the length study and the concurrent rotordynamic analysis, the 0.8 inch bearing length was chosen. The final design consideration was the depth of the recess. This was calculated using the criteria set forth by MTI in Pratt and Whitney Report (1967): the minimum recess depth should be set such that the pressure variation in the recess is one-tenth of the film pressure drop, the maximum depth should be chosen such that the ratio of the orifice and recess volume to the film volume should be less than 1.0. Given these criteria, the recess depth recommendation was:

$$0.007 \text{ in} < \text{depth} < 0.043 \text{ in.}$$

The final hydrostatic journal bearing design parameters were as follows:

Orifice diameter = 0.030 in
Number of recesses = 6
Recess dimensions = 0.22 x 0.237 in
Recess depth = 0.007-0.0043 in
Bearing diameter = 1.0 in
Bearing length = 0.8 in
Radial clearance = 0.00125 in
Estimated leakage = 0.2 lbm/s/bearing

Figure 22A - Final Bearing Design



TESTER DETAIL DESIGN AND ANALYSIS

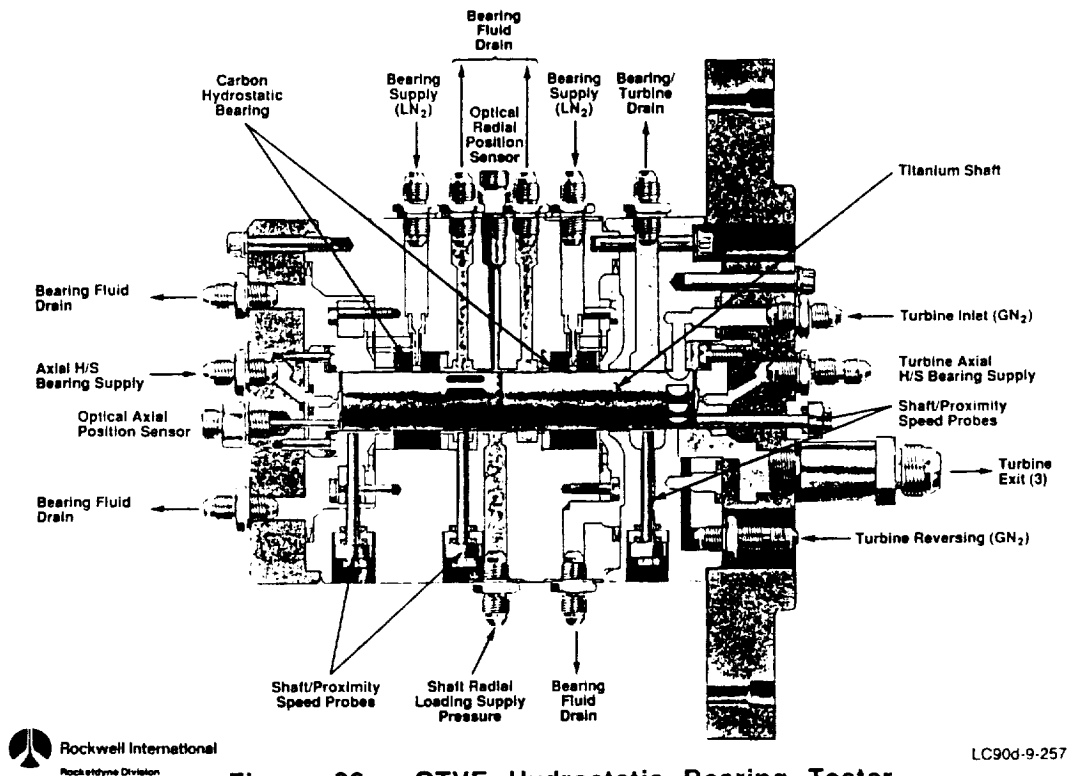


Figure 23 - OTVE Hydrostatic Bearing Tester

TESTER DESIGN

Efforts in the detail design phase of this program have resulted in the cross section shown in Figure 23. The tester is being designed, fabricated, and assembled, to test through multiple stop and start cycles. The testing will determine the wear resistance and flow requirements of hydrostatic bearing element materials, when operating with a Titanium shaft in liquid hydrogen. The design speed of the tester shaft is 200,000 RPM, similar to that of the 7.5K pound thrust OTVE HPFTP (RI/RD 92-127 Final Report).

The features of the tester cross section, Figure 23, include two shaft supporting radial hydrostatic test bearings that are replaceable with hydrostatic bearing elements of different materials. The materials selected are P5N Carbon for the first series of tests, and K162B Kentanium, a hard ceramic, for the second series of tests. These radial hydrostatic bearings are pressure fed proportional to shaft speed squared, to simulate pump pressure build up, through radial isolation pins, see Fig. 22A, that are designed to isolate the bearing to housing diametral interfaces from high fluid pressure.

The shaft is one inch in diameter and six inches long. Titanium has been selected for the shaft material for two reasons. A rotordynamic analysis of the tester has indicated the need for a

material with titanium's stiffness to weight ratio and at least one of the HPFTP bearing journals will likely be the hub of a Titanium impeller.

The shaft has a Terry turbine machined at one end that is powered by gaseous hydrogen to drive the shaft to 200,000 RPM. There are seven forward turbine nozzles and two reversing nozzles located over the terry turbine. The time required to accelerate the shaft to 200,000 RPM is calculated to be approximately 1/2 second, neglecting friction. During testing a two second ramp to 200,000 RPM is planned.

A set of reversing nozzles are aimed at the same set of terry turbine buckets and are intended to stop the shaft, along with the frictional fluid drag of the hydrostatic bearings, from 200,000 RPM. These two reversing nozzles generate approximately 10% of the torque of the forward nozzles and an analysis of the coast down time required for the shaft to slow from 200,000 RPM to zero is presented in Appendix A.

The forward set of turbine nozzles provide power to turn the shaft and as a result apply an eight pound axial load toward the non-turbine end of the shaft. This axial load is reacted by an axial hydrostatic thrust bearing made of the polymer Kel-F. The axial hydrostatic bearings, located at both ends of the shaft, are pressure fed with liquid hydrogen at constant supply pressure. An analysis of the axial hydrostatic bearings is presented in Appendix B.

The radial side loading device, consisting of a single hydrostatic pad, is located over the shaft at the mid-point between the two radial hydrostatic bearings. This device will be used to apply shaft side load to simulate turbopump volute discharge shaft loadings. The pressure supplied to the radial loader will be proportional to shaft speed squared to simulate radial load build up as the turbopump speed increases. An analysis of the radial loader is presented in Appendix C.

Instrumentation designed to monitor shaft motion consists of six eddy current probes to monitor shaft orbit, speed, and radial and axial position. Three fiberoptic probes will provide redundant monitoring of shaft orbit, speed, and axial position.

The greatest challenge in the design of the tester was in the mounting of the P5N Carbon bearing element to a housing. The difference in the thermal expansion rates of the P5N Carbon and most common housing metals is such that structural analysis of the assembly of the P5N bearing and housing predicted that the P5N bearing would fail at cryogenic temperatures. The objective is to maintain at least a line to line fit at the diametral interface of the bearing element O.D. and mating housing I.D. at LH₂ temperatures and yet have sufficient fit at ambient temperature to accomplish line boring of the assembly. A search was made to find a material that is more compatible with the P5N. Invar was selected as this material for the housing.

Invar is used as the mount ring material in some of the carbon seals in the SSME HPFTP. The utilization of Invar allows the assembly of the P5N Carbon and Invar housing at ambient temperatures and maintains a sufficient diametral interference at LH₂ temperatures.

Axial restraint is required on the bearing elements to keep the tensile stress field around the isolation pin holes within acceptable levels. This restraint is applied by axial retainers which are bolted to each end of the main housing and apply axial force to each bearing stack, see Fig. 24.

The solution to the thermal expansion problem between the P5N Carbon bearing element and the supporting housing was solved by selecting Invar 36 as the housing material in this tester. This material may not be applicable to the turbopump however, as the thermal expansion problem is merely transferred to another diametral interface - between Invar 36 and the turbopump housing. Further analysis is needed on this issue. A turbopump compatible hydrostatic bearing material/design needs to be developed. A solution may be offered in the second bearing material selected for testing, Kentanium.

A heat transfer analysis of the tester is presented in Appendix D.

ROTOR DYNAMIC ANALYSIS

Rotor dynamic analysis has been performed on the OTV hydrostatic bearing tester and is presented along with the finite element analysis and related design iterations. The analyses consist of linear damped critical speed and stability calculations. The final configuration analyzed was found to be acceptable from a rotor dynamic standpoint.

Several design iterations of the bearing tester have been analyzed for critical speeds and rotor dynamic stability. In all, three different rotor material properties were analyzed in combination with numerous bearing configurations. Also, a hollow shaft was partially analyzed. The rotor dynamic analysis of each design iteration is described below. The end results of each analysis are maps of mode damped natural frequency versus running speed and modal damping (log dec) versus running speed. The damped natural frequency maps show what the frequency of each mode is at any given shaft speed. A speed value that has a forward rotor mode with a frequency equal to the speed is a critical speed.

Baseline Analysis: Steel Shaft

The rotor model consists of a uniform beam, 1 inch in diameter broken into 10 finite element cylindrical beam elements, and has 44 degrees of freedom in all. The tester employs a terry turbine as its drive element. The shaft is radially supported by two hydrostatic bearings using liquid hydrogen as the working fluid. Table 4 shows the stiffness, damping and cross-coupled values for these bearings for the various cases analyzed. All values are for a shaft speed of 200,000 RPM. Note that the stability ratio, $K_{xy}/C_{xx} \omega$ (where ω is the angular velocity in radians per second), is 50% for each set of coefficients. This means that any rotor mode with a frequency below 50% of shaft speed will be unstable.

Table 4 - K_{xx} , K_{xy} , and C_{xx} for Various Bearings at 200,000 RPM

Set #	\odot in	Clearance mils	Delta P psi	Length in	K_{xx} lbs/in	K_{xy} lbs/in	C_{xx} lbs-s/in	$K_{xy}/C_{xx}\omega$
1	1.0	1.25	2000	0.4	352380	28279	2.7	50%
2	1.0	1.25	2000	0.8	632379	138785	13.3	50%
3	1.0	1.25	2000	1.2	806732	318265	30.5	50%
4	1.0	1.25	1000	1.2	424557	248229	23.8	50%
5	1.0	1.25	4000	1.2	1494694	407091	39.0	50%
6	1.0	1.25	1000	0.8	332810	108253	10.4	50%
7	1.0	1.25	4000	0.8	1171690	177532	17.0	50%

Figures E-1 and E-2 (Appendix E) show the damped natural frequency and stability maps for this model. Figures E-3 and E-4 show the mode shapes for these two modes along with the bearing locations. (mode shapes indicate relative response amplitudes, not absolute response amplitudes). The first two critical speeds are below 40,000 RPM and each mode appears as two curves which diverge at increasing speed. The lower frequency curve is the backward component of the mode, and is not important. The higher frequency curve is the forward component of the mode. When a forward component frequency equals shaft speed, that speed is a critical speed. The stability map of Figure E-2 shows the log decs for the first two rotor modes. The first mode is shown unstable (log dec <0) at low speeds. The predicted instability of the first mode at low speed is probably not valid as the hydrostatic bearing coefficients are poorly defined at those conditions. The stability of the second mode is acceptable.

This design is unacceptable because of the questionable stability of the first mode, and the potential for resonance of the second mode. Note that the frequency of the second mode very closely parallels the 45 degree line in Figure E-1. This means that the frequency of the mode

will very closely track running speed, thereby creating a near resonant condition over nearly all of the operating range of the tester. That is, the high vibration usually experienced only when passing through a critical speed will persist and be maintained over as much as the entire operating range. This condition must either be avoided altogether by designing away from it, or by taking measures to reduce the response to acceptable levels (precision balance, or high damping).

To improve the rotordynamics of the tester the first step taken was to consider different bearing configurations. Alternate pressure differences were evaluated leading to the conclusion that the maximum available pressure difference of 2000 psi was required. Also, six different sets of bearing axial locations were evaluated. The set shown in Figures E-3 and E-4 provided the most improved rotordynamics. The length of the bearing was also evaluated. For the target application of an OTV turbopump, 0.8 inches was considered the maximum allowable bearing length. For the tester it was shown that the longest bearing possible was needed for its maximum stiffness, and thus 0.8 inches was chosen. Also, an unduly long bearing may be subject to adverse affects from shaft tilt.

Revised Analysis: Hollow Steel Shaft

A hollow steel shaft was considered as a means of raising the critical speeds and enhancing the stability of the tester. The analysis of this configuration was not completed however, as the available manufacturing techniques to fabricate a closed end hollow shaft were considered inadequate to produce a shaft which could satisfy the balancing requirements of this application.

Revised Analysis: Aluminum Shaft

A solid aluminum shaft was considered as a means of raising the critical speeds and enhancing the stability of the tester. Figures E-5 through E-8 show the damped natural frequencies, log decs, and mode shapes for this configuration. In this case the damped natural frequency of the first mode is seen to closely track running speed, and thus is not acceptable.

Revised Analysis: Titanium Shaft

A solid Titanium shaft was considered as a means of raising the critical speeds and enhancing the stability of the tester. Figures E-9 through E-12 show the damped natural frequencies, log decs, and mode shapes for this configuration. This case was deemed acceptable as the margins between operating speed and the damped natural frequencies, combined with the log dec margins against instability, yielded an adequate rotordynamic configuration.

STRUCTURAL ANALYSIS

A stress analysis of the OTV hydrostatic bearing tester has been performed. The radial hydrostatic bearings analyzed are made of Carbon P5N and Kentanium. The structural design criteria is met for all of the tester components except for the Kentanium radial hydrostatic bearings mounted in the Invar housing at the room temperature condition. In the assembled condition, peak stresses at the radial flow holes in the bearings result in safety factors below those required. However, these peak stress occur in a compressive stress field and crack propagation is not expected.

A structural analysis has been performed on the OTV hydrostatic bearing tester. The design criteria used to evaluate the structural integrity of the bearing tester is defined below.

$$(F.S.)_{ult} \geq 1.4$$

$$(F.S.)_{yld} \geq 1.1$$

Two materials were selected for testing of the radial hydrostatic bearings. The selected materials are Carbon P5N and Kentanium in combination with a Titanium shaft. Material properties for Carbon P5N and Kentanium are shown in Table F-1. To achieve adequate bearing stiffness, the hydrostatic bearings were designed to have a specified clearance at steady-state operation. To simulate the OTVE HPFTP, a bearing clearance of 0.0018 to 0.0024 inches (diametral) was required at a shaft operating speed of 200,000 RPM. A bearing feed pressure of 2000 psi, sump pressure of 300 psi, and a bearing exit pressure at the orifice of 1267 psi are predicted for this operating condition. Since the bearing exit pressure varies both in the circumferential and in the axial direction along the inner diameter of the bearing, an equivalent pressure at the inner diameter of the bearing of 842 psi was utilized in all stress calculations.

Prior to operation, the tester is to be chilled with liquid hydrogen. Stress calculations associated with chill and operating conditions were performed using an average tester temperature of -380 degrees F. Reviewing Table F-1, it can be seen that the coefficients of thermal expansion and strength of Carbon P5N are low. Since the inner diameter of the bearing is to be line bored after the bearings are installed into the bearing housing, an interference fit between the bearing and the housing is required at room temperature. With this condition, and the fact that the strength of Carbon P5N is low, a material with a low coefficient of thermal expansion was selected for the bearing housing to allow for an interference fit between the bearing and the housing at room temperature and minimizing the

interference at cryogenic temperatures. The material chosen for the bearing housing material is Invar 36. Material properties of Invar 36 are shown on Table F-1.

Isolation pins, Fig. 24, are installed in the radial bearings to isolate the bearing/housing interface from the 2000 psi bearing inlet pressure. Since Carbon P5N has a low elastic modulus, the pressure at the bearing outer diameter must be low to maintain low stresses in the bearing. With the isolation pins installed, it was assumed that the pressure at the outer diameter of the bearings is equal to the sump pressure, 300 psi. For this design, a uralite sealant on the pins is required at installation to assure that leakage does not occur.

Using the steady-state operating conditions, the required bearing fits and shaft clearances at assembly were determined. Results are shown in Figures F-1 and F-2 for the Carbon P5N and Kentanium bearings, respectively. A summary of the peak stresses in the radial hydrostatic bearings are shown on Table F-2. The calculated stresses account for stress concentration and area reduction factors associated with the bearing feed holes. Reviewing Table F-2, the critical stress in the Carbon P5N and Kentanium bearings occurs when the bearing is press fit into the housing at ambient conditions.

Reviewing Table F-2, peak stresses in the Carbon P5N bearing are -17302 psi (hoop) and 5286 psi (axial). The corresponding factors of safety are 2.02 on compressive ultimate strength and 1.32 on tensile ultimate strength. Although the design factor of 1.4 on ultimate strength is not met for this bearing, this condition must be accepted. Any less fit between the bearing and housing could result in separation of the interface and thus result in a lower bearing stiffness. Since Carbon P5N is a brittle material, a bearing retainer was designed to apply an axial preload to the bearing when it is assembled. The axial preload will prevent the bearing from moving axially in case bearing cracking occurs.

In Table F-2, the peak stresses in the Kentanium bearing are shown to be -227,145 psi (hoop) and 75,638 psi (axial). The corresponding factors of safety are 1.02 on compressive ultimate strength and 3.07 on tensile ultimate strength. For this bearing, the design factor of safety on ultimate strength is not met for the peak compressive stress which occurs at assembly. Since Kentanium has a much higher coefficient of thermal expansion than Invar 36, a tight fit between the bearing and the housing is required at assembly to keep the bearing/housing interface from separating at operation. Since the peak stress occurs at the radial flow holes, the stress away from the holes decreases by a factor of three due to a stress concentration factor applied at the holes. If a crack begins at the holes at assembly, it should not propagate further since the bearing is in compression in the hoop direction.

The remaining tester components, housing, end caps, nozzle, shaft and thrust bearings were reviewed. The components were analyzed for pressure loads, interference fits, thermal loads, and centrifugal loads corresponding to room temperature and steady-state operating conditions. All of the components meet the structural design criteria for these conditions.

Bolt material, size and torque specifications for the tester assembly are shown in Figure F-3. The specified torques provide adequate preload to overcome separating loads and thermal mismatch of the parts.

HYDROSTATIC BEARING MATERIALS EVALUATION

Table 4 lists several materials that were evaluated for use as hydrostatic bearing material for application in the OTVE High Pressure Liquid Hydrogen Turbopump. The table also lists common material properties and four columns are devoted to what are known as thermal shock parameters. These thermal shock ($K_{IC}/E\alpha$ and $K_{ICk}/E\alpha$) parameters were used as the major criteria in this evaluation effort.

The parameters, $K_{IC}/E\alpha$ and $K_{ICk}/E\alpha$ are contrived material constants related to the material resistance factor for thermal stress, ΔT_f . This factor was initially developed by ceramists as a measure of instantaneous temperature difference (generated by a rapid quench) required to initiate fracture through thermal stress:

$$\Delta T_f = (\sigma_f (1 - \nu)) / E\alpha$$

where σ_f is material fracture stress (psi)
 E is Young's modulus (psi)
 ν is Poisson's ratio
 α is linear expansion coefficient (in/in $^{\circ}F$)

It is clear that materials with a high fracture stress and low modulus and expansion coefficient should exhibit high resistance to thermal shock. For more moderate rates of heat transfer it can be shown that:

$$\Delta T_f \propto (k \sigma_f (1 - \nu)) / E\alpha$$

where k is the thermal conductivity of the material.

The consideration of this factor in ranking tribological materials reflects the quasi-adiabatic nature of heat generation on highly loaded transient sliding contacts. Heat is generated at a rate equal to μPV per unit area where μ is the coefficient of friction, P is the contact stress and V the sliding speed. If PV is high, very steep temperature gradients are required to conduct heat away from the interface. In materials used in rubbing contact seal applications, for example, this is usually the performance limiting factor with material failure taking the form of surface cracking and spalling ("heat checking"). Where the "PV limit" for a particular material is known, its value is rated in the last column of Table 5. It should be noted that this

Table 5 - Hydrostatic Bearing Material Candidates

OTV: HYDROSTATIC BEARING MATERIAL CANDIDATES										
MATERIAL	NAME AND MANUFACTURER	E psi x 10 ⁶	α in/in°F	σ bend ₂ ksi	σ comp ksi	$\frac{k}{Btu/ft/}$ hr/°F	$\frac{K_{IC}}{ksi\sqrt{in}}$	$\frac{K_{IC}}{E \alpha}$ °F \sqrt{in}	$\frac{K_{IC}^k}{E \alpha}$ Btu \sqrt{in} ft hr	PV psi-ft/min
Carbon- Graphite	P-5N Pure Carbon	3.0	2.4 E-6	12.5	40	~5	1.8	250	1250	500,000
SiC	PS-9242 Pure Carbon	53.0	2.5 E-6	55 (4) 68 (3)	400	85	3	23	1925	500,000
PSZ	Nilsen	29.7	5.0 E-6	94 (3)	175	1.27	~8	54	68	
Si ₃ N ₄	NC-132 Norton	45.0	1.9 E-6	~150 (3)		18.5	~5	58	1080	
WC + Ni	K801 Kennametal	89.6	1.8 E-6	315 (3)	690	47.4	3	18	870	
Polyimide	Vespe1 SP211 DuPont	0.2	30 E-6	10.0	--	.44	--	--	--	100,000
TiC + Ni/Mo	K162B (Kennatium) Kennametal	59.0	4.1 E-6	235 (3)	610	11.1	9.6	77	860	
Carbon- Carbon	S.A.I.C.1	18.6	1.5 E-6	45	--	18	3.1	114	2106	

NOTES: 1 Scientific Applications International Corporation
2 Number in parentheses indicates 3- or 4-point bend test

is a system rather than a material property and as such is dependent on the application environment.

In its original form the material resistance factor for thermal stress was based on crack initiation. Since material failure only occurs following crack propagation, this criterion can be misleading. For non-homogeneous materials, a crack can be stopped by a discontinuity such as a pore or a second phase particle. This consideration has led more recently to the informal substitution of the fracture toughness K_{IC} for the fracture stress σ_f . In either form it should be noted that a clear and well established correlation between the thermal shock parameter and tribological performance has yet to be demonstrated. In these circumstances it should be used as guide to selection rather than a design parameter.

On this basis alone, SiC, would appear the most attractive candidate. Despite the fact that this material has been used successfully in some rubbing seal applications, the low expansion coefficient and brittle nature (low K_{IC}) of this material would present problems in applications having a wide operational temperature range. K162B has a more moderate thermal shock performance, but it does possess the highest expansion and toughness characteristics of the five wear resistance ceramic/cermet candidates. As such, it presents the most attractive candidate in this sub-group.

P5N has a high thermal shock parameter, probably the lowest friction coefficient of all the candidates, and a well established record, although sufficient mounting problems associated with the low coefficient of thermal expansion do exist.

Although the polyimide material has been used in some low speed/low stress cryogenic applications and possesses an attractive PV limit, its wear resistance needs to be evaluated for this application before a recommendation can be made. Evaluation of the material on the basis of thermal shock is inappropriate since the damage mechanism at high PV is softening/melting followed by excessive abrasive wear.

While the carbon-carbon materials have a great deal of potential, significant development is still required for tribological applications. Currently, costs appear to be prohibitive due to the high costs associated with engineering, manual lay-up and impregnation required for custom fabrication

TESTER FABRICATION AND ASSEMBLY

The fabrication of the majority of the tester components proved to be easily accomplished due to the simple design. Some complicated machining was required on the housing and nozzle but was accomplished without difficulty.

The shaft required some additional attention because of the tight tolerances required to insure good balance and fit up with the bearings. In addition, the shaft was ion implanted with nitrogen in the bearing areas for wear resistance, copper plated for eddy current instrumentation, Tiodized for optical target generation for fiberoptic instrumentation, and radioactively activated in the bearing areas for isotope wear detection.

All of the tester components are completely fabricated and are shown in Figures 24 through 28. Some partial assembly can be seen in Figures 25 and 27.

Figure 24 - Tester Components

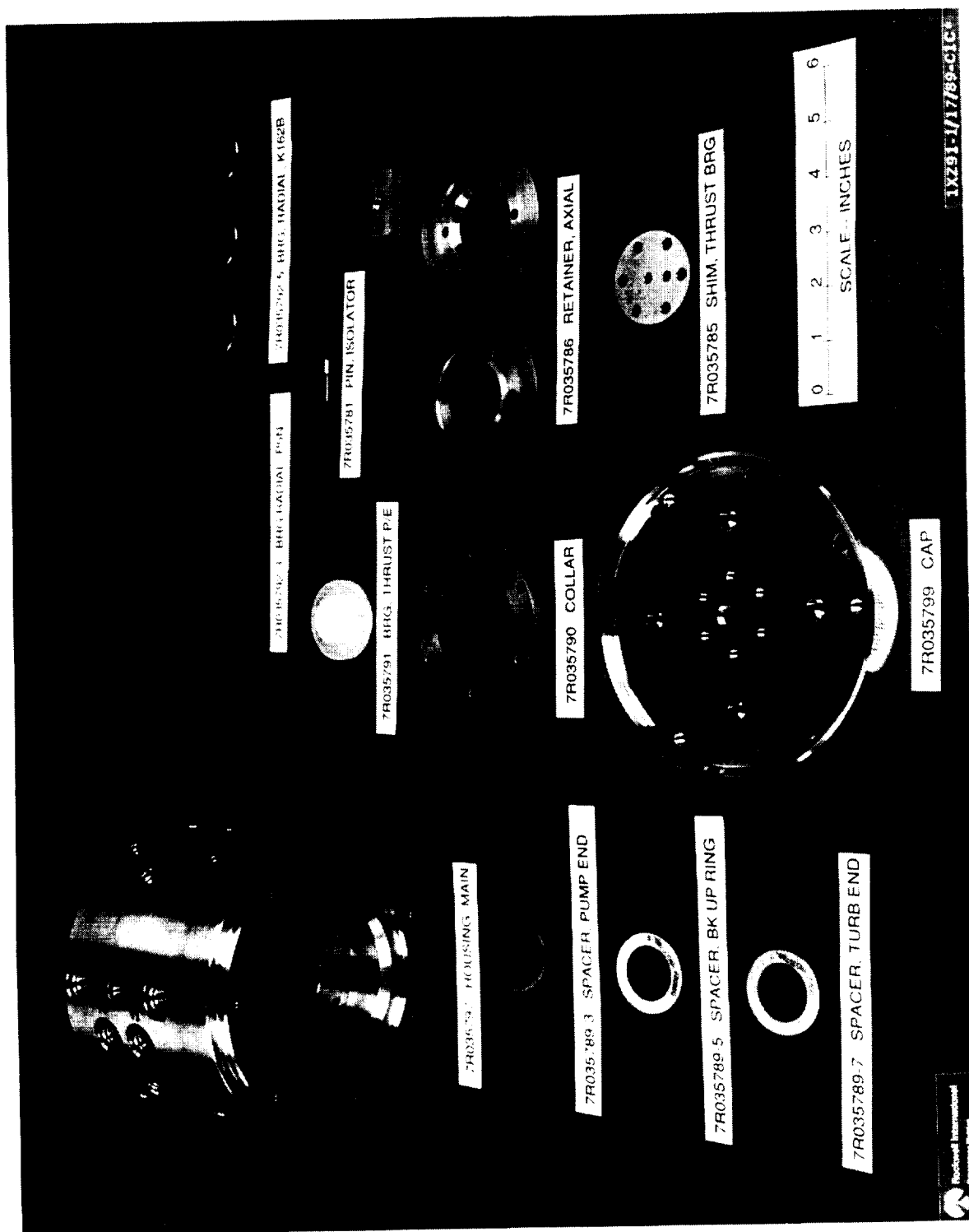


Figure 25 - Tester Nozzle and Baseplate

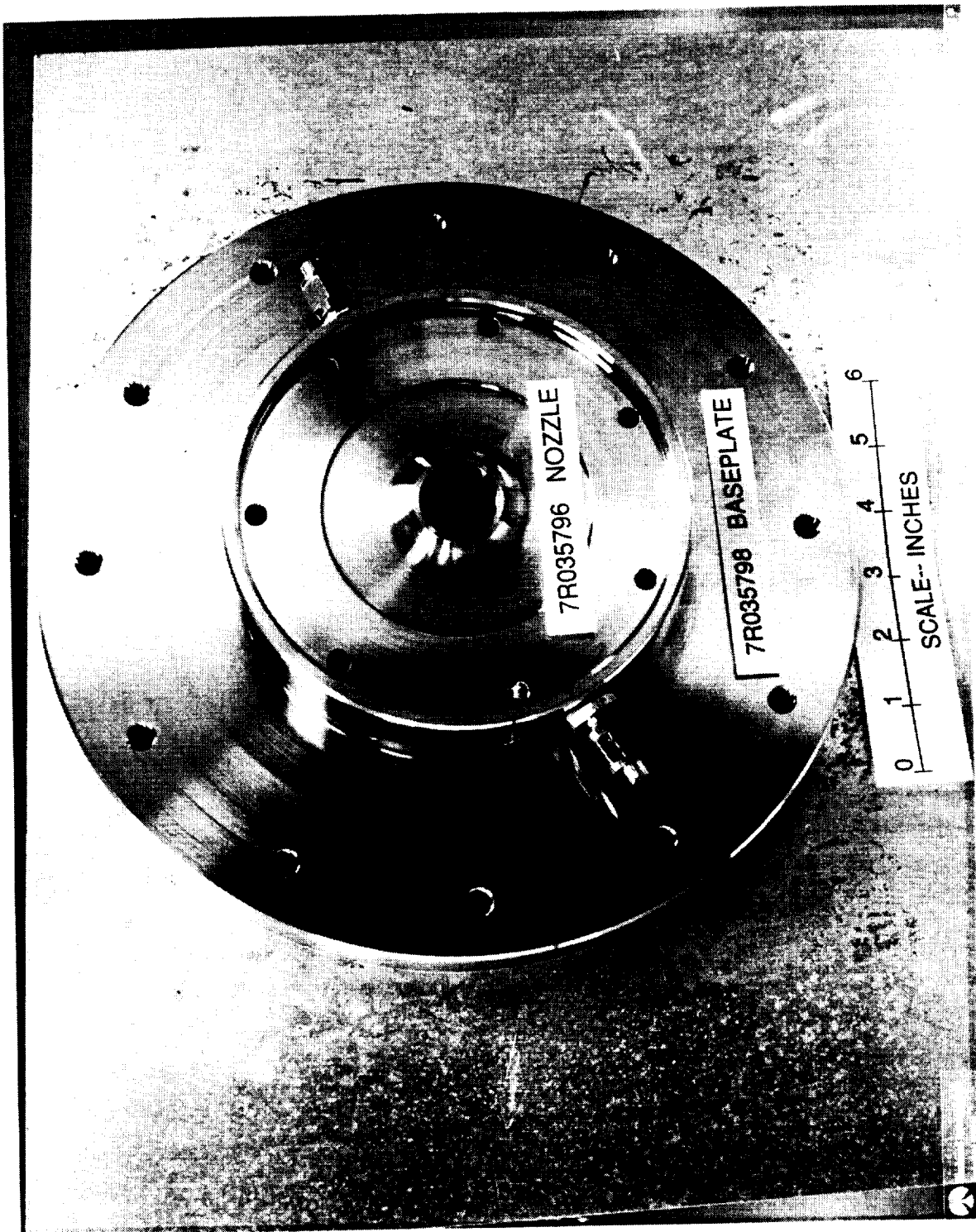
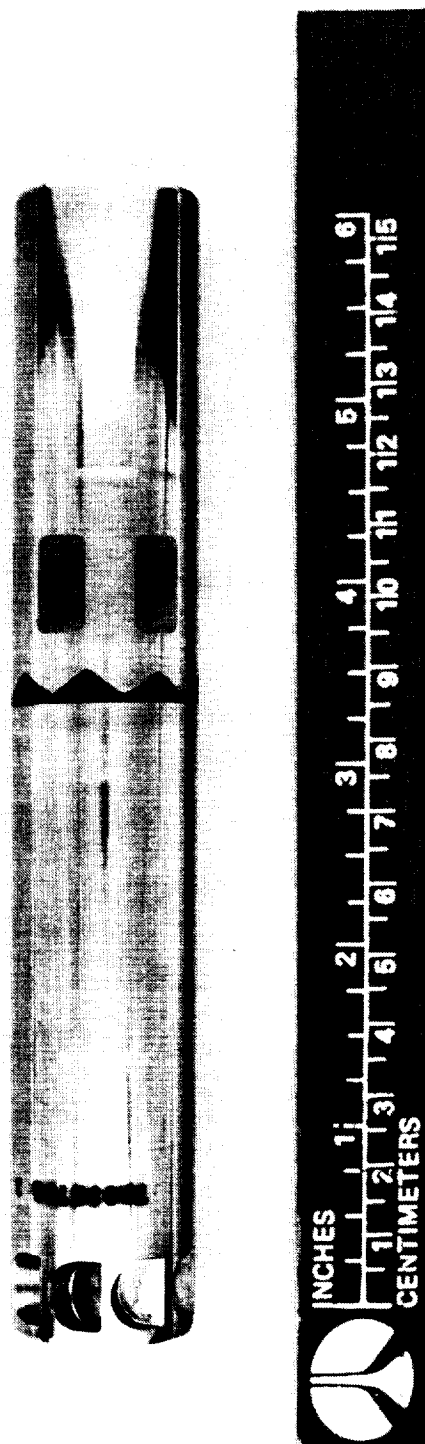


Figure 26 - Tester Shaft



ORIGINAL PAGE
BLACK AND WHITE PHOTOGRAPH

Figure 27 - Tester Baseplate

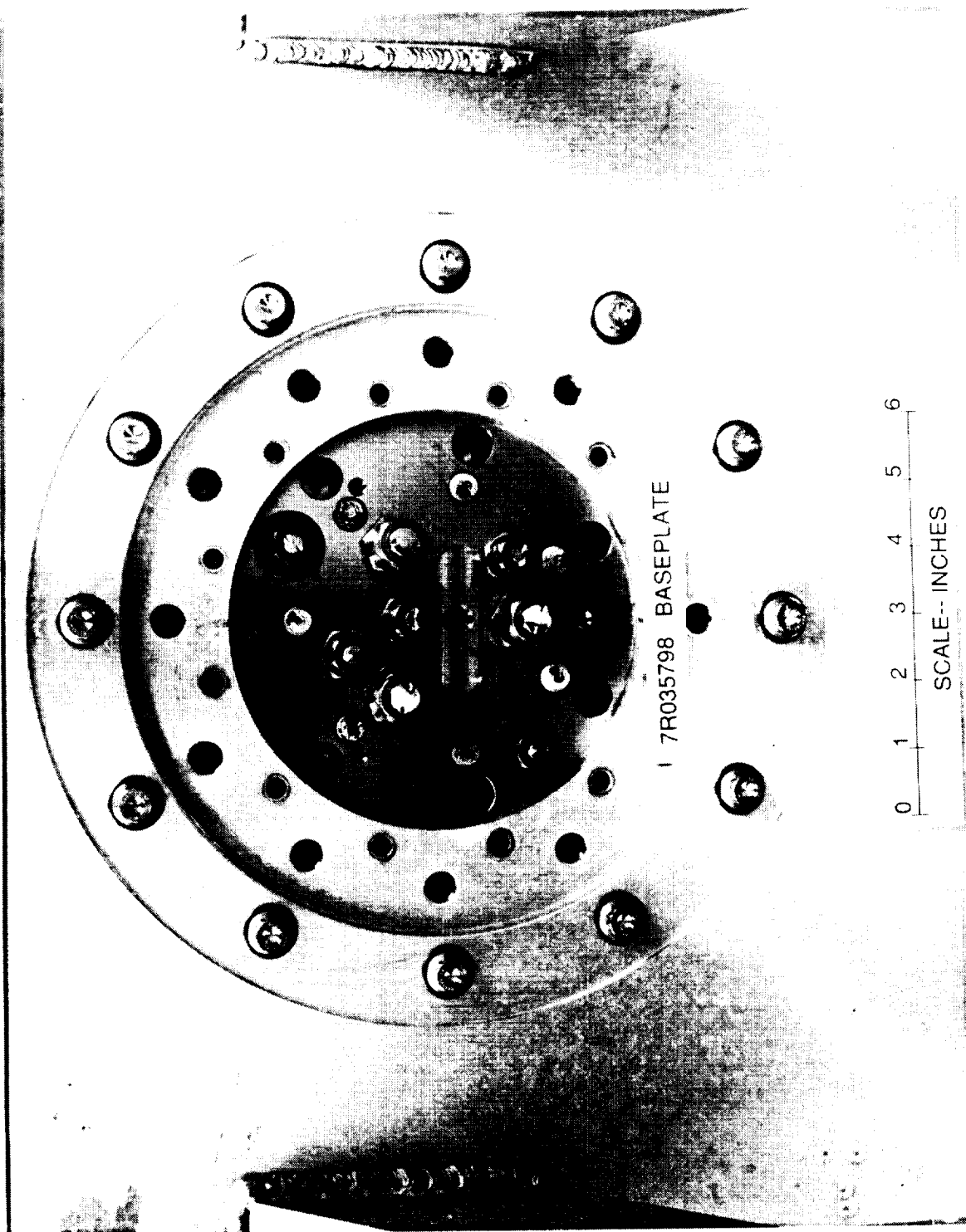
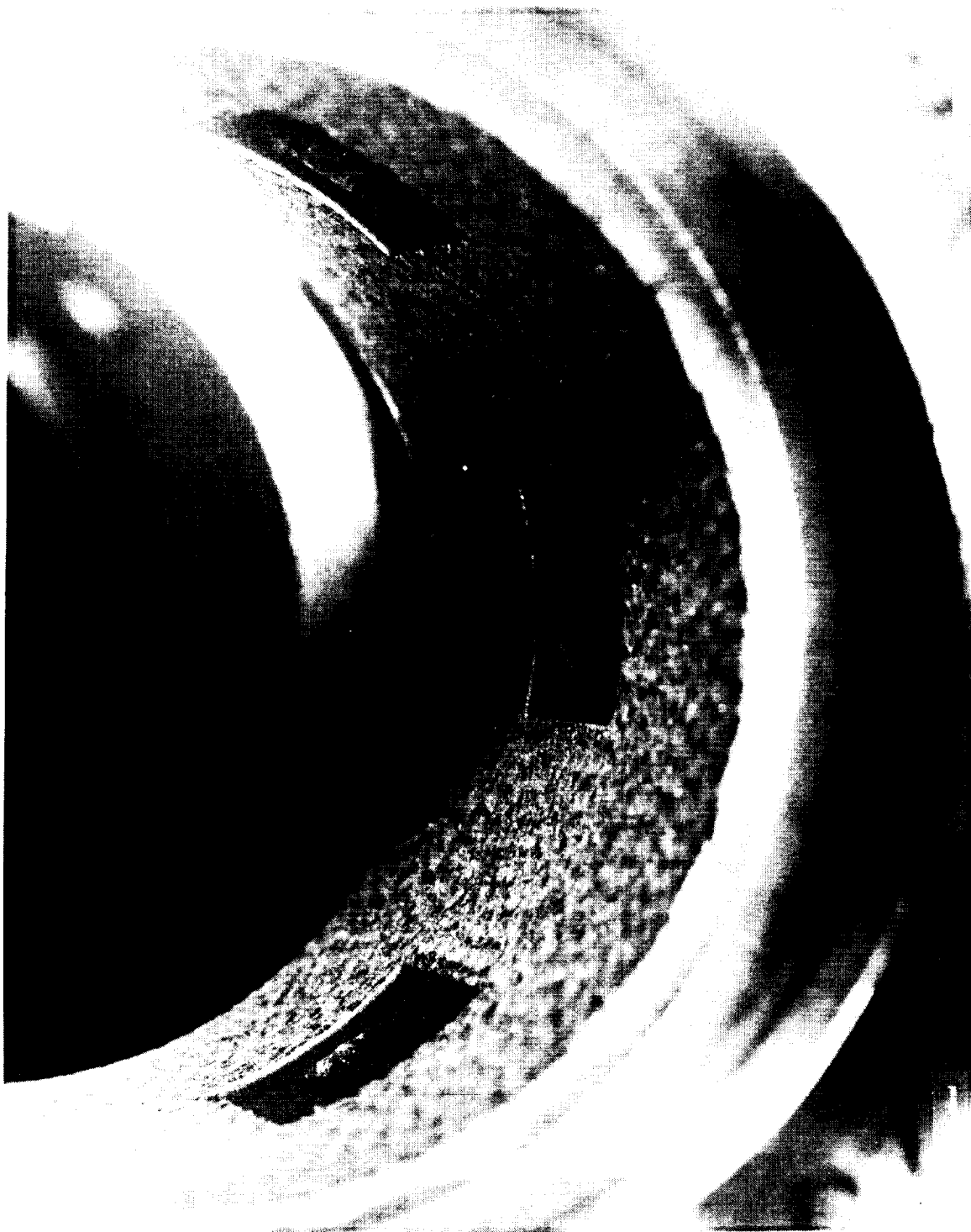


Figure 28 - Radial Bearing Inner View



ORIGINAL PAGE
BLACK AND WHITE PHOTOGRAPH

INSTRUMENTATION

Tester instrumentation is fully described in the OTVE Hydrostatic Bearing Tester Test Plan that is included as Appendix G.

Additional effort has been applied in the area of shaft position monitoring. Shaft orbit, axial position, and speed, have traditionally been measured using eddy current probes. Indeed, this tester includes six Bently eddy current probes designated to monitor shaft position. Measuring speed with an eddy current probe requires that a shaft surface interruption is in place so that the magnetic field of the eddy current probe is changed as the shaft revolves. Traditionally, this has been accomplished with "glitches", which are shallow, 0.005 inches, depressions in the shaft surface that change the magnetic field of the eddy current probe.

The high shaft speeds required for this tester cause two concerns with respect to "glitches." First, a single glitch will cause shaft unbalance that must be compensated for and secondly, at these high surface speeds some possibility exists that pumping and cavitation may occur. A pumping load may prevent reaching 200,000 RPM and cavitation damage could induce shaft imbalance.

These concerns have resulted in development of a copper plating procedure for Titanium. It has been demonstrated at the laboratory level that the eddy current probes will respond to a thin, 0.001 inch, interrupted layer of copper plate. This work is described in the OTVE Turbopump Condition Monitoring Final Report which was written under the OTV E-5 task. The shaft has been prepared with depressions on the outside diameter and one axial face, and these have been filled with copper plate. This will allow the use of eddy current probes to measure shaft RPM without the concerns caused by the unfilled surface depressions. The copper plating procedure is found in Appendix H.

In addition, a fiberoptic measuring method has been developed and demonstrated in the laboratory that will monitor shaft orbit, axial position, and speed while using only two fiberoptic probes. This work is also described in the aforementioned report. Provisions have been made to incorporate these fiberoptic measurement probes into this tester as backup to the eddy current probes. The eddy current probe and fiberoptic probe locations are specified in Figure 23.

Bearing and shaft surface wear rates will be monitored by geometric measurements and by radioactive isotope techniques. The surface of the shaft in the bearing areas will be activated to produce radioactivity that can be measured with time to determine if surface material has worn away and been removed from the site.

Bearing fluid flow rates will be measured by test facility instrumentation as described in the Hydrostatic Bearing Tester Test Plan found in Appendix G.

CONCLUSION

The imposed turbopump speed, load, cryogenic requirements, and the engine life and duty cycle of the OTV, motivated the selection of the hydrostatic bearings as the prime bearing candidate for this engine. Several materials were evaluated for the hydrostatic bearings of which the Carbon P-5N was chosen as the most promising for the high speed conditions.

The tester that was fabricated and assembled in this program, included a titanium rotor for high speed operation. This rotor was impregnated with copper plated surfaces in the shaft end and circumference for accurate measurements of speed and angular shaft position. These copper detectors allowed the elimination of the existing Bently speed measurement limitation of approximately 100,000 rpm. Currently both the Bently and the copper detectors are being used in the tester. Tiodize patterns were incorporated as fiber optic targets around the circumference of the shaft for accurate measurements of speed and axial shaft position. The titanium rotor was balanced to 0.01 gram/inches.

Funding limitations did not allow for any testing during this contractual effort. Rocketdyne funded and accomplished the testing under IR&D during fiscal years 1990 and 1991, consequent to this program. The test results have been documented in Rocketdyne IR&D technical reports entitled "Demonstration of Dual Rotor Supports" (Task 61152, Project 907.1) and "Small Bearing Technology Development" (Task 61894, Project 918.9).

It is recommended that this hydrostatic bearing tester be employed as a work-horse tester for other types of bearing and seal testing, such as foil bearings, hybrid bearings, and brush seals.

REFERENCES

- Aerojet Corp., 1965, "Hydrostatic Bearing Feasibility Program", Report AFRPL-TR-65-120
- Butner, M. and Murphy, B. T., 1986, "SSME Long-Life Bearings", NASA CR179455.
- Chaomleffel, J.P., 1983, "Influence des forces d'inerties en lubrification hybride", Doctoral dissertation, I.N.S.A. Lyon.
- Heller, S., 1974, "Static and Dynamic Performance of Externally Pressurized Fluid Film Journal Bearings in the Turbulent Regime", *ASEM J. of Lubrication Technology*, Vol. 96, July, pp. 381-390.
- Ho, Y. S. and Chen, N.N.S., 1980, "Dynamic Characteristic of a Hydrostatic Journal Bearing", *Wear*, Vol. 63, pp. 13-24.
- Ho, Y. S. and Chen, N.N.S., 1984, "Pressure Distribution in a Six-Pocket Hydrostatic Journal Bearing", *Wear*, Vol. 98, pp. 89-100.
- Mullan, P.J. and Richardson, H.H., 1964, "Plane Vibration of the Inherently Compensated Gas Journal Bearings; Analysis and Comparison with Experiment", *ASLE Trans.*, Vol. 7, pp. 277-287.
- Pratt and Whitney Corp., 1967, "Investigation of Hydrostatic Bearing for Use in High Pressure Cryogenic Turbopumps", Report AFRPL-TR-67-130.
- Rocketdyne, Rockwell Int., 1992, "Test Results of the RS-44 Integrated Component Evaluator Liquid Oxygen/Hydrogen Rocket Engine", RI/RD 92-127
- Raimondi, A.A. and Boyd, J., 1957, "An Analysis of Orifice & Capillary Compensated Hydrostatic Journal Bearings", *J. Lubr. Engr.*, Jan., pp. 28-37.
- Spica, P.W., Hannum, N.P., and Meyer, S.D., 1986, "Evaluation of a Hybrid Hydrostaic Bearing for Cryogenic Turbopump Application", NASA TM 87255.
- Yoshimoto, S. and Nakano, Y., 1984, "Stability of a Rigid Rotor Supported by Externally Pressurized Gas Journal Bearings with a Circular Slot Restrictor", *Bull. JSME*, Vol. 27, No. 225, March, pp. 561-568.
- Yoshimoto, S., Nakano, Y. and Kakubari, T., 1984, "Static Characteristics of Externally Pressurized Gas Journal Bearings with a Circular Slot Restrictor", *Tribology International*, Vol. 17, No. 4, August, pp. 199-203.
- Yoshimoto, S., 1988, "Static Characteristics of a Slot-Entry Gas Journal Bearing with Feeding Holes", ASME Paper No. 88-Trib-14.

APPENDIX A

OTV TESTER COASTDOWN STUDY

In generating the Hydrostatic Bearing Tester Test Plan, it was important to estimate the liquid hydrogen usage for one cycle of the tests. One cycle consists of a start, accelerate to 200,000 rpm, dwell for one second, and decelerate to stop.

A study was carried out to determine the time for the test shaft to coastdown to a stop during one cycle of operation and the resulting total leakage for one cycle. This was done using the following equation of motion:

$$\Sigma T = I \ddot{\theta} \quad (\text{Equation A.1})$$

where T is the torque on the shaft, I is the moment of inertia of the shaft, and $\ddot{\theta}$ is the angular acceleration of the shaft. The torque on the shaft consists of the torque from the two hydrostatic bearings and the reversing torque from the turbine. The reversing turbine torque was assumed unknown, later estimated at 15% of forward torque. Therefore it becomes an independent variable. The hydrostatic bearing torque is known from calculations and can be expressed as an exponential function of speed.

$$T_b = a \dot{\theta}^b \quad (\text{Equation A.2})$$

Substituting equation A.2 into equation A.1 yields a simple first order differential equation in shaft speed, ω , where $\omega = \dot{\theta}$. The values for a and b are determined from a curve fit of analysis results from the HBEAR code developed from the Theory of Artiles et al (1982). This equation was numerically integrated using standard numerical techniques for various values of turbine torque. The leakage and stiffness of the bearing, which can also be expressed as an exponential function of speed, were calculated at each time step. When the load capacity of the bearings became less than the weight of the shaft and the applied load from the radial loader, coastdown was complete. The calculated leakage function could then be integrated to yield total hydrostatic bearing leakage. The leakage from the axial thrust bearing and the radial loader were assumed to be speed independent. Therefore, total leakage was calculated by multiplying the leakage from the radial loader and thrust bearing by the total coastdown time and adding it to the integrated leakage total of the hydrostatic bearings. Several cases of turbine torque were run; one with a constant torque value and one with a speed dependent turbine torque which was assumed to be a multiple of the hydrostatic bearing torque. The results from the constant

torque cases are given in Figures A-1 thru A-4. Figures A-1 and A-2 show the coastdown time as a function of torque. Figure A-1 is for a turbine torque range of 1 to 5 and Figure A-2 is for a range of 0.1 thru 1.0. As expected, the more turbine torque, the faster the shaft stops. Figures A-3 and A-4 show the corresponding data for the total leakage mass as a function of torque for the same two torque range cases. The results of the variable torque cases are shown in Figures A-5 and A-6. Figure A-5 shows the coastdown time for turbine torques which are 0 to 10 multiples of the hydrostatic bearing torque. Figure A-6 shows the corresponding plot for the leakage mass.

Figure A-1 - Turbine Torque vs Coastdown Time (Range: 1 to 5 in-lbf)

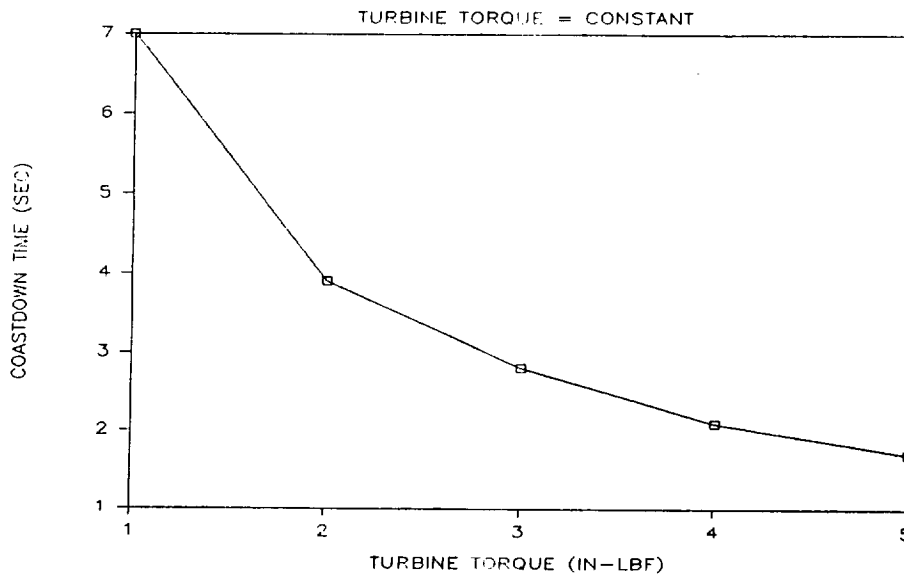


Figure A-2 - Turbine Torque vs Coastdown Time (Range: 0.1 to 1 in-lbf)

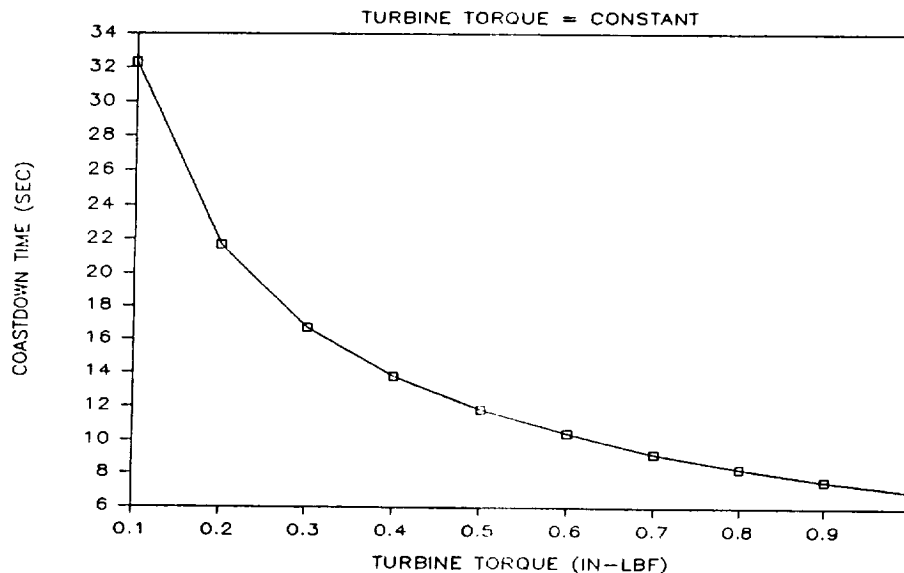


Figure A-3 - Turbine Torque vs Leakage Mass (Range: 1 to 5 in-lbf)

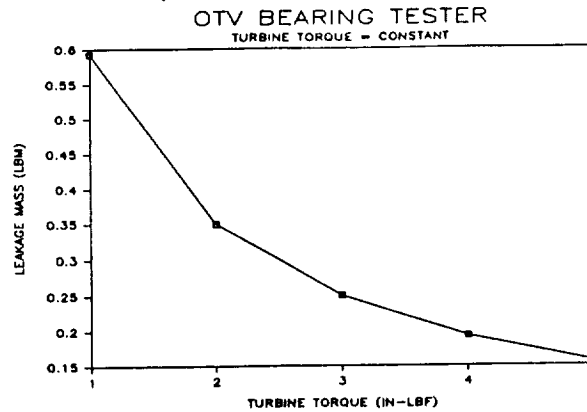


Figure A-4 - Turbine Torque vs Leakage Mass (Range: 0.1 to 1 in-lbf)

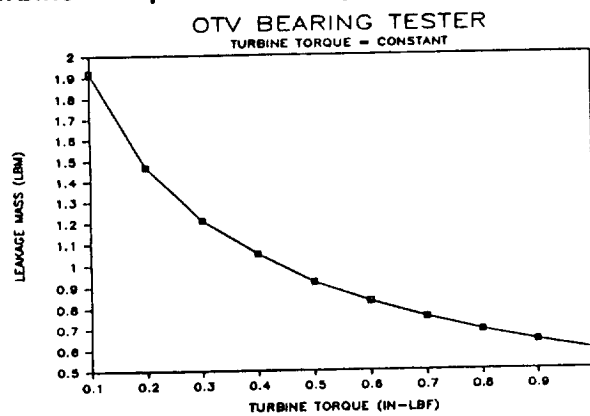


Figure A-5 - Speed vs Coastdown Time

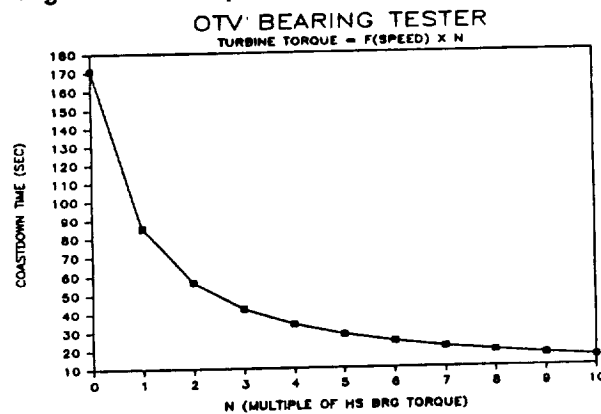
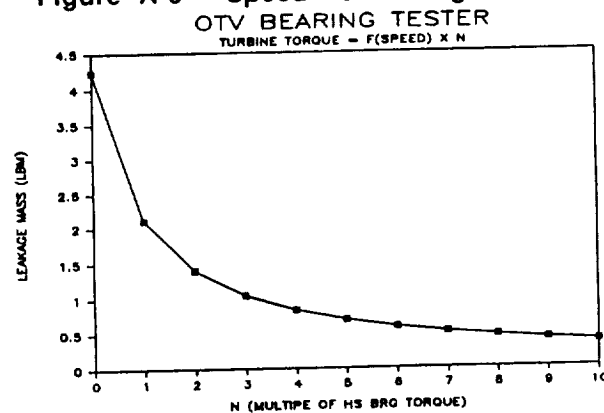


Figure A-6 - Speed vs Leakage Mass



APPENDIX B

OTV AXIAL THRUST BEARING DESIGN

There are many references in the open literature for the analysis of axial thrust bearings. However, all the references neglect the effects of centrifugal inertia. At 200,000 rpm, the effects of centrifugal inertia become very important. Therefore an analysis and computer program were developed to handle this problem. The equation of motion for a single recess thrust bearing is:

$$\frac{dP}{dr} = - \frac{6 m \mu}{\pi \rho r h^3} + \frac{3 r \pi \rho \omega^2}{10}$$

where,

- P is pressure (psi)
- h is clearance (inches)
- r is radial coordinate (in)
- m is flow rate (lb_m/sec)
- μ is viscosity (lb_m/ft-s)
- ρ is density (lb_m/ft³)
- ω is shaft speed (rad/s)

Equation 1 can be integrated to yield the pressure distribution. The solution algorithm requires that the mass flow rate, m, be iterated until the pressure boundary conditions are met. The pressure distribution can then be integrated to yield the load capacity of the bearing. The thrust bearing design requirement was to support 20 lb at a 0.005 inch clearance. To meet the load capacity requirement and avoid any potential instability problems, an orifice compensated bearing was chosen. The bearing recess diameter was iterated until this requirement was met. For liquid hydrogen, this resulted in a recess diameter of 0.36 inches. For gaseous hydrogen the requirement cannot be met. Other types of thrust bearing designs were investigated such as the four sector pad design, however, they did not prove to be effective for this application.

The recess depth for the axial thrust bearing was evaluated using the previously described method for journal bearings. The analysis yielded the following recess depth limits:

$$0.0055 \text{ inches} < \text{depth} < 0.0095 \text{ inches}$$

The natural frequency of the axial thrust bearing system was evaluated using design curves from MTI Gas Bearing Design Handbook and course notes, for undamped natural frequency for the thrust bearing system of 32 Hz. For a nine bucket turbine, this frequency would be excited at 212 RPM.

The final thrust bearing design is as follows:

Orifice diameter = 0.050 in.

Orifice length = 0.10 in.

Recess diameter = 0.36 in.

Operating clearance = 0.002 in.

Recess depth = 0.0055-0.0095 in.

Supply pressure = 2000 psi

Recess pressure = 375 psi

Estimated leakage = 0.075 lb_m/s

APPENDIX C

RADIAL LOAD DEVICE

A noncontacting radial loading device was needed to simulate the effects of side load on the bearings. This shaft radial loading device consists of a single hydrostatic bearing pad machined in the side of the invar housing and maintained in close proximity of the shaft surface. The device is to apply a shaft side load varying with shaft speed squared from 0 to 30 lbs while being supplied with pressure that varied with shaft speed squared from 0 to 864 psi. The previously described hydrostatic bearing analysis code was used to analyze the design. The geometry chosen for the pad was based on previous design experience. The geometry description was:

Number of recesses = 1
 Recess Dimensions = 0.34 by 0.34 in.
 Pad axial length = 0.6 in.
 Pad circumferential length = 0.45 in.
 Radius of loader = 1.0 in.

The effects of radial clearance and orifice diameter on the leakage and load capacity of the loader were investigated. The results were as follows:

CLEARANCE (IN)	ORIFICE DIAMETER (IN)	LEAKAGE (LBM/S)	LOAD (LBF)
0.001	No ΔP	18.74	65.2
0.001	0.025	3.21	19.4
0.001	0.030	4.13	26.2
0.002	No ΔP	24.91	36.6
0.002	0.030	5.25	6.50
0.002	0.040	8.46	12.7
0.003	No ΔP	31.08	27.9

Based on this information, the uncompensated (no pressure drop across the orifice) pad with the 0.002 in. radial clearance was selected.

APPENDIX D

THERMAL ANALYSIS

A thermal analysis was performed on the OTV bearing tester. No thermal problems were identified.

The first analysis was to determine the amount of heat which would be lost from the bearing tester through polyurethane insulation. The dimensions of the tester were taken to be a cylinder 6 inches in diameter and 10 inches long. A parametric analysis was performed to determine the amount of heat lost as a function of insulation thickness, and calculate how much of a temperature rise the hydrogen flow would have based on an assumed hydrogen flow rate of 0.2 lb/sec. The calculation was based upon the assumption that the outside surface temperature of the insulation was at ambient and the inside surface temperature was at liquid hydrogen temperature. The following equation was employed to conduct this calculation:

$$\text{Total Heat Rate} = \text{Heat Rate Through End} + \text{Heat Rate Through Cylindrical Insulator}$$

or

$$Q_{\text{TOTAL}} = 2 \pi k \Delta T ([L / \ln (r_o/r_i)] + [D^2 / (4 \Delta X)])$$

where,

L = length of tester (ft)

ΔT = temperature drop across the insulation ($^{\circ}\text{F}$)

r_o = outside radius of insulator (ft)

r_i = inside radius of insulator (ft)

k = thermal conductivity (Btu/ft/hr/ $^{\circ}\text{F}$)

The results that were obtained using the above equation are summarized below:

Insulation Outside Radius, In.	4	5	6	7	8
Insulation Thickness, In.	1	2	3	4	5
Insulation Energy Loss, Btu/Hr	150.5	82.83	59.95	48.34	41.30
Temperature Rise of Hydrogen Flow, $^{\circ}\text{F}$	0.123	0.070	0.050	0.040	0.030

Next, a calculation was made to determine the heat transfer through the shaft. For the calculation, the temperature difference through the shaft (ΔT) was assumed the maximum possible, ie 480 °F. The shaft is one inch in diameter so that the area (A) is 0.785 in². The distance from the terry turbine to the first bearing (L) is 1.2 inches. The heat flow down the shaft is calculated (assuming the thermal conductivity, k, of the shaft at 11 Btu/ft/hr/°F) to be 288 Btu/hr using the following equation:

$$Q = (A k \Delta T) / L$$

If the flow, W, of liquid hydrogen is 0.1 lb_m/sec, a temperature rise of 0.5 °F is calculated using the following equation:

$$\Delta T = Q / (W C_p)$$

where C_p = specific heat at constant pressure (Btu/lb_m/°F).

The temperature rise in the near bearing of one half degree should not be of concern.

Another analysis was performed to calculate the energy into the hydrogen produced by the turbine shaft viscous shear force in the hydrogen. The calculation was performed using the equation:

$$E = T \omega \pi^2 D^2 L$$

and

$$T = \mu \omega (\pi D / g)$$

where Viscosity, $\mu = 3.2 \times 10^{-5} \text{ N}\cdot\text{s}/\text{m}^2 = 2.15 \times 10^{-5} \text{ lb}_m/\text{ft}\cdot\text{s}$

Shaft Speed = ω (rad/s)

Shaft Diameter = D (ft)

Shear Stress = T (lb_f/ft²)

Bearing Length = L (ft)

Energy = E (Btu/s)

Gap = g (ft)

The energy into the hydrogen produced by the turbine shaft viscous shear was calculated to be 0.685 Btu/Sec. This energy will not produce a measurable increase in the hydrogen flow temperature. The mass of the tester was estimated by considering it as a solid cylindrical metal and was determined to be 82 lbs. The amount of energy needed to reduce this mass from room temperature to liquid hydrogen temperature was calculated to be 4420 BTUs using the following equation:

$$E = (\text{Mass}) (\text{Specific Heat}) (T_{\text{initial}} - T_{\text{final}})$$

where Specific Heat = 0.11 Btu/ (lb_m °F)

$$T_{\text{initial}} = 70 \text{ °F}$$

$$T_{\text{final}} = -420 \text{ °F}$$

For a tester temperature reduction to liquid nitrogen temperature (-320.5 °F), the energy was determined to be 3521 Btu's. The amount of nitrogen needed to be boiled to absorb this energy by the heat of vaporization, H_v , was calculated to be 18 lbs. The equation employed to conduct this calculation is:

$$M \text{ of } N_2 = E / H_v \text{ of } N_2$$

where $H_v \text{ of } N_2 = 198 \text{ Btu/lb.}$

The duration to cool the tester to -320 °F was determined to be approximately 20 minutes for the 18 lbs of nitrogen calculated. The tester temperature measurements have been reviewed and found to be adequate.

APPENDIX E

ROTORDYNAMIC ANALYSIS

**Figure E-1 - Rotor Spin Speed vs Damped Natural Frequency
(Hydrostatic Bearings & Laby Seal)**

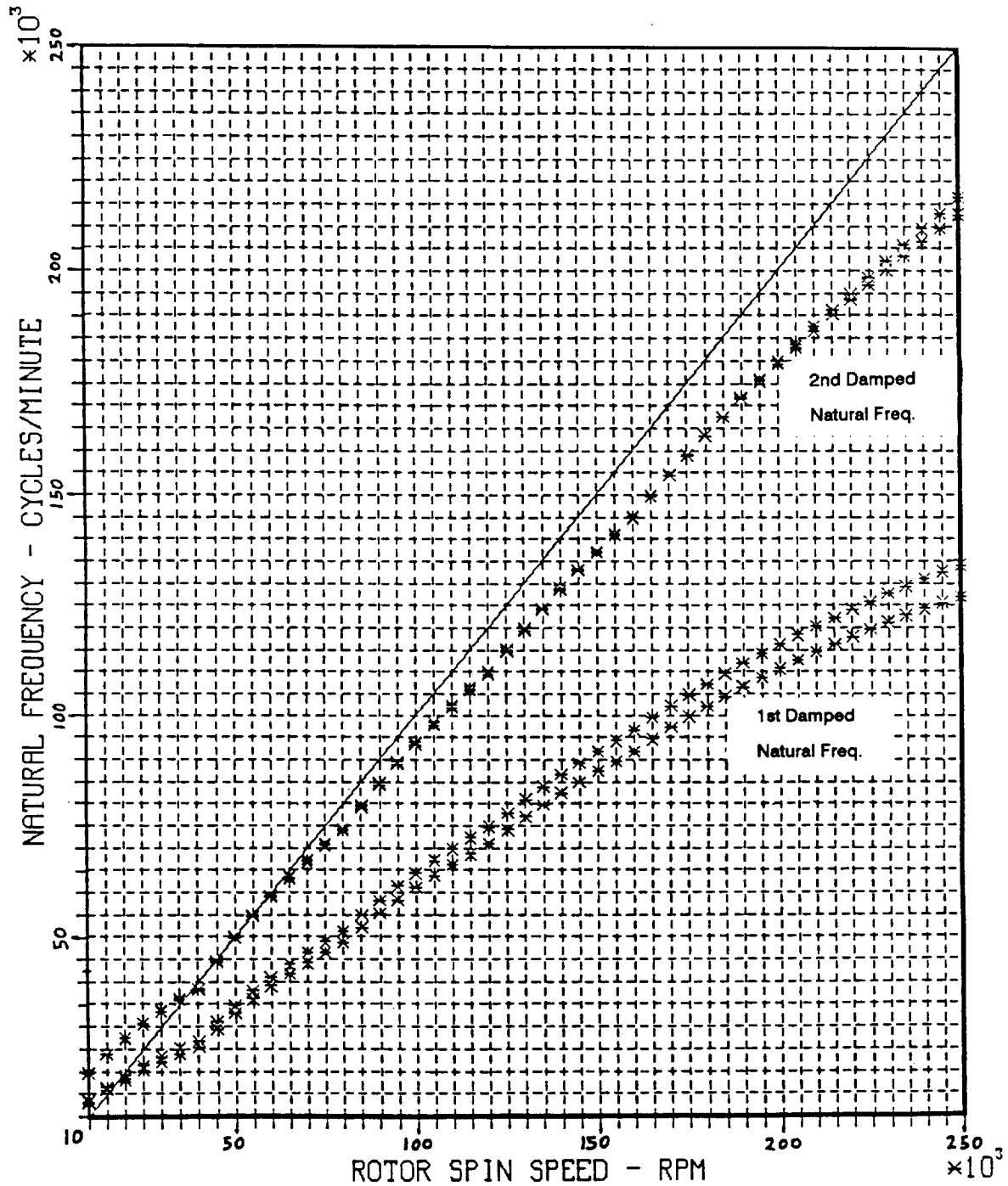
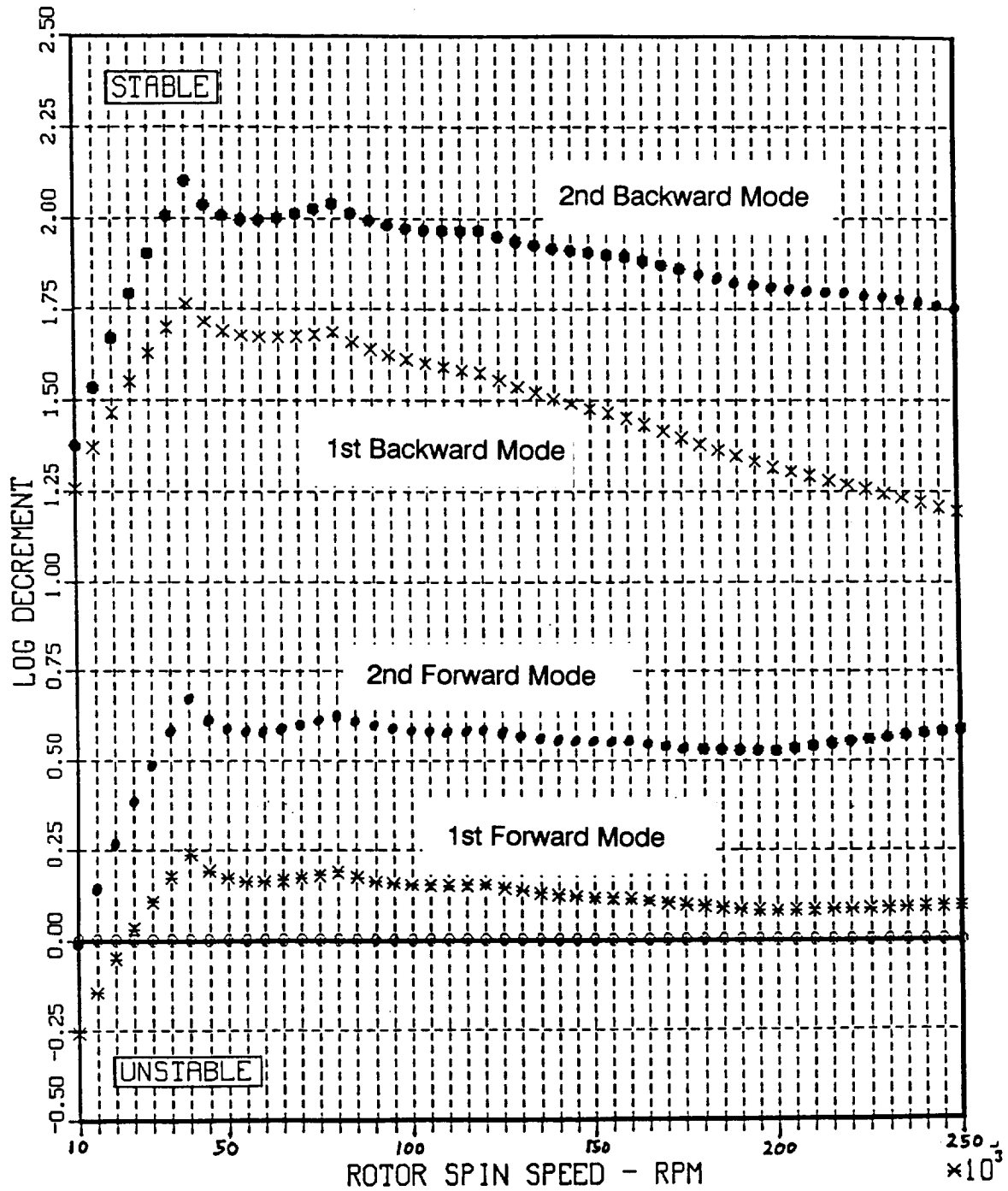
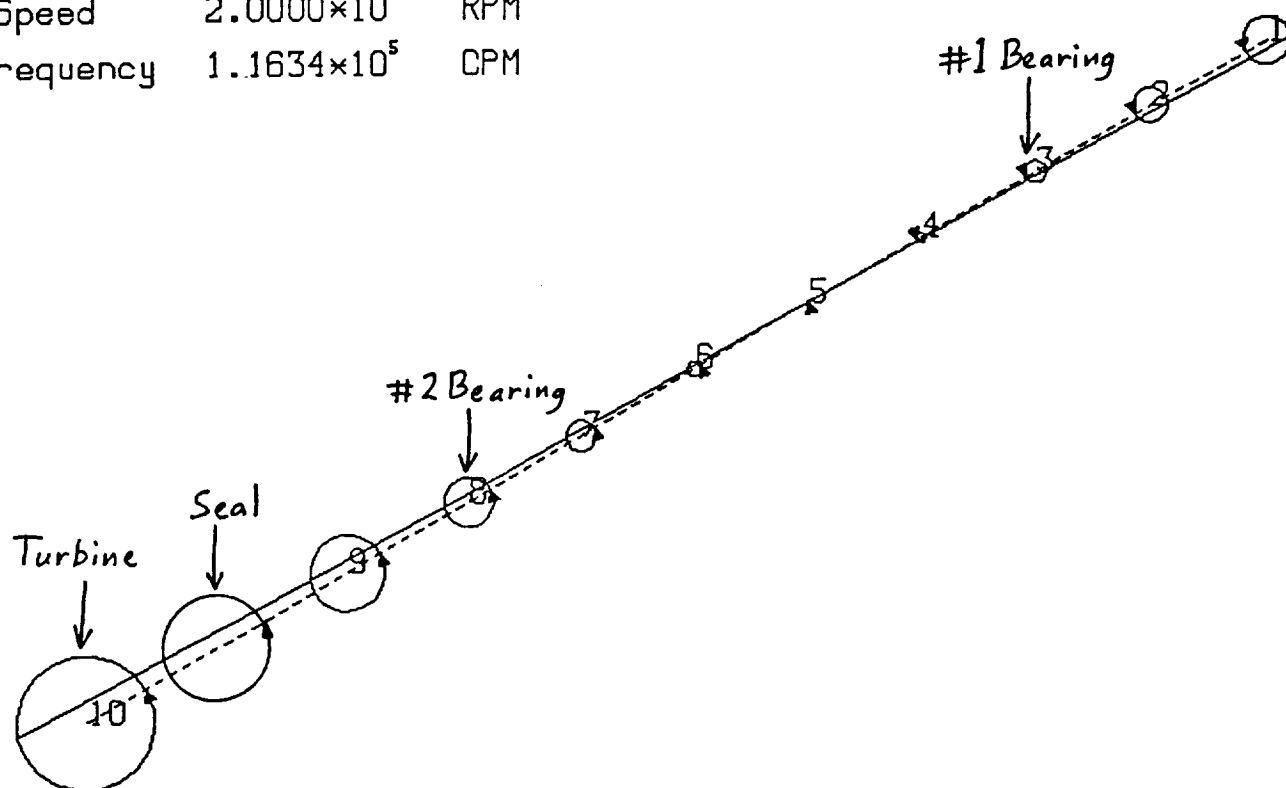


Figure E-2 - Rotor Spin Speed vs Log Decrement
(Hydrostatic Bearings & Laby Seal)



**Figure E-3 - First Critical Rotor Group Mode Shape
(Hydrostatic Bearings & Laby Seal)**

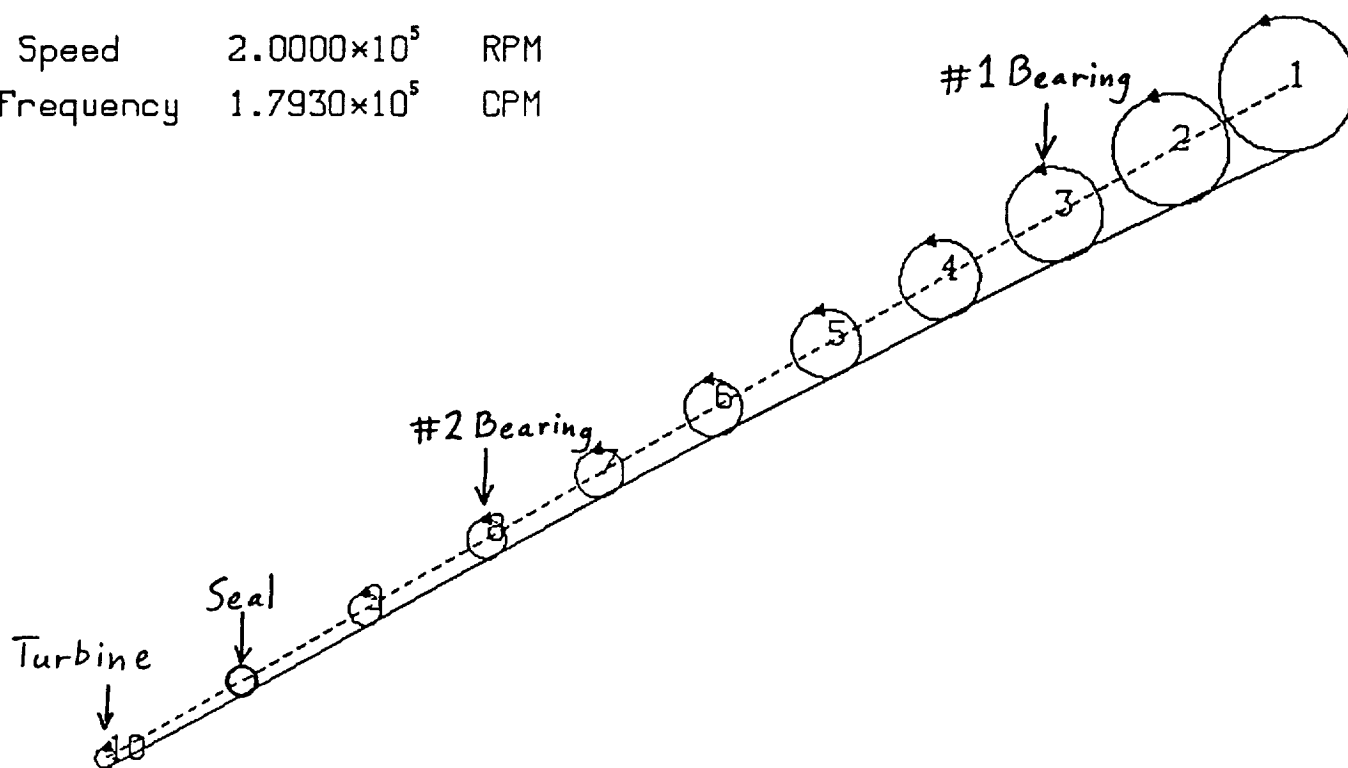
Spin Speed 2.0000×10^5 RPM
Nat Frequency 1.1634×10^5 CPM



STATION 10 ORBIT - FORWARD PRECESSION

Figure E-4 - Second Critical Rotor Group Mode Shape
(Hydrostatic Bearings & Laby Seal)

Spin Speed 2.0000×10^5 RPM
Nat Frequency 1.7930×10^5 CPM



STATION 1 ORBIT - FORWARD PRECESSION

Figure E-5 - Rotor Spin Speed vs Damped Natural Frequency
(Hydrostatic Bearings & Aluminium Shaft)

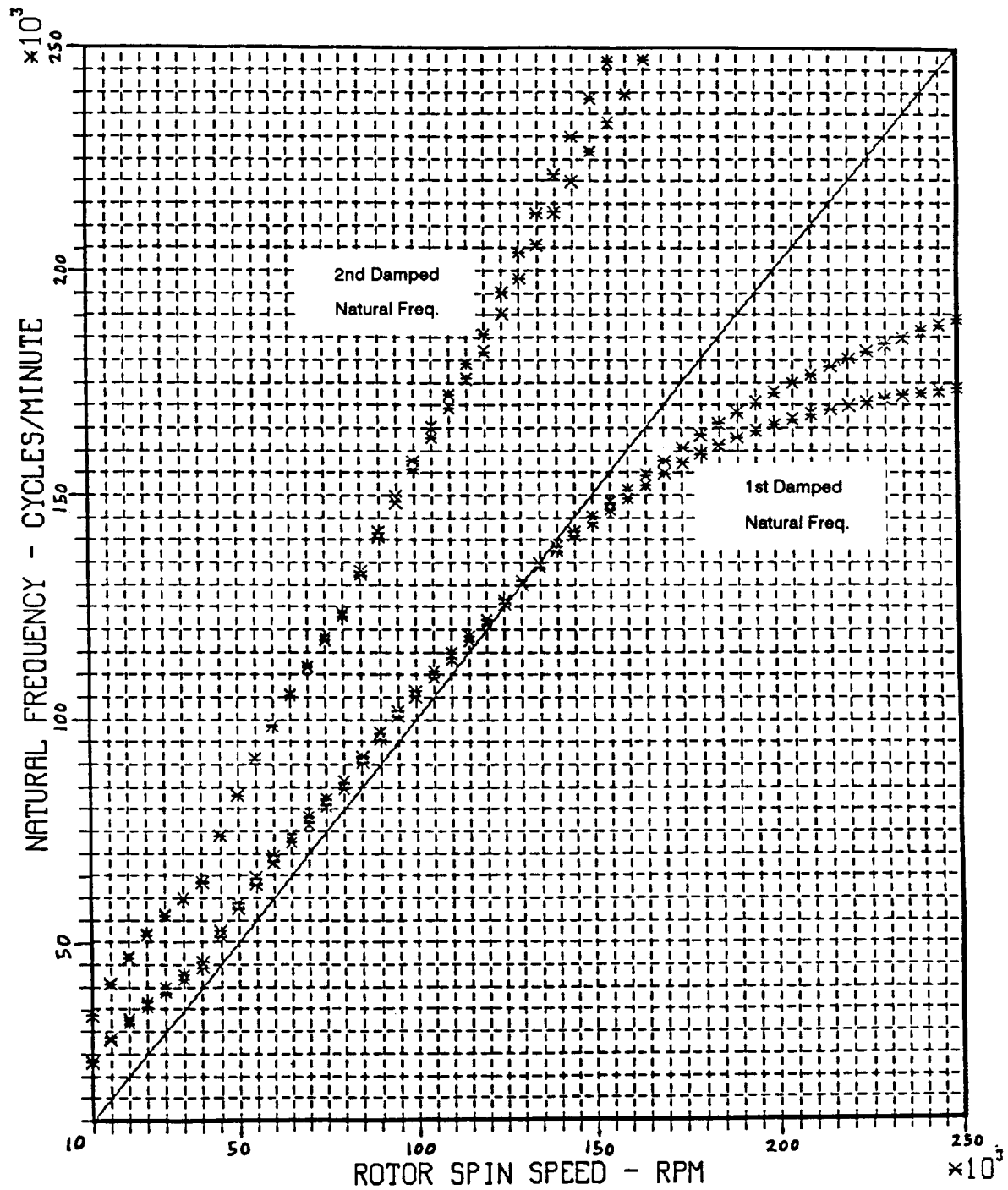


Figure E-6 - Rotor Spin Speed vs Log Decrement
(Hydrostatic Bearings & Aluminium Shaft)

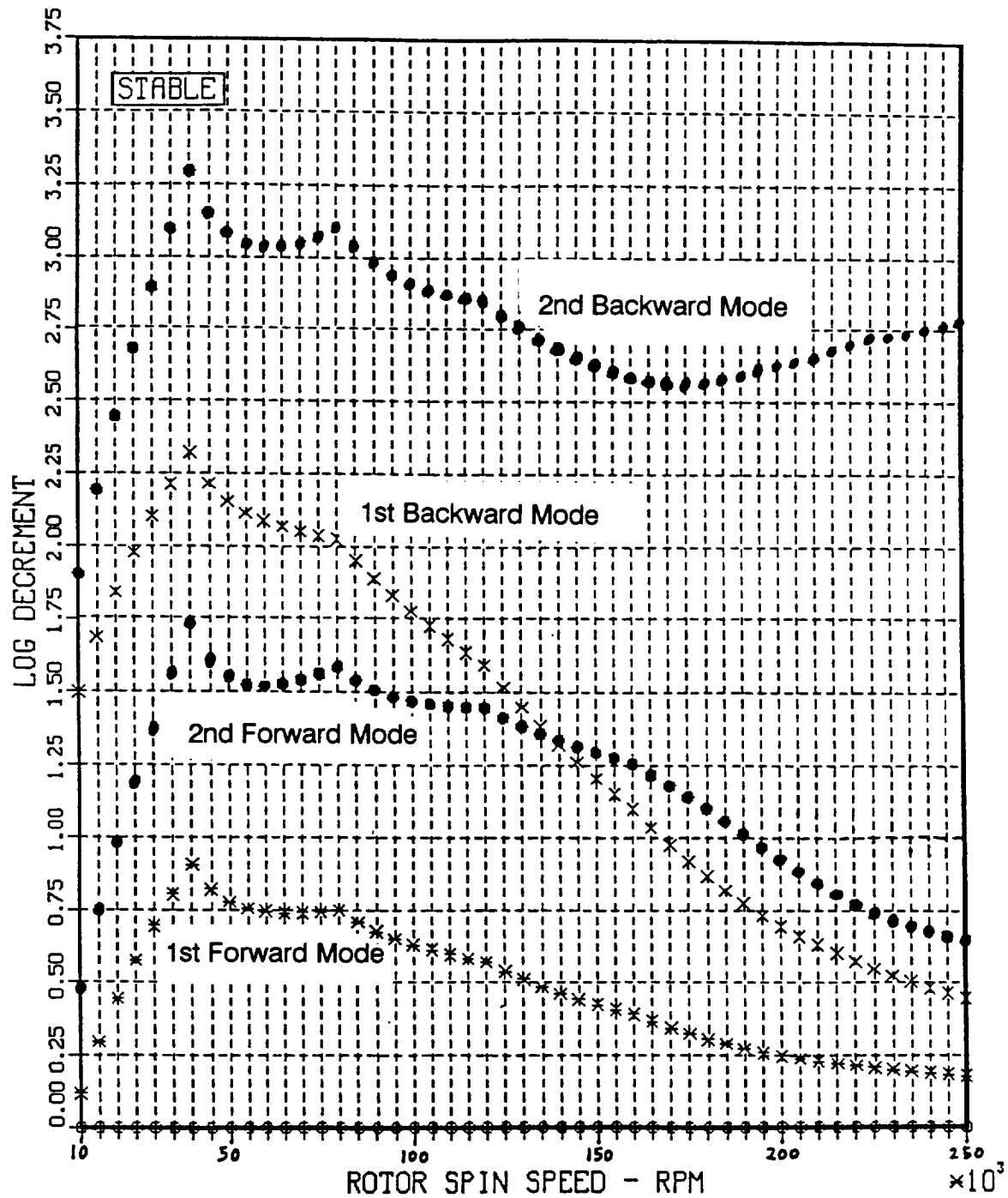
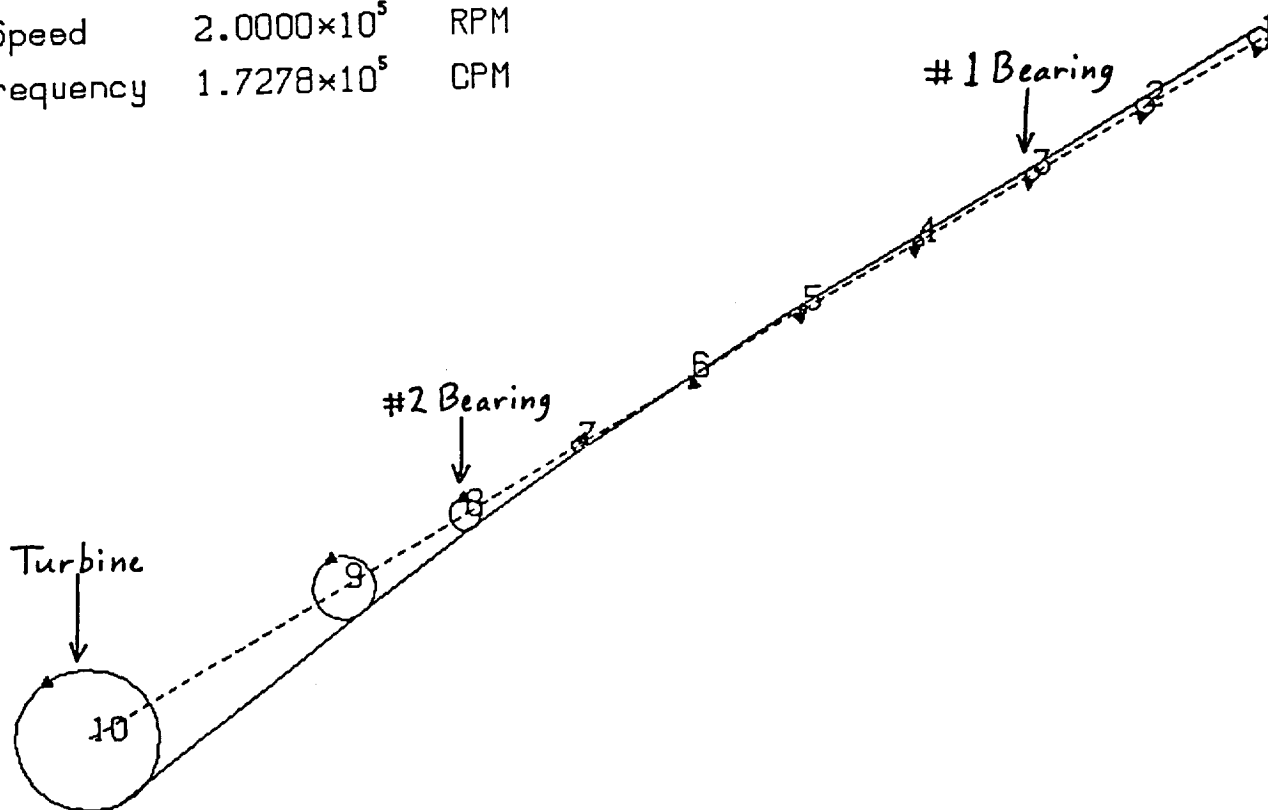


Figure E-7 - First Critical Rotor Group Mode Shape
(Hydrostatic Bearings & Aluminium Shaft)

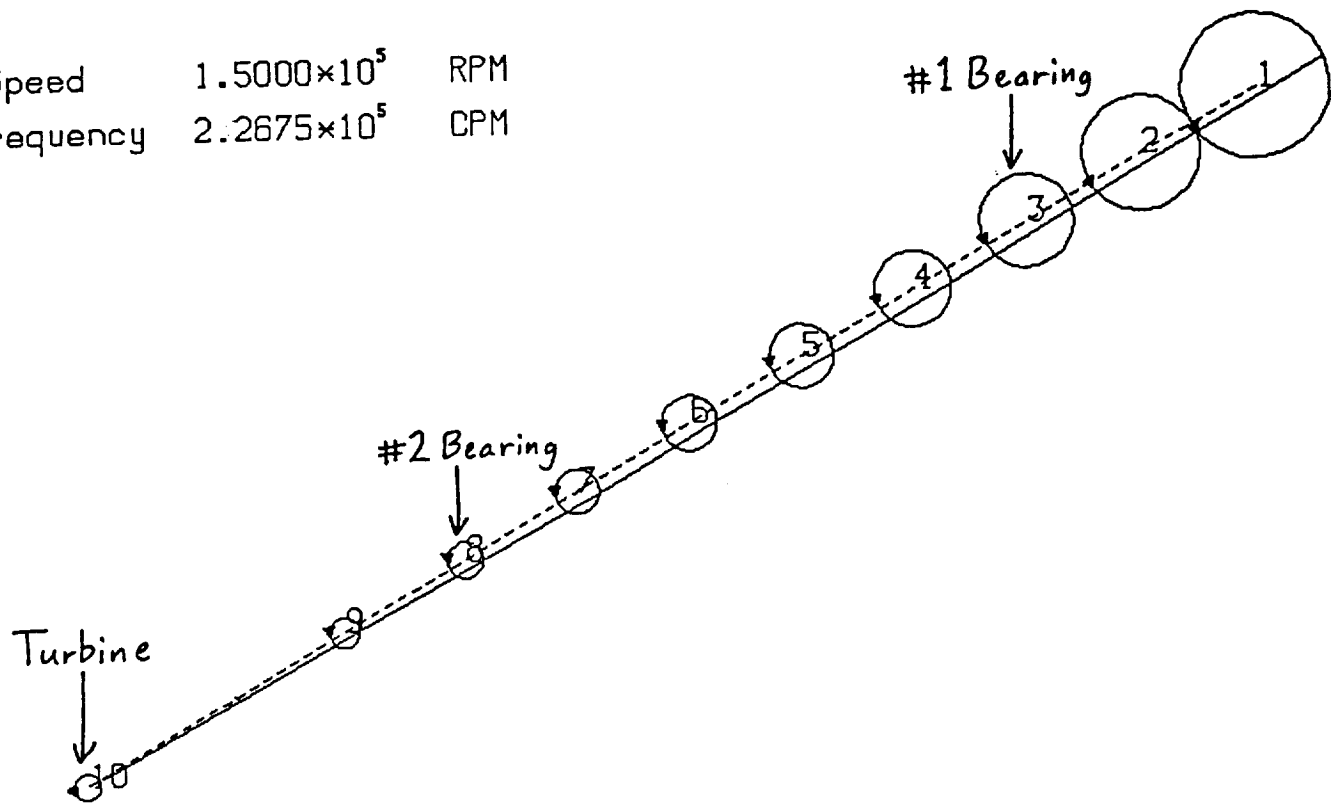
Spin Speed 2.0000×10^5 RPM
Nat Frequency 1.7278×10^5 CPM



STATION 10 ORBIT - FORWARD PRECESSION

Figure E-8 - Second Critical Rotor Group Mode Shape
(Hydrostatic Bearings & Aluminium Shaft)

Spin Speed 1.5000×10^5 RPM
Nat Frequency 2.2675×10^5 CPM



STATION 1 ORBIT - FORWARD PRECESSION

Figure E-9 - Rotor Spin Speed vs Damped Natural Frequency
(Hydrostatic Bearings & Titanium Shaft)

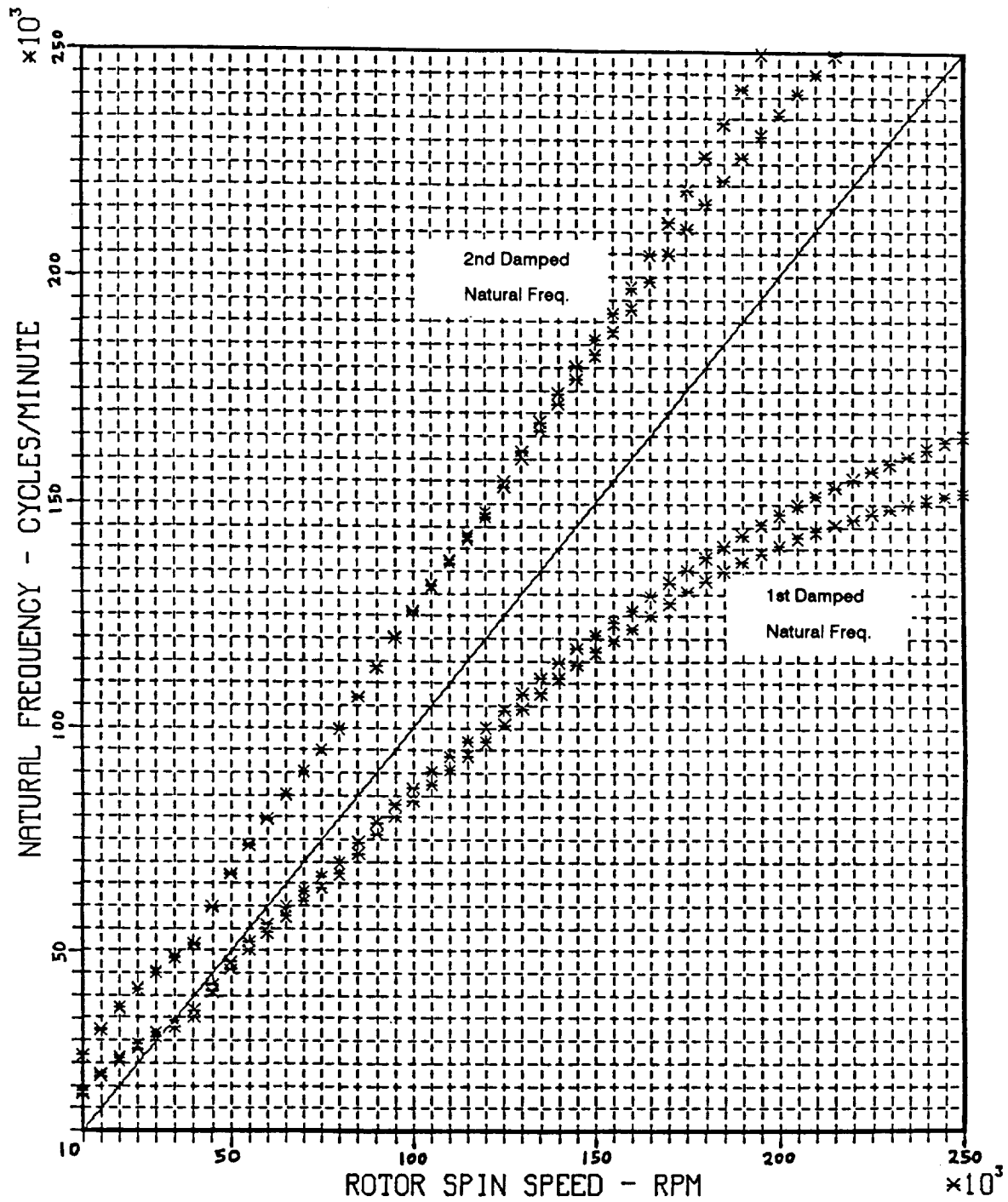
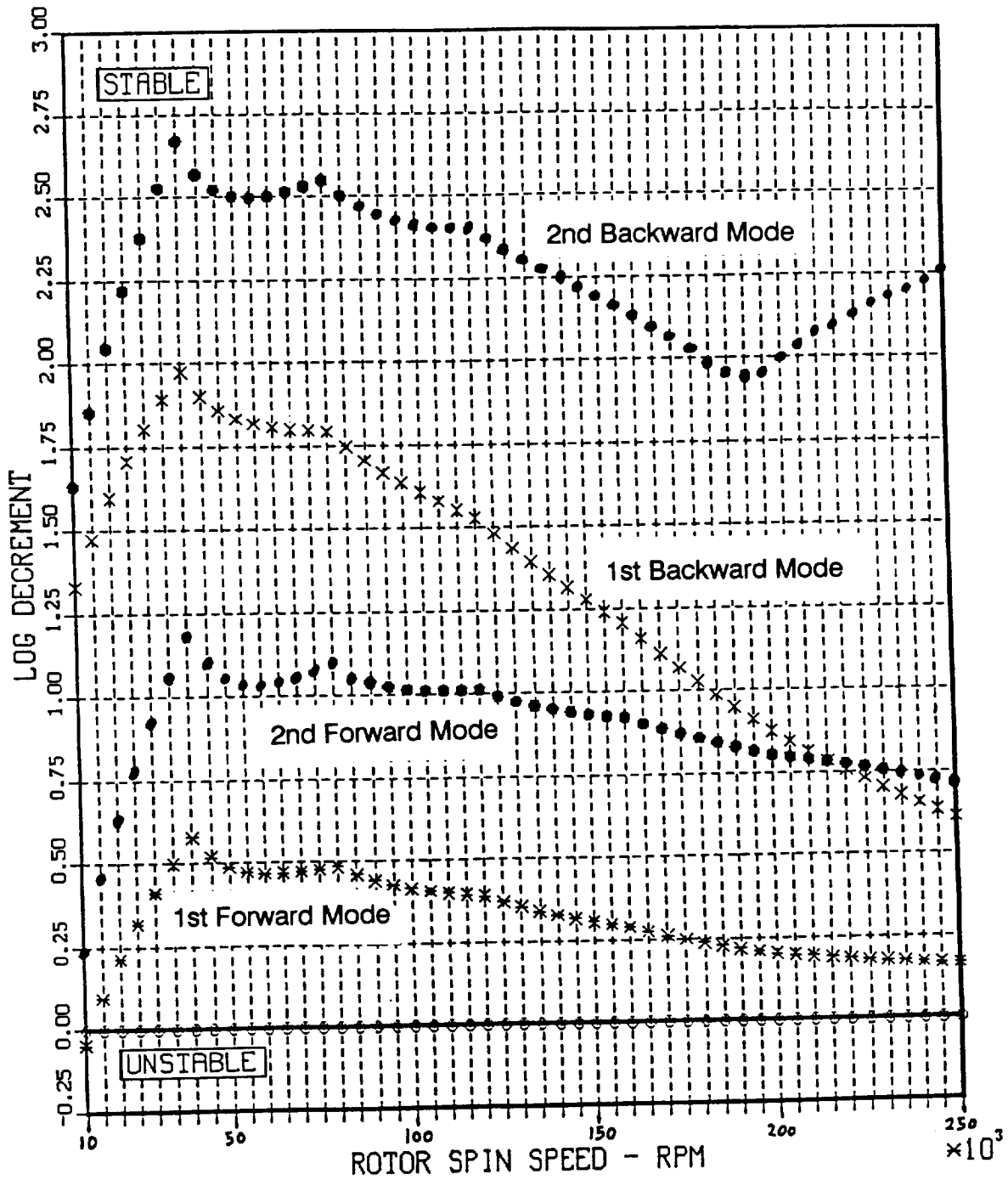
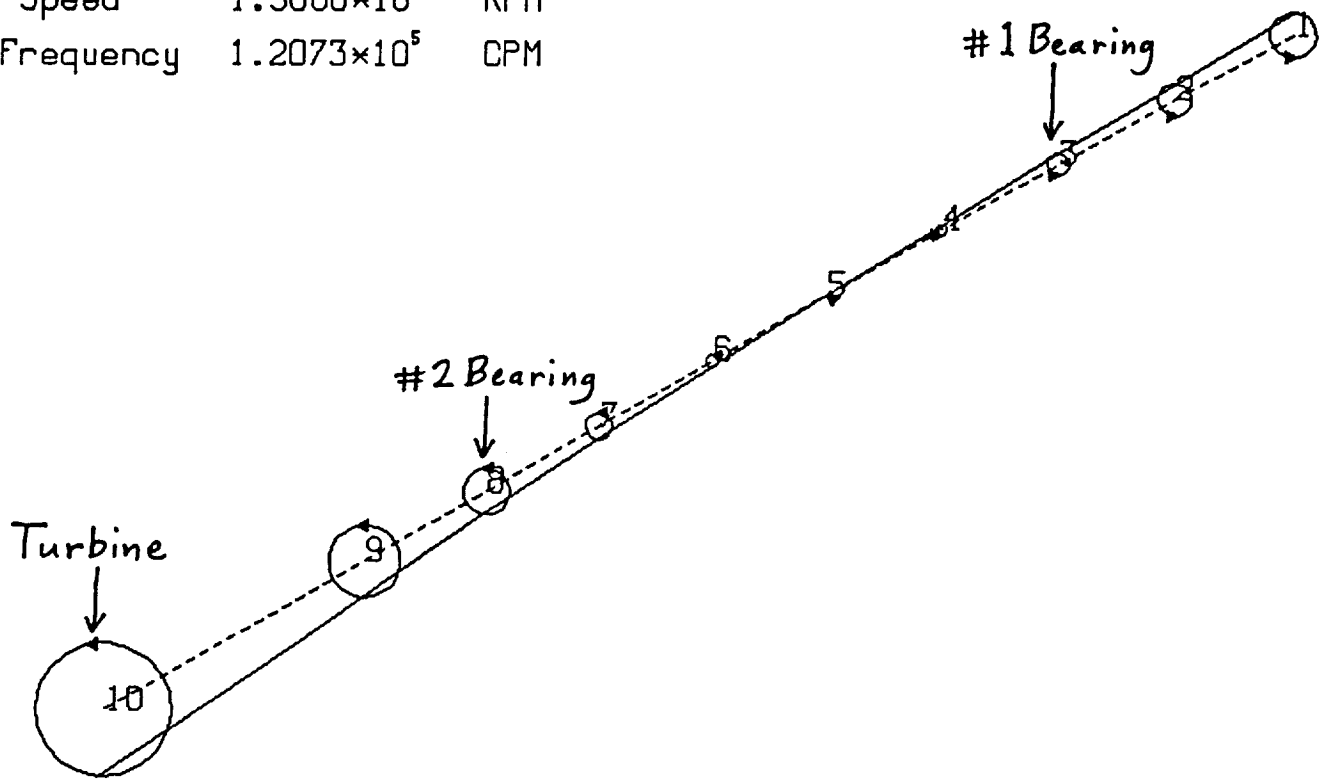


Figure E-10 - Rotor Spin Speed vs Log Decrement
(Hydrostatic Bearings & Titanium Shaft)



**Figure E-11 - First Critical Rotor Group Mode Shape
(Hydrostatic Bearings & Titanium Shaft)**

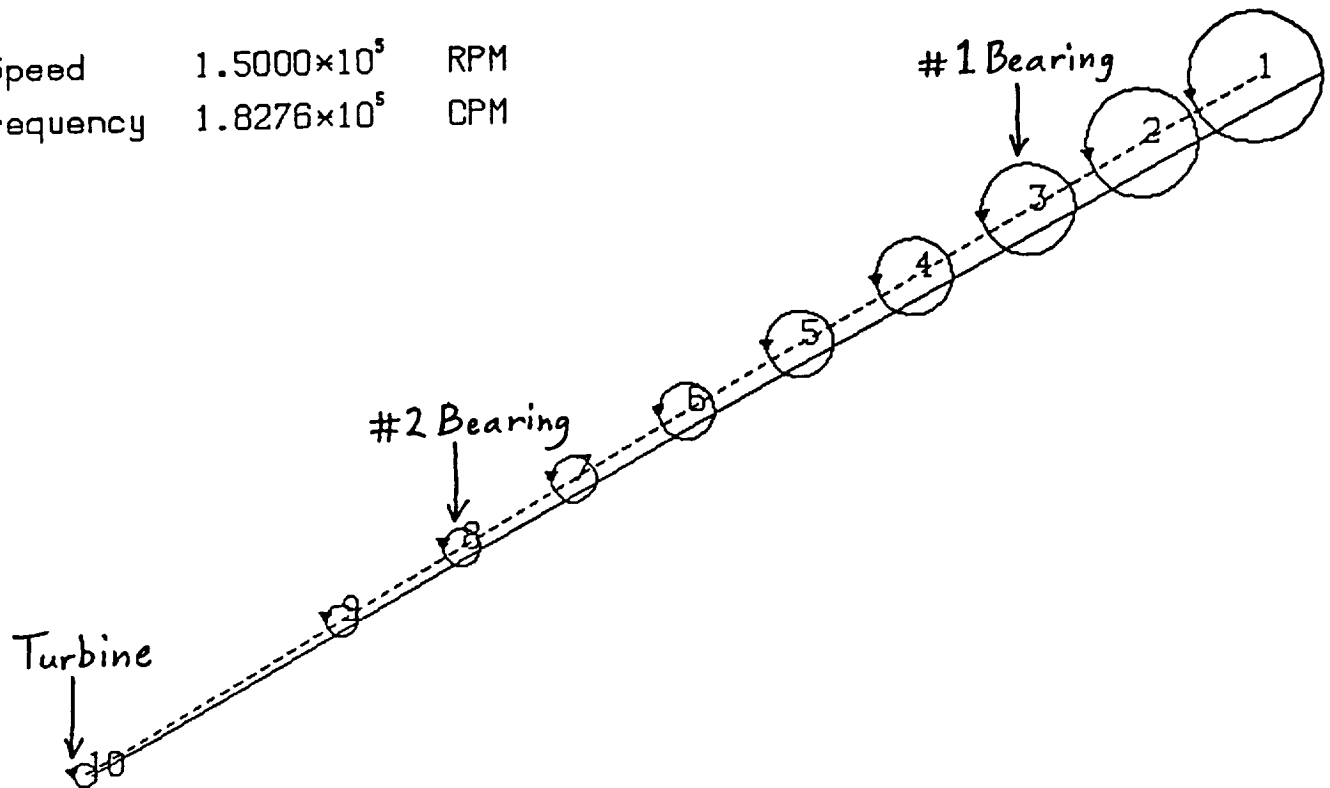
Spin Speed 1.5000×10^5 RPM
Nat Frequency 1.2073×10^5 CPM



STATION 10 ORBIT - FORWARD PRECESSION

Figure E-12 - Second Critical Rotor Group Mode Shape
(Hydrostatic Bearings & Titanium Shaft)

Spin Speed 1.5000×10^5 RPM
Nat Frequency 1.8276×10^5 CPM



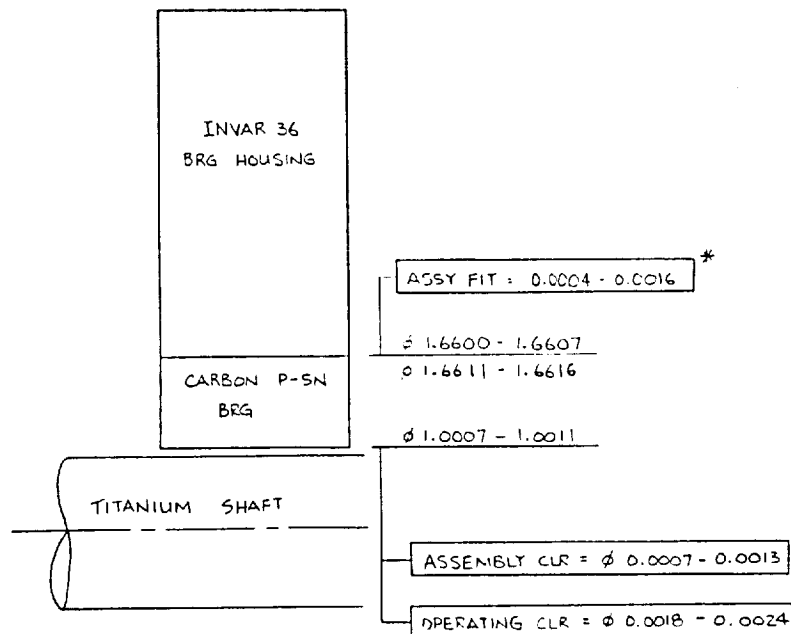
STATION 1 ORBIT - FORWARD PRECESSION

APPENDIX F: STRUCTURAL ANALYSIS

Table F-1 - Material Summary

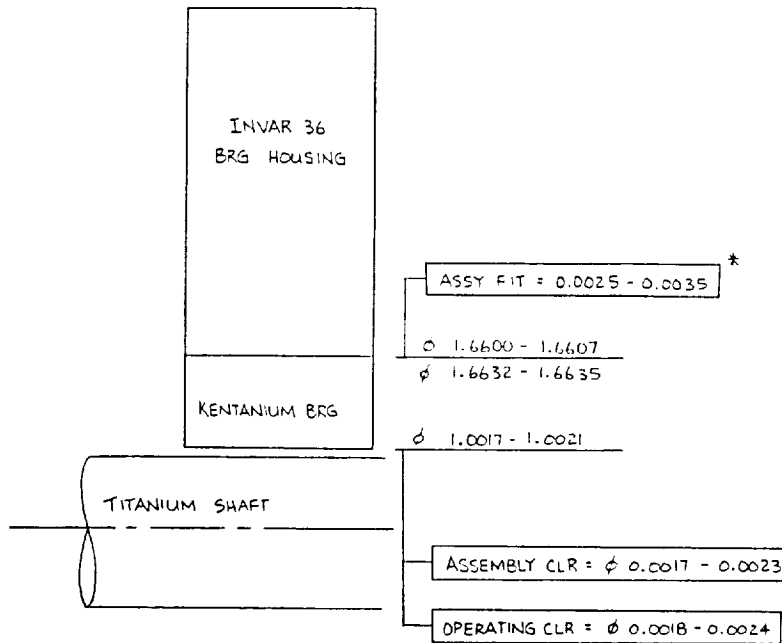
MATERIAL NAME	ELASTIC MODULUS (PSI)	COEFFICIENT OF THERMAL EXPANSION (IN/IN-°F)	MATERIAL STRENGTH @ 70 F (ksi)				MATERIAL STRENGTH @ -300 F (ksi)			
			F _{tu}	F _{cu}	F _{ty}	F _{cy}	F _{tu}	F _{cu}	F _{ty}	F _{cy}
CARBON P-5N	3.00E+06	1.220E-06	7	35	7	35	7	35	7	35
KENTANIUM	5.73E+07	4.110E-06	232							
INVAR 36	1.96E+07	7.500E-07	60	60	35	35	100	100	60	60
INCO 625	3.11E+07	5.330E-06	103	103	52	52	160	160	83	83
INCO 718	3.02E+07	5.330E-06	110	110	72	72	160	160	92	92
A286	3.05E+07	6.000E-06	140	140	96	96	194	194	129	129

Figure F-1 - Carbon P-5N Hydrostatic Bearing



* RESULTING FIT @ OPERATION = 0.00024 - 0.00145 IN (DIAMETRAL)

Figure F-2 - Kentanium Hydrostatic Bearing



* RESULTING FIT @ OPERATION = 0.0000 - 0.0010 IN (DIAMETRAL)

Table F-2 - Stress Summary

BRG MAT'L & PARAMETER DESCRIPTION	ASSEMBLY (W/O AXIAL PRELOAD)		ASSEMBLY (WITH AXIAL PRELOAD)		CHILL		OPERATION	
	HOOP	AXIAL	HOOP ⁽¹⁾	AXIAL ⁽²⁾	HOOP ⁽¹⁾	AXIAL ⁽²⁾	HOOP ⁽¹⁾	AXIAL ⁽²⁾
CARBON P-5N BRG:								
PEAK STRESS (PSI)	-15859	5286	-17302	5822	-13766	3891	-12542	3483
MINIMUM F.S.	2.21	1.32	2.02	1.39	2.54	1.8	2.79	2.01
KENTANIUM BRG:								
PEAK STRESS (PSI)	-226915	75638	-227145	75352	-65912	21959	-61211	20393
MINIMUM F.S.	1.02	3.07	1.02	3.08	3.52	>4.0	3.79	>4.0

(1) Based on maximum axial preload
(2) Based on minimum axial preload

Figure F-3 - Bolt Torque Specifications

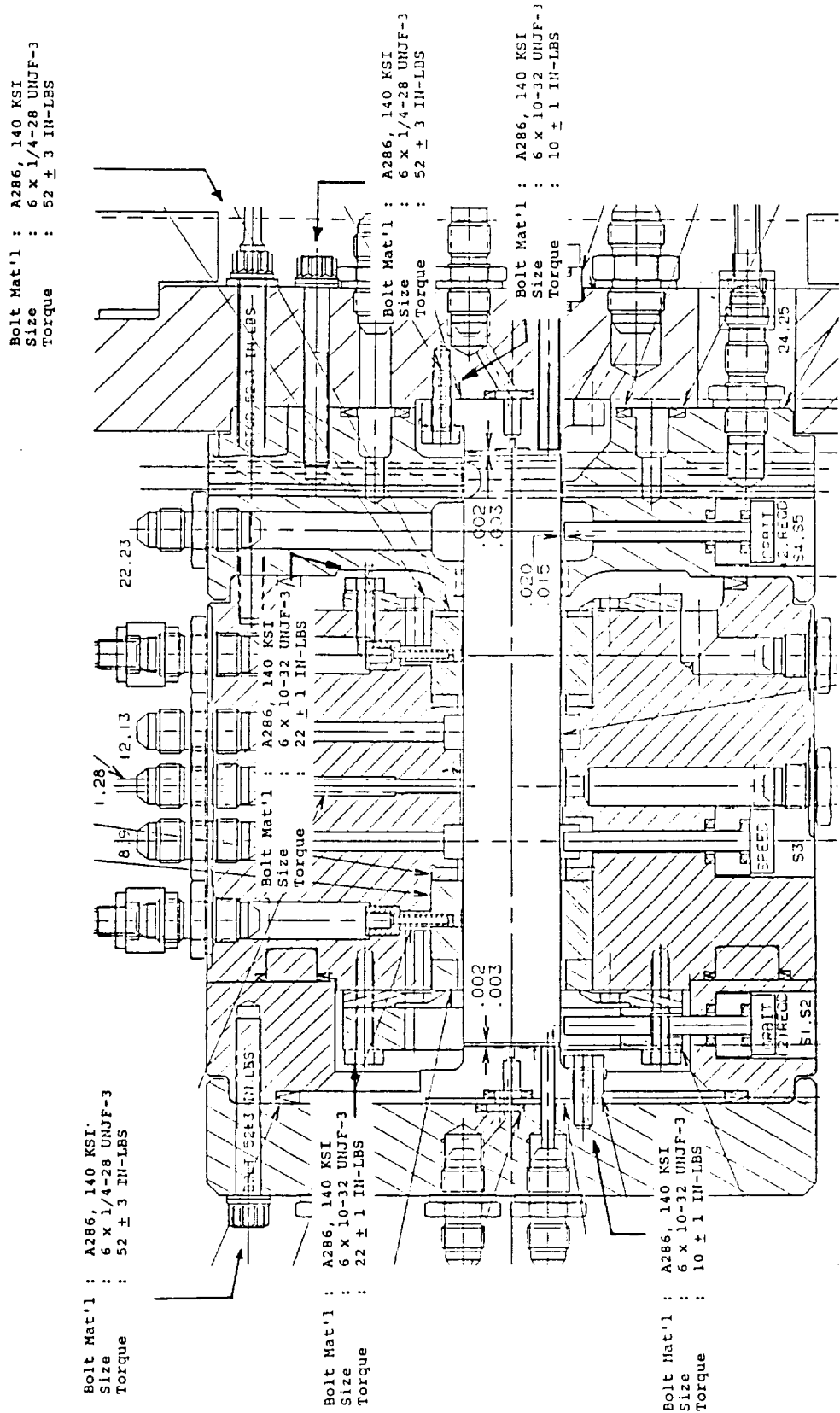
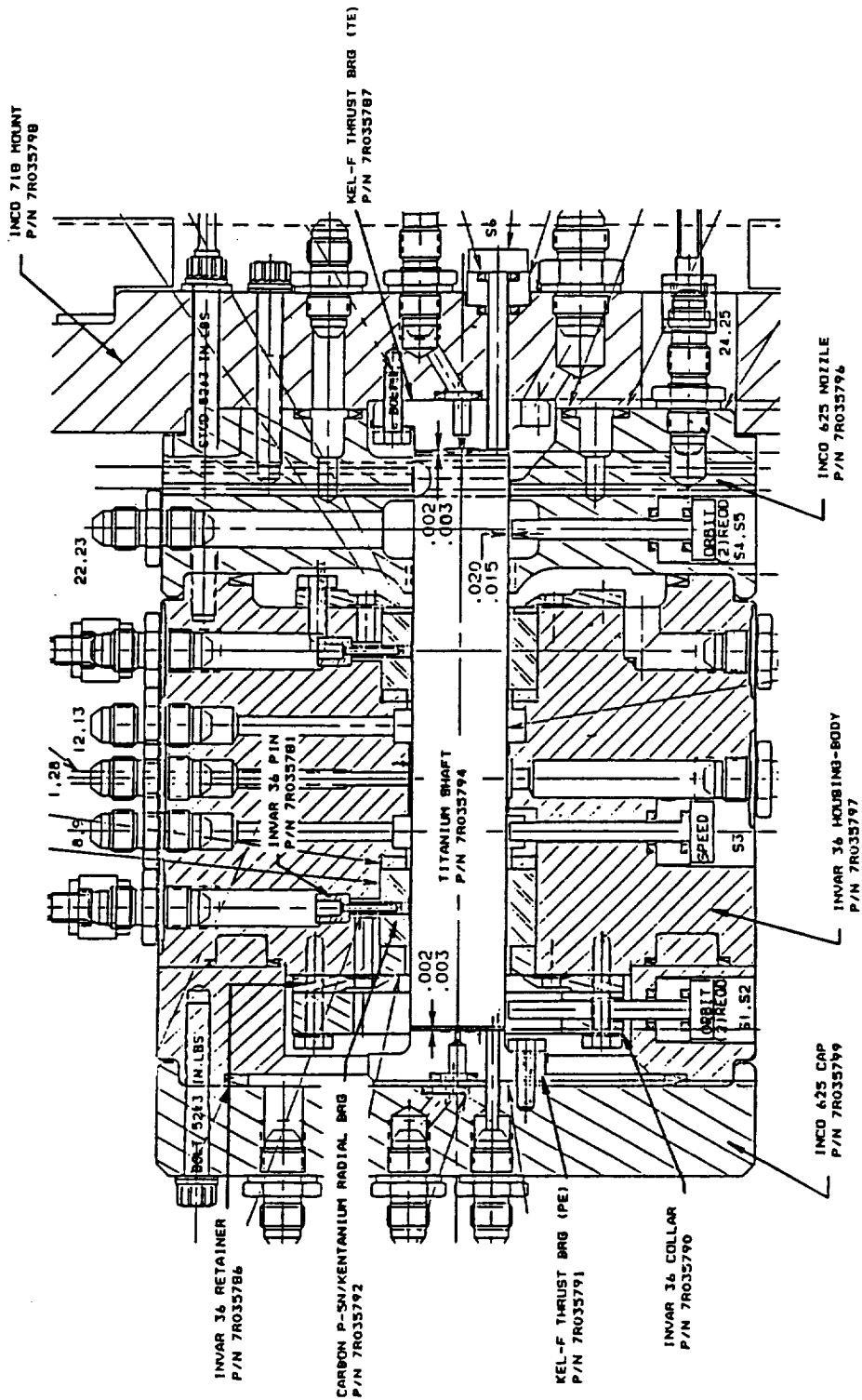


Figure F-4 - Tester Materials



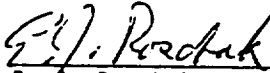
APPENDIX G

TEST PLAN


ORBIT TRANSFER ROCKET ENGINE TECHNOLOGY PROGRAM
CONTRACT NAS3-23773

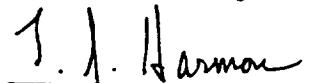
OTVE HYDROSTATIC BEARING TESTER TEST PLAN

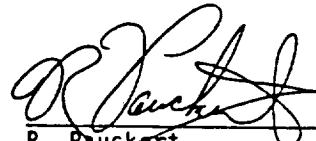
Prepared by:

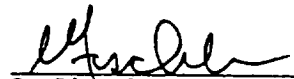

E. D. Roschak, OTVE Turbomachinery
Advanced Rotating Machinery

Approved by:


N. C. Gulbrandsen
Manager, Technology Projects
Advanced Rotating Machinery


T. J. Harmon
Project Engineer
Orbit Transfer Vehicle Engine


R. Pauckert
Project Manager
Orbit Transfer Vehicle Energy

 8/23/88
S. Fischler
Manager
Advanced Programs, Test

1680a/paw

OBJECTIVE

The Orbital Transfer Vehicle (OTV) Technology Program, Task B.6 - High Speed Turbopump Bearings, will develop the basic materials and design technology required to achieve extended life capabilities of high-speed cryogenic turbopump bearings. This capability will be demonstrated with full-scale hydrostatic bearings, operating to 200,000 RPM in high-pressure liquid hydrogen environment, simulating 100 start-up and shutdown transients and steady-state operation. The objectives of this program are to determine life and durability of various bearing materials and to establish flow and pressure requirements for these bearings.

This test program will evaluate two different hydrostatic bearing material combinations and quantify bearing wear to identify the best performing materials. The test program will consist of a series of tests during which wear will be quantified by isotope detection techniques, visual and microscopic inspection, dimensional checks and data analysis. Instrumentation will be used to obtain pressures, temperatures, and flows, isoplots, synchronous tracking, amplitude spectra and orbital plots.

This test plan presents the program approach, program and testing schedule, hardware description, facility requirements, hardware/facility interfaces, and the test matrix necessary to complete the proposed test program and demonstrate the extended life requirements of the bearing materials.

APPROACH

The high-speed bearing task (B-6) of Contract NAS3-23773 is divided into 8 subtasks and are described below:

Subtask I Bearing Limits and Concept Evaluation

During this task, the conceptual evaluation of bearings for high-speed turbopumps and the conceptual layout of the tester

will be accomplished. The tester will utilize radial and axial thrust bearings operating in a liquid hydrogen (LH₂) environment and powered by a turbine integral with the shaft.

Subtask II Detail Design - Bearing Tester

The tester will be designed during this subtask based on the criteria listed in Table I of Appendix A.

Subtask III Bearing Material Selection

The test bearing material analysis and selection will be performed during this subtask based on the criteria listed in table II of Appendix A. Procurement and fabrication of the selected materials will also occur during this subtask.

Subtask IV Tester Fabrication

The activities associated with this subtask include fabrication of tester components and inspection of critical dimensions/interfaces and vendor-supplied parts and assembly of the tester.

Subtask V Design and Layout of the Test Facility

The efforts of this subtask will produce a test plan and test facility layout.

Subtask VI Test Facility Preparation

The facility layout conceptualized in Subtask V will be constructed. Activities include facility preparation, instrumentation installation, installation of the tester, pretest readiness review, and running of checkout tests.

Subtask VII Testing (Reference Test Matrix)

The activities associated with this subtask include start-up testing, verification of facility and test parameter controls, verify all instruments are operating properly, cycle testing, duplication of start-stop and steady-state testing, data recording, inspection of 2 material bearing combinations, and data analysis and evaluations. Securing the facility upon completion of the test program will also be done under this subtask.

Subtask VIII Reporting

SCHEDULE

Figure 1 shows the program and test schedule.

HARDWARE DESCRIPTION

The Orbital Transfer Vehicle (OTV) Technology Program Hydrostatic Bearing Tester cross section shown in Figures 2 and 3, utilizes a free-floating 1-in.-diameter by 6-in.-long shaft, the two test radial hydrostatic bearings, one radial loading hydrostatic bearing, two axial hydrostatic shaft center positioning thrust bearings, a terry turbine integral to the shaft and a tooth-on-stator labyrinth seal. The tester will simulate a liquid hydrogen environment common to small, high-speed turbopumps. The goal of the tester is to investigate and demonstrate possible hydrostatic bearing materials and designs that are capable of withstanding a minimum of 100 start and stop transients as well as the rotordynamic forces typical of turbopumps operating at 200,000 RPM.

Of the three radial hydrostatic bearings, the two outboard units are the actual test specimens, while the center bearing will be used as a shaft radial

OTV Program Schedule

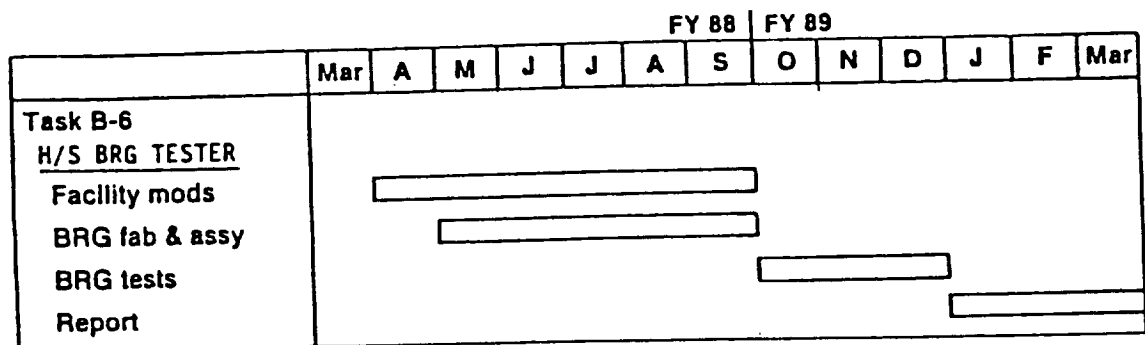


Figure G-1 Program and Test Schedule

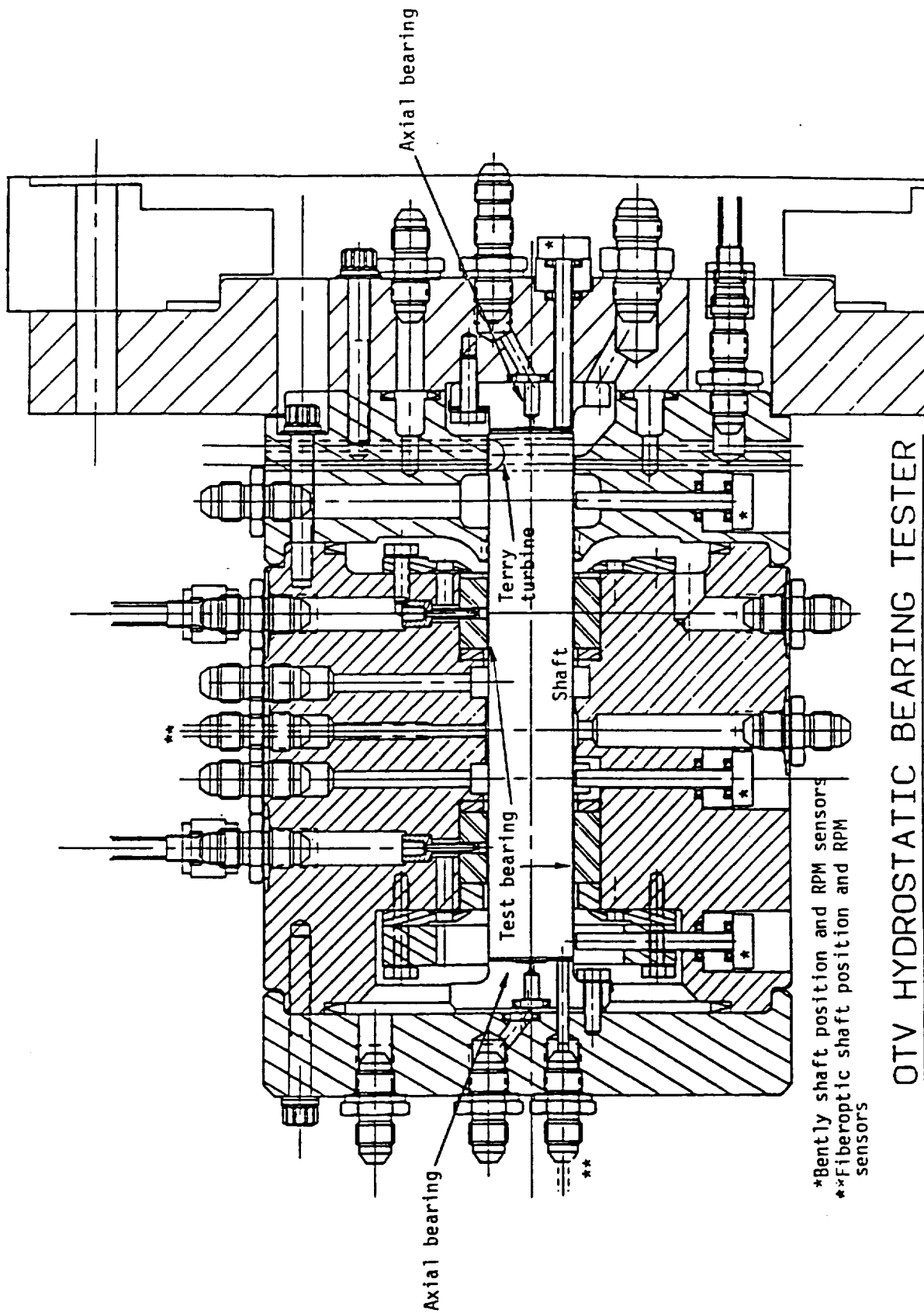


Figure G-2 Tester Hardware

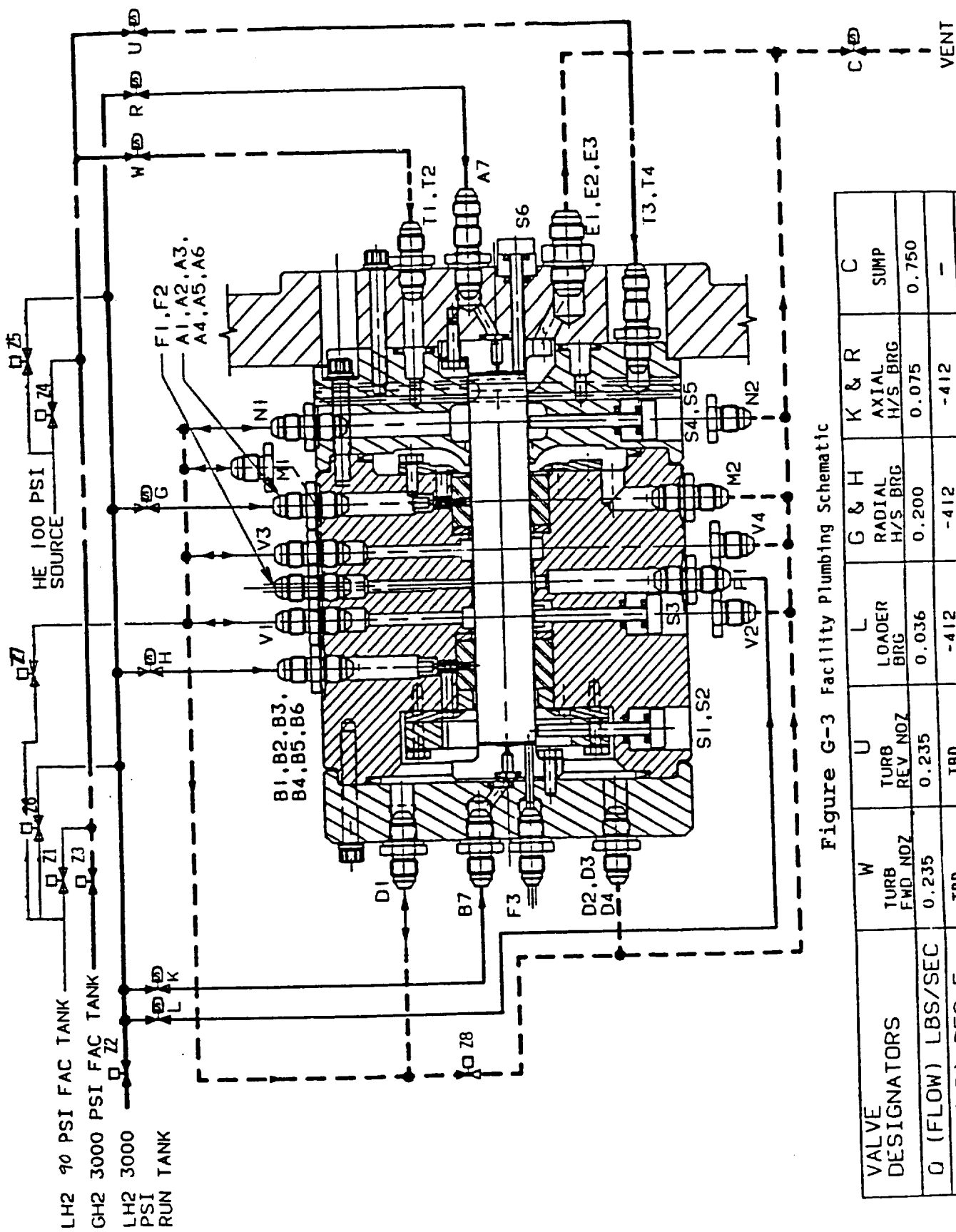


Figure G-3 Facility Plumbing Schematic

VALVE DESIGNATORS	W TURB FWD NOZ	U TURB REV NOZ	L LOADER BRG	G & H RADIAL H/S BRG	K & R AXIAL H/S BRG	C SUMP
Q (FLOW) LBS/SEC	0.235	0.235	0.036	0.200	0.075	0.750
T (TEMP) DEG F	T80	T80	-412	-412	-412	-
Q (TEMP) DEG F	1000	3000	816	2300	2000	300

loading device. The test hydrostatic bearings have the following characteristics:

- 0.03-in.-diameter orifices
- 6 recesses per bearing
- 0.00250 in. diametral clearance
- 0.2 lbm/s per bearing estimated leakage
- Inlet pressure to vary as a function of speed squared up to 2300 psig (ref Figure 4).

Radial loads will be applied to the shaft via a radial loader pad. This pad has the following characteristics:

- No orifice
- 1 recess
- 0.002 in. radial clearance
- 0.036 lbm/sec estimated leakage
- Inlet pressure to vary as a function of speed squared up to 816 psig.

Two materials are planned for the test bearings. These materials are carbon P5N and kentanum. The carbon P5N is the same material that is commonly used in turbopump shaft seals. The kentanum is a ceramic material that represents the hard end of the material spectrum. Test bearing changeout requires machining of the bearing in place. Consequently, all hardware builds will be done at the Rocketdyne EDL facility.

Two hydrostatic thrust bearings will be incorporated to axially stabilize the shaft. Since there is an axial load produced by the turbine during operation, the pad pressure will provide a corrective balancing force to prevent the shaft from rubbing on the thrust bearing. The axial hydrostatic thrust bearings have the following characteristics:

- 0.050-in.-diameter orifice
- 0.002-0.003 in. axial clearance

OTV HYDROSTATIC BEARING TEST

SPEED VS TIME PROFILE

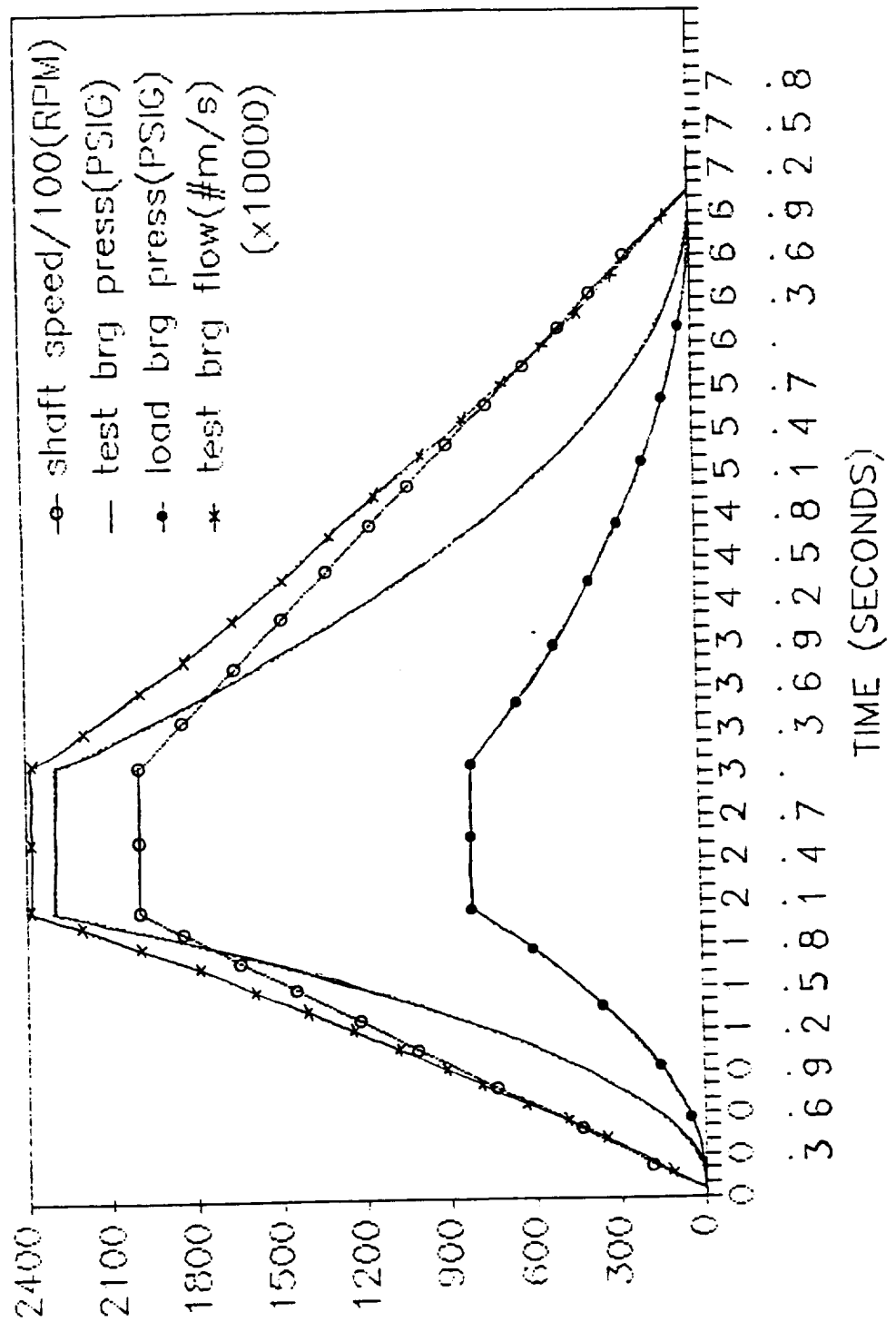


Figure G-4 Speed/Pressure vs Time

0.075 lbm/s estimated leakage
2000 psig supply pressure.

The radial and axial shaft position will be monitored with special Bently proximeter probes and fiber optic probes. Speed is measured via a Bently and a fiber optic probe.

The terry turbine, which will translate the gaseous hydrogen flow into rotational motion, is machined into the shaft. The turbine has 7 inlet nozzles and 9 buckets to provide the necessary flow to obtain 200,000 RPM while minimizing the axial load potential. Braking torque will be applied via 2 reversing nozzles. The tooth-on-stator labyrinth seal is used to prevent the leakage of liquid hydrogen into the turbine cavity while the tester is rotating.

FACILITY REQUIREMENTS

General

Tester port identifications can be found in Table A which also lists port sizes, flow, and pressures.

It is the test facility's responsibility to install and remove the test hardware and to supply the propellant pressurant, drains, the stated instrumentation (per Table B), and the data acquisition and facility control systems required to perform the tests set forth in this test plan.

The bearing tester assembly as received by the test facility will consist of the bearing tester mounted on test fixture 7R0016001. This tester assembly shall be bolted to the test facility stand via the test fixture 7R0016001 so that the tester shaft is horizontal.

The plumbing will consist of fluid fittings installed in the assembly. All fluid fittings will be 1/4-inch tube size with the exception of the three turbine vent fluid fittings which are of 3/8 tubing size.

A facility-supplied manifold will be constructed that circles the assembly and will supply LH_2 to fittings A1 through A6. This manifold will be controlled by servo-valve "G" as shown in Figure 3. Similarly, a facility-supplied manifold will be constructed that circles the assembly and will supply LH_2 to fittings B1 through B6. This manifold will be controlled by servo-valve "H" as shown in Figure 3.

Servo-valve "R" will supply and control LH_2 to fitting A7, the turbine side axial hydrostatic bearing. Servo-valve "K" will supply and control LH_2 to fitting B7, the nonturbine side axial hydrostatic bearing. Servo-valve "W" will supply and control GH_2 to fittings T1 and T2, the forward turbine nozzles. Servo-valve "U" will supply and control GH_2 to fittings T3 and T4, the reverse turbine nozzles. Servo-valve "L" will supply and control LH_2 to fitting P1, the shaft radial loader.

Fittings V1 through V4, M1, M2, N1, N2, E1 through E3, and D1 through D4 will be manifolded together and controlled by servo valve "C" to provide a constant sump pressure of 300 psig.

Valves Z1 through Z7 are remotely controlled facility valves and valve Z8 is a remotely controlled on/off valve that is utilized during chill.

Upon completion of the installation, including plumbing and valving, the system will be leak checked with helium pressurized to 3,000 psig. After all leaks are repaired, the system will be purified with helium heat cycled and vacuum cycled to remove all moisture.

A hardware insulation housing will be constructed that will provide thermal insulation to prevent loss of chill during tester operation. Access must be provided for isotope wear detection equipment. Also, an LH_2 external tracer line and an external heater tracer line will be installed.

Chill Procedure

The valve positions to accomplish chill will be as follows: Valves Z2, Z3, Z4, Z5, and Z8 will be closed. Valves Z1, Z6, Z7, and all other valves, with the exception of sump valve "C" which will be controlling back pressure, will be open until chill is accomplished. As chill is accomplished, valves Z1, Z6, and Z7 will be closed and the flow of high-pressure LH_2 and GH_2 will be controlled as described in the test request.

Flow Requirements (Pressure, Flowrate & Time)

A simplified propellant and pressurant supply schematic is shown in Figure 3 to diagram the major interface components.

The liquid Hydrogen system shall be capable of pressure to 3000 psig and 0.75 lb/sec for approximately 180 seconds duration before having to retank. As shown in the schematic, Figure 3, the liquid hydrogen flow system is split into five parallel systems as follows:

- 1&2) The first two systems will regulate flow to the two test hydrostatic bearings.
- 3) The third system will regulate the supply pressure to the radial load hydrostatic bearing.
- 4&5) The last two systems will control the axial shaft position by supplying the axial thrust bearings with centering flow.

The gaseous hydrogen flow system is split into two systems as follows:

- 1) The terry turbine drive system.
- 2) The terry turbine reversing nozzle system.

A turbine drive system is required to drive the terry turbine that is capable of flowing gaseous hydrogen (GH_2). Additionally, a heat exchanger may be placed downstream of the drive valve that will be immersed in liquid nitrogen. The turbine requires a 3000-psig source at 0.23 lb/sec. The turbine exhaust system will be a mixed flow of liquid and gaseous hydrogen.

All of the tester's discharge lines will be manifolded together and regulated to maintain a constant 300-psig backpressure, ref Figure 3.

Listed below are the maximum pressures and flowrates the test program requires for the various media:

<u>Parameter</u>	<u>Pressure Range</u>	<u>Flow Range</u>
Liquid hydrogen (LH ₂)	0-3000 psig	0 - 0.75 lbm/sec
Gaseous hydrogen (GH ₂)	0-3000 psig	0 - 0.50 lbm/sec
Gaseous helium (He)	0-50 psig	0 - 500 scim

Flow Control Requirements

Special facility controls are necessary to support the test plan. Since the OTV turbopump builds pump discharge pressure, and subsequent radial shaft loads, as a function of speed squared, the inlet pressure to the test hydrostatic and radial loading bearings must increase as a function of speed squared. Since the objective of this program is to accurately simulate the OTV pump bearing environment, an accurate representation of the OTV pump start-up and shutdown transients is required. To accomplish this, the test hydrostatic and radial loading bearings inlet pressures must be adjusted as a function of speed squared. Figure 4 defines the desired shaft speed versus time and radial hydrostatic bearing pressure versus time profiles:

The turbine drive valve will control the shaft speed using a speed feedback signal from the Bently speed proximeter probe or a fiber optic probe. The hydrostatic test bearing supply valve and the radial load bearing supply valve will use the same speed feedback signal to control pressures that are proportional to speed squared. Care must be taken in the control of shaft speed during start-up so that excessive shaft overspeed is not encountered with the rapid acceleration rate expected. Caution must be exercised to minimize the time spent between 20,000 rpm and 60,000 rpm. In this speed range, the shaft is operating near the first critical speed.

In order to avoid excessive LH₂ leakage, the flow to the two axial hydrostatic bearings must be limited to 0.075 lbm/sec maximum for each bearing.

A servo valve will be required to control the hydrostatic bearing sump and turbine exhaust cavity pressure. As previously stated, all of the tester's discharge lines will be manifolded together and maintained at a constant backpressure of 300 psig.

Table E lists the OTVE hydrostatic bearing tester valve sequencing for one cycle. There will be 1-second dwell at zero RPM between cycles.

Instrumentation

Table B represents the tester instrumentation and data acquisition requirements. The table shows the recording device, the number required of each parameter, the range, method of recording the data (static vs. dynamic), whether the parameter is to be displayed real time, and who is to supply the thermocouple, transducer, Bently, accelerometer or probe.

Table C lists the operational limits of the tester. The nominal or expected range is listed as well the redlines.

Table D describes the accelerometer instrumentation ranges and limits which will be set for three accelerometers, one for each spacial axis.

Table F lists the OTVE hydrostatic bearing tester parameters that will be used for temperatures, pressures, and flows. Shaft RPM will be designated at "N."

Bearing wear will be monitored by isotope wear detection techniques. The test bearing internal diameters will be irradiated to generate radioactive isotopes to a minimal depth on the IDs. As the bearing ID is worn away, radioactive particles are carried out of the tester through the sump system. A portable radioactivity detector measures the decrease in the radioactivity level emanating from the bearings. These measurements will be made posttest day and will not interface with testing. All necessary permits will be in place and all safety procedures will be adhered to.

Table G-1 OTV H/S Bearing Tester Port Identification

Port Number	Description	Size MS Tube	Media/ Valve	Flow Rate (lb/sec)	Nominal Pressure (psig)	Maximum Pressure (psig)*
A1-A6	TURB SIDE H/S BRG	1/4	LH ₂ /"G"	0.2	2300	3000
B1-B6	NONTURB SIDE H/S BRG	1/4	LH ₂ /"H"	0.2	2300	3000
A7	TURB SIDE AXIAL H/S BRG	1/4	LH ₂ /"R"	0.075	2000	3000
B7	NONTURB SIDE AXIAL H/S BRG	1/4	LH ₂ /"K"	0.075	2000	3000
P1	SHAFT RADIAL LOADER	1/4	LH ₂ /"L"	0.036	816	1500
T1-T2	TURB FWD NOZZLE	1/4	GH ₂ /"W"	0.235	532	1500
T3-T4	TURB REV NOZZLE	1/4	GH ₂ /"U"	0.235	3000	3000
S1-S2	NONTURB SIDE SHAFT ORBIT BENTLY PROBES	--	--	--	--	--
S3	SHAFT RPM BENTLY PROBE	--	--	--	--	--
S4-S5	TURB SIDE SHAFT BENTLY PROBES	--	--	--	--	--
S6	TURB SIDE SHAFT AXIAL BENTLY PROBE	--	--	--	--	--
F1-F2	SHAFT ORBIT, AXIAL, AND RPM FIBER OPTIC PROBE	(CONAX FITTING)		--	--	--
F3	NONTURB SIDE SHAFT AXIAL FIBER OPTIC PROBE	(CONAX FITTING)		--	--	--
N1-N2	LABY VENT	1/4	LH ₂ /"C"	--	300	350
M1-M2	TURB NOZZLE HSG VENT	1/4	LH ₂ /"C"	--	300	350
E1-E3	TURBINE EXHAUST	3/8	LH ₂ /"C"	--	300	350
V1-V4	LOADER & H/S BRG VENT	1/4	LH ₂ /"C"	--	300	350
D1-D4	END CAP BRG VENT	1/4	LH ₂ /"C"	--	300	350

*NOTE: VALVING SHOULD BE SET UP TO CONTROL TO NOMINAL PRESSURE VALUES BUT ACCOMMODATE MAX VALUES SHOWN

Table G-2
Standard and Special Instrumentation
Dynamic Tests
(Sheet 1 of 2)

All data will be recorded on test facility data acquisition systems. The program will supply the hardware and instrumentation necessary for using the Isotope Wear Detector.

Parameter	Device	No. / Rqd.	Range	/Recording Device/		CRT Display	/ Recording Device /	
				Digital	FM Tape		Test Fac	Program Supplied
/TEMPERATURES								
/ RADIAL BEARINGS	TEMP BULBS	2	/60 to -420F	X	/	X	/	
/ AXIAL BEARINGS	"	2	"	X	/	X	/	
/ LOADER BEARINGS	"	1	"	X	/	X	/	
/ TURBINE FWD NOZZLE	"	1	"	X	/	X	/	
/ TURBINE REV NOZZLE	"	1	"	X	/	X	/	
/ SUMP	THERMOCOUPLE	4	"	X	/	X	/	
/	/	/	/	/	/	/	/	
/	/	/	/	/	/	/	/	
/PRESSURES								
/ RADIAL BEARINGS	TRANSDUCER	2	0-3000 PSIG	X	/	X	/	
/ AXIAL BEARINGS	"	2	0-2000 PSIG	X	/	X	/	
/ LOADER BEARING	"	1	0-1000 PSIG	X	/	X	/	
/ TURBINE FWD NOZZLE	"	1	0-1000 PSIG	X	/	X	/	
/ TURBINE REV NOZZLE	"	1	0-3000 PSIG	X	/	X	/	
/ SUMP	"	1	0-300 PSIG	X	/	X	/	
/	/	/	/	/	/	/	/	
/DELTA PRESSURES (FLOW)								
/ RADIAL BEARINGS	TRANSDUCER	2	50 PSIG	X	/	X	/	
/ AXIAL BEARINGS	"	2	50 PSIG	X	/	X	/	
/ LOADER BEARING	"	1	50 PSIG	X	/	X	/	
/	/	/	/	/	/	/	/	
/TESTER ACCELERATION								
/ (X, Y & Z)	ACCELS	/1 PER /PLANE	0-10 g's RMS	/	(3)X	(3)X	/	

Table G-2
Standard and Special Instrumentation
Dynamic Tests
(Sheet 2 of 2)

All data will be recorded on test facility data acquisition systems. The program will supply the hardware and instrumentation necessary for using the Isotope Wear Detector.

Parameter	Device	No Rqd.	Range	Recording Device			Recording Device		
				Digital	Tape	FM	Display	Test Fac	Program
								Supplied	Supplied
/SHAFT SPEED									
/ 1 BENTLY PROBE	BENTLYS	1	/0-500K RPM	X	X		(CRT)		X
/ 1 FIBER OPTIC PROBE	FIBER OPTIC	1	/0-500K RPM	X	X		X		X
/FLOW RATES							(P.C.)		
/ RADIAL BEARINGS	ORIFICE	2	/0-0.2 #/s				X		X
/ AXIAL BEARINGS	"	2	/0-0.075 #/s				X		X
/ LOADER BEARING	"	1	/0-0.036 #/s				X		X
/SHAFT RADIAL MOTION									
/ 2 SETS OF 2 BENTLYS	BENTLYS	/2 SETS/0-0.005"			(4)X		(SCOPE)		X
/		/ OF 2							
/ 1 SET OF 2 FIBER OPTI/	FIBER OPTIC	2	"		(2)X		(SCOPE)		X
/									
/SHAFT AXIAL POSITION							(CRT)		
/ 1 AXIAL BENTLY	BENTLY	1	/0-0.010"	X	X		X		X
/ 2 FIBER OPTIC PROBE	FIBER OPTIC	2	/0-0.010"	X	X		X		X
/									
/MISCELLANEOUS							(O-GRAPH)		
/ TIME	IRIG	1		X	X		X		X
/ SUMP	"	1	0-300 PSIG	X			X		X

Table G-3
Standard and Special Instrumentation
Dynamic Tests
Hardware Limitation

PARAMETER	DEVICE	NO. RQD.	NOMINAL RANGE	LOCATION	REDLINE
<u>TEMPERATURES</u>					
RADIAL BRGS	TEMP BULB	2	/60 to -420°F	VALVES G&H	*
AXIAL BRGS	"	2	"	VALVES K&R	*
LOADER BRG	"	1	"	VALVE L	--
TURBINE (FWD)	"	2	/60 to -320°F	VALVE W	--
TURBINE (REV)	"	1	"	VALVE U	--
SUMP	THERMOCOUPLE	5	/60 to -420°F	PORTS D1, V1, V3, E1 & M1	--
<u>PRESSURES</u>					
RADIAL BRGS	TRANSDUCER	1	/0-2300 PSIG	VALVES G&H	3000 PSIG
AXIAL BRGS	"	1	/0-2000 PSIG	VALVES K&R	3000 PSIG
LOADER BRG	"	2	/0-1000 PSIG	VALVE L	1500 PSIG
TURBINE (FWD)	"	1	/0-1000 PSIG	VALVE W	1500 PSIG
TURBINE (REV)	"	1	/0-3000 PSIG	VALVE U	3000 PSIG
SUMP	"	1	/0-300 PSIG	VALVE C	350 PSIG
<u>TESTER ACCELERATION</u>					
(X, Y & Z)	ACCELS	/1 PER /PLANE	/0-5 g's RMS	ACCEL BLOCK	/10 g's RMS
<u>SHAFT SPEED</u>					
1 BENTLY PROBE	BENTLY	1	/0-200K RPM	PORT S3	250 KRPM
1 FIBER OPTIC PROBE	FIBER OPTIC	1	"	PORT F1	"
<u>SHAFT RADIAL MOTION</u>					
2 SETS OF 2 BENTLYS	BENTLYS	/2 SETS/ /OF 2	/0.0-0.001"	S1, S2, S4, S5	ORBIT
1 SET OF 2 F.O.P.	FIBER OPTIC	/1 SET /OF 2	/0.0-0.001"	PORTS F1&F2	--
<u>SHAFT AXIAL POSITION</u>					
1 AXIAL BENTLY	BENTLY	1	/0 - 0.003"	PORT S6	--
1 AXIAL F.O.P	F.O.	1	/0 - 0.003"	PORT F3	--
<u>FLOW RATES</u>					
RADIAL BEARINGS	ORIFICE	2	/0-0.2 #/s	VALVES G&H	--
AXIAL BEARINGS	"	2	/0-0.075 #/s	VALVES K&R	--
LOADER BEARING	"	1	/0-0.036 #/s	VALVE L	--
TURBINE FWD NOZZLE	"	1	/0-0.235 #/s	VALVE W	--
TURBINE REV NOZZLE	"	1	/0-0.235 #/s	VALVE U	--

*THE TEST CYCLES WILL START WHEN TEMPERATURES TD4, TV2, TV4, AND TM2 REACH -415°F AND TEST WILL CUT OFF WHEN THESE TEMPERATURES REACH -400°F.

Table G-4
ACCELEROMETER INSTRUMENTATION PARAMETERS

Accelerometer Amplitude Redline	10 g rms
Frequency Range	0 to 4,200 Hertz
Time Delay	20 millisec
Reset Time	10 millisec
Tascos Cut-Off Criteria	One of Three (non-voting)

Table G-5
OTVE H/S BRG TESTER VALVE SEQUENCING

<u>Valve</u>	<u>On</u>	<u>Off</u>	<u>Control Parameter</u>	<u>Limit</u>
"C" Sump	-0.3 S	N=0+0.3 S	Pressure	350 psig
"R" Turb Thrust Brg	-0.2 S	N=0+0.2 S	Flow	0.08 lb/S
"K" Thrust Brg	-0.2 S	N=0+0.2 S	Flow	0.08 lb/S
"W" Turb Fwd Nozzle	0.0 S	N=200krpm+1S	Shaft Spd	250 krpm
"U" Turb Rev Nozzle	N=200krpm+1S	N=0	Shaft Spd	3,500 psig
"G" Turb Rad Brg "A"	0.0 S	N=0	N ²	3,500 psig
"H" Rad Brg "B"	0.0 S	N=0	N ²	3,500 psig
"L" Rad Loader	0.0 S	N=0	N ²	1,500 psig

Note: Sump valve "C" will be full open during chill and controlling during test cycles.

Table G-6
OTVE H/S BEARING TESTER PARAMETER IDENTIFIERS

	<u>T*</u>	<u>P*</u>	<u>DP</u>	<u>PORT</u>	<u>FLOW*</u>
Turbine H/S Bearing "A"	TG	PG	PPG	"A"MN	WG
Nonturbine H/S Bearing "B"	TH	PH	PPH	"B"MN	WH
Turbine Axial Bearing	TR	PR	PPR	A7	WR
Nonturbine axial bearing	TK	PK	PPK	B7	WK
Loader Bearing	TL	PL	PPL	P1	WL
Turbine Forward Nozzle	TW	PW	PPW	"T"MN	-
Turbine Reverse Nozzle	TU	PU	PPU	"T"MN	-
Sump	TD4	-	-	D4	-
Sump	TV2	-	-	V2	-
Sump	TV4	-	-	V4	-
Sump	TM2	-	-	M2	-
Sump	TC	PC	-	-	-

*Displayed during test

HARDWARE/FACILITY INTERFACES

The tester shown in Figure 2 will be assembled at the Rocketdyne EDL facility. Posttest data analysis will determine when or if removal by APTF personnel of the bearing housing subassembly is required. Inspection of the bearings will consist of, but not limited to, isotope wear detection measurements, visual and microscopic inspections, and dimensional checks.

The tester will be held in place via a 7-bolt hole pattern that is 10 in. in diameter and is drilled for 3/8-in. bolts. The tester is 6 in. in diameter by 10 in. long (reference Tester Assembly Drawing No. 7R035800).

TEST MATRIX

The initial test runs will be exploratory in nature. During chill-down, it is important that the shaft does not rotate. A controlled steady flow of GH_2 through the turbine brake nozzles should prevent shaft rotation. After chill-down (the tester is considered "Chilled Down" when LIQUID hydrogen is flowing completely through the test bearing), several tests are to be performed. They are:

1) Quantify Shaft Radial Movement

While flowing hydrogen to the test bearings at various pressures specified by Engineering, gradually (approximately 100 psi/sec) increase the radial load bearing pressure to 1000 psig. Record pressure, flow, and shaft movement via the Bentlys and fiber optic probes.

2) Facility Control and Tester Response Checkouts

Gaseous hydrogen is to be trickled into the turbine area through the seven forward turbine nozzles and the two turbine reversing nozzles to clear the turbine area of liquid hydrogen. The test hydrostatic

bearing supply pressures will be applied at 2300 psig, the forward turbine nozzles will be shut down, and the reversing nozzles will be pulsed at 500 psig. Instrumentation readouts will be monitored for shaft rotation. If no rotation is noted, then the reversing nozzle pressure will be increased in 25-psig increments up to 3000 psig max or until shaft rotation is noted. Once shaft rotation is noted, the rotation will be maintained at 5,000 to 10,000 RPM. While the shaft is still coasting, the forward turbine nozzles will be applied gradually to stop the shaft and change the direction of rotation to the forward direction. The shaft will be brought up to a speed of 80,000 RPM, the forward turbine nozzles will be shut down, and the reversing nozzles will be applied at 3000 psig and the time required to stop the shaft will be noted. Speed, pressures, flows and shaft movement shall be recorded. The test will be placed on a temporary hold to assess the coastdown time impact. The system will be returned to chill mode.

All instrumentation (static and dynamic) will record time, speed, pressures, temperatures, flows, displacement and acceleration.

Upon completion of the aforementioned checkout test and the test request reviewed and revised based on previous exploratory tests, the terry turbine will be pulsed to start the shaft spinning. The pressure of the pulse required to get the shaft spinning and the RPM the shaft reaches will be recorded. The shaft will then be accelerated to 80,000 RPM and immediately the turbine supply pressure will be cut to zero and the reversing nozzles of the terry turbine will be activated at a pressure of 3000 psig. The time required for the shaft coast to zero RPM will be recorded. The shaft will then be accelerated to 100,000 RPM and the reversing nozzles will again be activated. The time required for the shaft to coast to zero RPM will be recorded. This coastdown time information is required to plan the remaining test matrix. This procedure is to be repeated up to the maximum tester speed

of 200,000 RPM. At each speed level the following parameters will be checked for redline:

- Speed
- Pressure (inlet and sump)
- Temperatures (inlet and sump)
- Flow (inlet and sump)
- Accelerometers
- Shaft axial position
- Shaft orbit
- Facility control and recording equipment.

Additional checkout tests are required to verify rotordynamic calculations. To accomplish this, the tester is to be brought up to speed at a hydrostatic bearing supply pressure of 2,300 psig. With speed held constant, the pressure to the bearings will then be slowly reduced until the supply pressure equals the indicated pressures in the following table:

<u>Speed</u>	<u>Pressure</u>
80,000 RPM	620 psig
120,000 RPM	1,020 psig
160,000 RPM	1,580 psig
200,000 RPM	2,300 psig

Once the checkout tests have been completed and the facility and tester are functioning properly, the testing will proceed in the following manner:

Tests 1-30 Test Bearing Material #1 per the Time/Speed/Pressure profile illustrated in Figure 4.

Inspect Bearings for wear (if necessary).

Tests 31-100 Continue testing of Bearing Material #1 per Figure 4 profile up to 100 cycles.

Pending results of posttest data analysis, remove assembly from the facility and ship to EDL for installation of Bearing Material #2.

- Tests 101-130 Test Bearing #2 per the Time/Speed/Pressure profile illustrated in Figure 4.
- Inspect Bearing for wear (if necessary).
- Tests 131-200 Continue testing of Bearing Material #2 per Figure 4 profile up to 100 cycles.
- Pending posttest data analysis, remove assembly from test stand and ship to EDL.

APPENDIX H

COPPER PLATING METHOD

THE FOLLOWING BATHS WILL BE REQD FOR THE
COPPER ELECTROPLATING PROCEDURE:

- a.1. ENBOND HP 127S.
ENBOND HP 127S 70 GRAMS/LITER.
TEMPERATURE: 190°F.
TANK: MILD STEEL.
CAUTION: SOLUTION IS CAUSTIC.
- a.2. TERNARY ACID PICKLE.
ACTANE 70: 30 GRAMS/LITER.
CONC. SULFURIC ACID 6.5% BY VOLUME.
CONC. NITRIC ACID (70%) 12.5% BY VOLUME.
ROOM TEMPERATURE.
TANK: PLASTIC OR RUBBER LINED.
CAUTION: SOLUTION CONTAINS FLOURIDE.
- a.3. ACTANE TI2000.
USE FULL STRENGTH.
pH 1.7-1.8 (USE pH PAPER TO MEASURE pH).
TEMPERATURE: 158°F.
TANK: POLYPRO OR PLASTIC LINED.
HEATER: TEFLON COATED.
CAUTION: SOLUTION CONTAINS FLOURIDE.
- a.4. 10% HYDROCHLORIC ACID.
CONC. HYDROCHLORIC ACID: 10% BY VOLUME.
WOOD'S NICKEL STRIKE. (STANDARD).

COPPER ELECTROPLATE SHAFT IN DESIGNATED AREAS
AS FOLLOWS:

- b.1. ENBOND 127S BATH.
IMMERSE FOR 5 MINUTES.
COLD WATER RINSE, TWO RINSES.
- b.2. TERNARY ACID PICKLE.
IMMERSE FOR 60 SECONDS OR UNTIL UNIFORM GAS-
ING IS OBSERVED. (RECORD THE TIME).
COLD WATER RINSE.
- b.3. ACTANE TI 2000.
IMMERSE FOR 10 MIN OR UNTIL A DARK GREY SUR-
FACE APPEARANCE IS NOTICED.
(RECORD THE TIME).
COLD WATER RINSE.

